Delfim Diniz Costa

Licenciado em Ciências de Engenharia Mecânica

Proposal of a methodology for the design of the installation of turrets on aircrafts – the approach on the aerodynamic influences

Dissertação para obtenção do grau de Mestre em

Engenharia Mecânica

Orientador: Prof. Doutor Daniel Vaz, Professor Auxiliar, FCT/UNL

Co-Orientador: Prof. Doutor António José Freire Mourão, Professor Associado, FCT/UNL

Co-Orientador: Eng. João Rui Duarte, OGMA – Indústria Aeronáutica de Portugal, S.A.

Júri:

Presidente: Prof. Doutor João Cardoso, Professor Auxiliar, FCT/UNL

Vogal: Prof. Doutor Daniel Vaz, Professor Auxiliar, FCT/UNL

Arguente: Mestre Rui Pereira, OGMA – Indústria Aeronáutica de Portugal, S.A.

Arguente: Doutor Eric Dider, Bolseiro de Pós-Doutoramento do LNEC, DHA, Núcleo de Portos e Estruturas Marítimas

FACULDADE DE CIÊNCIAS E TECNOLOGIA
UNIVERSIDADE NOVA DE LISBOA

Setembro de 2015

Proposal of a methodology for the design of the installation of turrets on aircrafts – the approach on the aerodynamic influences

Delfim Diniz Costa

Licenciado em Ciências da Engenharia Mecânica

Proposal of a methodology for the design of the installation of turrets on aircrafts – the approach on the aerodynamic influences

Dissertação apresentada à Faculdade de Ciências e Tecnologia da Universidade Nova de Lisboa para a obtenção do grau de Mestre em Engenharia Mecânica

Setembro 2015

A todos aqueles que me transmitem conhecimento...

Acknowledgements

Firstly, I would like to express my sincere gratitude to Eng. João Rui Duarte, for his support throughout the whole thesis development.

Besides Eng. João Rui Duarte, I would like to thank my advisors Professor Daniel Vaz and Professor António Mourão, for their guidance during the work.

I also want to thank Yevhen Doloshytskyy, for his friendship and cooperation during these last few years.

I extend my gratitude to my family, for always being there for me and making this possible.

Finally, a special “thank you” to my Mafalda, for being a part of my life.

Abstract

The present work has its origin on the necessity of enabling a design certified company, or DOA (Design Organization Approval), to perform a modification; this modification is the installation of EO/IR (Electro-optical infrared) sensors on aircrafts. The subject of interest in this dissertation lies on the aerodynamic impact of the modification on the aircraft.

The primary purpose of the present thesis is the creation of a methodology that regards the design stage of the modification. This methodology serves as guidance to the DOA design team that is assigned to the design of the modification. The methodology includes a recommendation to the certification of the modification; it contains a method intended to decide the location of the installation of the sensors on the aircraft; it also comprises of a design structure specifically adapted to the modification in study.

Regarding the aerodynamic impact, it is studied the aerodynamic analysis' tools, which allows one to relate the different stages of design to the most suited tools to each stage.

A case study is performed with the purpose of not only validating the methodology which was created but also to giving a first approach to the preliminary design of the modification. As example, there are used the Lockheed Martin C-130 aircraft and the FLIR Star Safire III sensor.

Keywords: EO/IR sensors, aerodynamic study, preliminary design, design methodology

Resumo

O presente trabalho nasce da necessidade de capacitar uma empresa certificada para projeto, ou DOA (Design Organization Approval), para realizar uma modificação: a instalação de sensores EO/IR (Electro-optical infrared) em aeronaves. De entre vários aspectos necessários estudar, esta dissertação cobre o impacto aerodinâmico da modificação na aeronave.

Como principal objetivo da dissertação está a criação de uma metodologia de abordagem na fase de projeto da modificação. Esta metodologia tem a funcionalidade de assistir a equipa de projeto da DOA no momento em que esta esteja a iniciar o projeto da modificação. A metodologia inclui uma recomendação relativamente à certificação da modificação, um método destinado a decidir a localização dos sensores na aeronave bem como uma organização da estrutura do projecto gerada especificamente para a modificação em questão.

Relativamente ao impacto aerodinâmico, é feito um levantamento das ferramentas de análise aerodinâmica que permite associar as diferentes etapas do projeto aos métodos mais adequados de análise aerodinâmica.

É efetuado um caso de estudo por forma a não só validar a metodologia criada bem como dar uma primeira aproximação do projeto preliminar da modificação em estudo. Como exemplo são usados a aeronave Lockheed Martin C-130 e o sensor FLIR Star Safire III.

Palavras-chave: sensores EO/IR, estudo aerodinâmico, projeto preliminar, metodologia de projeto

List of contents

List of figures

List of tables

Acronyms and nomenclature

AC – Air Conditioning

AD – Axiomatic Design

APU – Auxiliary Power Unit

CAD – Computer Aided Design

CCM – Certification Compliance Matrix

CD – Customer Domain

Cd – Drag Coefficient

CFD – Computational Fluid Dynamics

CP – Certification Plan

Cp – Pressure Coefficient

CQD – Certification and Qualification Domain

CS – Certification Specification

DNS – Direct Numerical Simulation

DOA – Design Organization Approval

DSM – Design Structure Matrix

EASA – European Aviation Safety Agency

EO – Electro Optical

FAA – Federal Aviation Administration

FD – Functional Domain

FEM – Finite Element Method

IAS – Indicated Airspeed

IR – Infrared

ISA – International Standard Atmosphere

LES – Large Eddy Simulation

LSCB – Least Square Cell Based

MTOW – Maximum Takeoff Weight

N-S – Navier-Stokes

PhyD – Physical Domain

ProD – Process Domain

QCM – Qualification Compliance Matrix

QP – Qualification

RANS – Reynolds Averaged Navier-Stokes

TAS – True Airspeed

TI – Turbulent Intensity

TLS – Turbulence Length Scale

1 Introduction

1.1 Motivation

The purpose of this work is based on the necessity of a design certified company or Design Organization Approval (DOA) to be certified on the specific modification of turrets installation on aircrafts. This thesis aims at being a first approach to the modification regarding the aerodynamic concerns and the methods of analyzing the aerodynamic impact of the installation of a multi-sensor turret on the aircraft.

The scope of the work is separated into two fields, the design methodology and the aerodynamic theory and analysis. Since the whole process consists of striving to perform the best modification, which implies the fastest, most economical and technically viable solution, there are not only single technical issues to be tackled; any modification or repair is attached to the design and certification compliance of the entire procedure. This is the reason why it is so important, in the aviation industry, to always account for not only the technical development of a solution but also how the procedure is going to be implemented regarding its organization and the certification requirements.

Simultaneously to the aerodynamic impact study, it is also developed the structural impact and structural design study **[1]**; combining both studies results in a more complete amount of information regarding the desired modification.

The major benefit of studying the design phase of a project essentially lies on the amount of commitment on the project on the mentioned phase. Figure 1.1 demonstrates that around 80% of the overall cost of a project is decided by the end of the design phase. This means that regardless of what has been actually invested on the project, by the end of the design stage, most of the decisions for the remaining stages are already made. So a thorough study on the design phase may demonstrate to be very cost-effective.

Other design-related aspect of the motivation for this thesis is the success analysis of the modification. It is in the best interest of the DOA that the modification may be performed successfully. The definition of success is relative so in Figure 1.2 it is represented the Iron Triangle which includes the three most important criteria to check whether a project is successful or not. This method only considers operational criteria; it does not include economical, institutional or regulatory factors that are also relevant to the feasibility of a project.

Cost, Quality and Time are generically the main three concerns of the management of a project. So this thesis has the purpose of reducing time and cost on the design phase of the modification while increasing the quality (quality of information in terms of results and aerodynamic analysis' methodology) of the project.

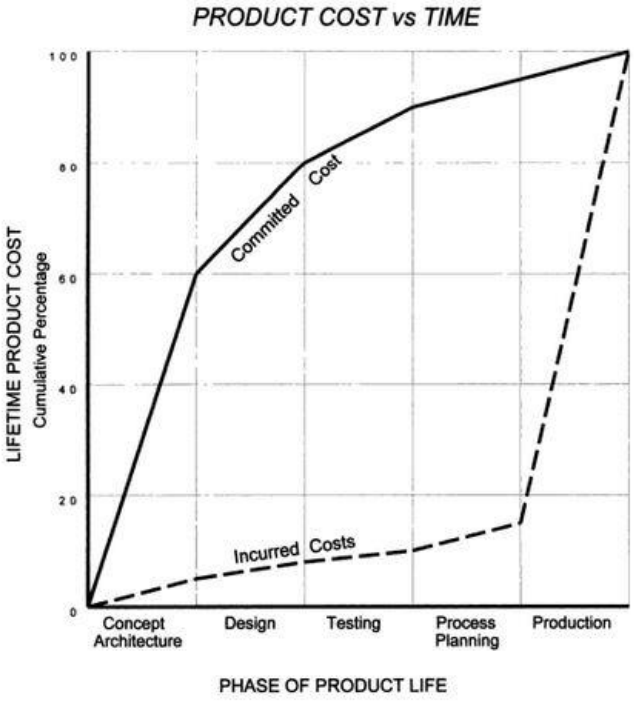

Figure 1.1 – Comparison between commited and incurred costs on different stages of a product development **[2]**.

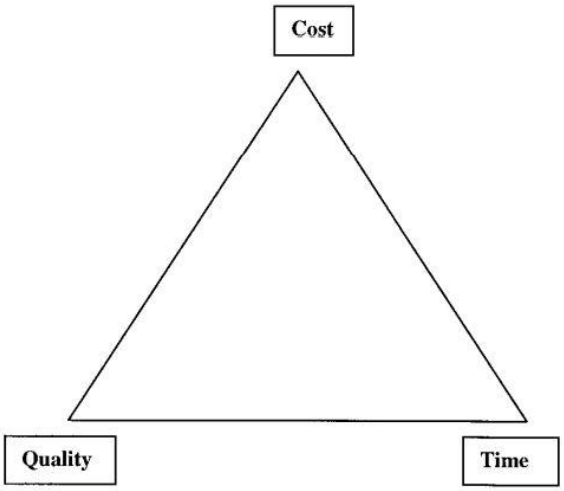

Figure 1.2 – The Iron Triangle **[3]**.

Although not specifically approached in this study, a crucial concern to take into account on the modification is aeroelastic phenomena. "*The aeroelastic behavior is determined by studying simultaneously the influence of the interaction of vibrational dynamics, structural elasticity and aerodynamics"* **[4]**. As seen on Figure 1.3 the interaction may be described by a triangle that treats inertial forces, elastic forces and aerodynamic forces respectively; each of these forces interact with each other as these are not independent. In the center of the triangle the aeroelastic phenomena are presented; these are flow-induced vibrations, being it forced

response and flutter (see more on forced response vibration and flutter on **[4]**). These phenomena do not occur in every situation on an aircraft, however these are common in many different locations, being one of the main locations of concern the wings.

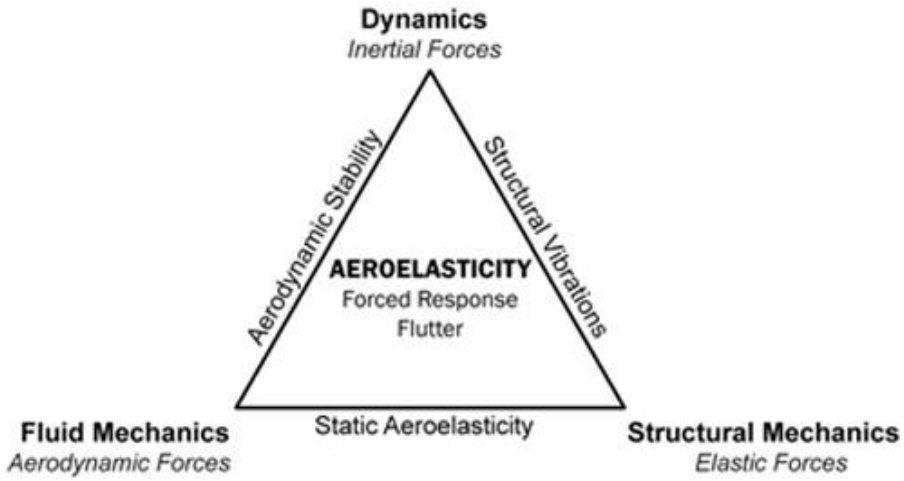

Figure 1.3 – The Collar Triangle **[4]**.

The development of the present work results from the cooperation between Faculdade de Ciências e Tecnologia – Universidade Nova de Lisboa and the company OGMA – Indústria Aeronáutica de Portugal, S.A..

1.2 Objectives

In order to provide a solution to the DOA entity's needs regarding a design methodology and an aerodynamic analysis always bearing in mind the regulatory and organizational requirements, the main output of the present work is a methodology tailored to the installation of multi-sensor turrets on aircrafts. This methodology allows the DOA to have a starting point in terms of aerodynamic analysis needs and the study by Doloshytskyy (2015) **[1]** has the same purpose regarding the structural analysis and design.

Figure 1.4 is a flowchart describing how the study is conducted. The outputs may be seen as minor objectives required to achieve a well-grounded major objective, being it the group of recommended actions related to the design procedures and the aerodynamic analysis.

As objectives, this work does not include:

- The certification compliance procedure for the modification, which may have differences depending on the type of aircraft or the location of the turret installation;
- The specifics of the design process. The intent is a methodology that regards guidelines for the design process, focusing on the preliminary design.

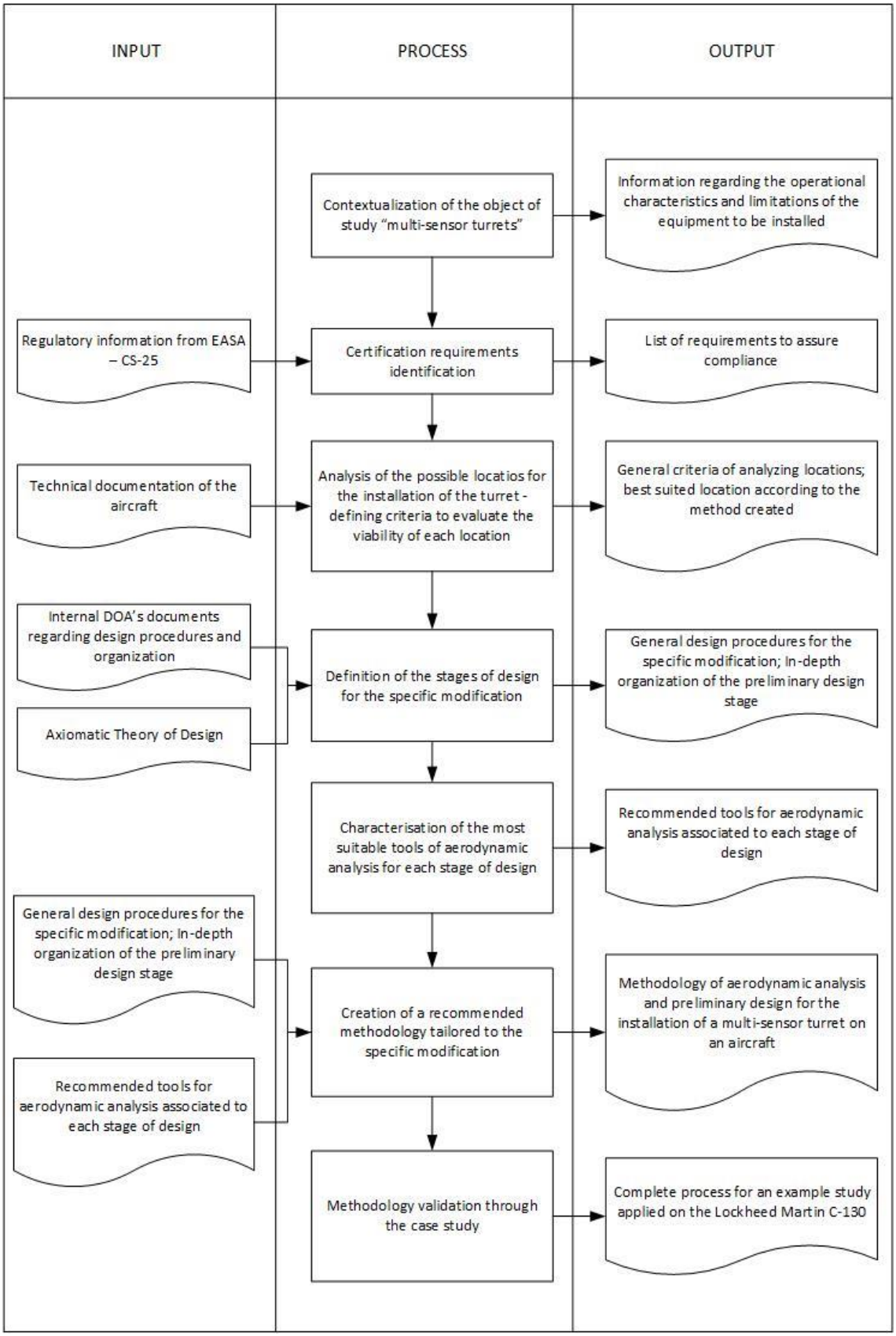

Figure 1.4 – Flowchart of the thesis outputs.

1.3 Thesis structure

The document is composed of eight chapters, being the first the introduction and the last the conclusion. As mentioned it regards two principal technical fields, the design methodology and the aerodynamic analysis.

The second chapter is related to the regulatory context of the modification. It gives a brief context of the existing regulations and also a recommendation of the requirements needed to comply for the certification of the procedure.

The third chapter is a brief overview of the equipment to be installed, the multi-sensors. Its applicability, main characteristics and functionalities are presented.

The forth chapter is related to the viability of the turret's locations to be installed on the aircraft. It regards the methodology created to choose the location for the installation of the turret on the aircraft; the methodology includes criteria that are applicable to other types of aircraft.

On the fifth chapter, the specific design methodology of the modification is addressed. A contextualization of the specific design methodology with the axiomatic design theory is done. Several layers of the methodology are constructed with increasingly amounts of detail on each one. In this methodology the intent is to optimize the existent design procedure of the DOA to the particular modification required.

Chapter six is: an overview of the aerodynamic analysis tools, the numerical computation considerations and a group of recommendations for the DOA relating the most suitable tools to apply in each stage of design. It also regards a set of considerations regarding the specific preliminary design steps. One of the purposes of this chapter is for the reader to have an extensive view of which are the most expedite tools, as well as the most precise ones. This information allows one to decide which tools to apply in which stages of the project.

On the seventh chapter, an example analysis is performed, a case study that includes every step of the preliminary CFD analysis.

Chapter eight includes the concluding remarks of the thesis and the future developments in order to allow further studies on the subject.

2 Aeronautical regulation

2.1 Introduction

For the last decades, the aviation industry has been growing exponentially and the enormous increase in air traffic has forced the organization and security measures to be much fiercer. Adding this fact to the obvious reasons of the intent of minimizing the prospect of accidents or incidents regarding airplanes in any way, the creation of regulatory organizations was inevitable. EASA (European Aviation Safety Agency) and FAA (Federal Aviation Administration) are the principal regulators on the aviation industry, being the former the European regulator and the latter the regulator from the USA. The main focus of EASA is the "*strategy and safety management, the certification of aviation products and the oversight of approved organizations and EU member states*" **[5]**.

2.2 Structure of regulation

The approved organizations mentioned include every company which has interference on any part of an aircraft, being this interference related to maintenance, production, assembly, modification or design, among others. This study is associated to a modification on an aircraft, more specifically to the design of the modification. In order for a company to be authorized to perform the design of the modification is has to be certified by EASA; a company which is certified to conduct designs of modifications or repairs on aircrafts is a DOA.

Among many regulations, there is the CS-25 which is a list of requirements or certification specifications (CS) related to the category of "Large Aeroplanes" in which the Lockheed Martin C-130 in included since it has a Maximum Takeoff Weight (MTOW) higher than 5670 Kg. This list includes regulations regarding every aspect of the design, characteristics, operations and security of an aircraft.

Although for military purposes there is no legal obligation of complying with the CS-25 requirements, unless agreed otherwise from both the DOA and the client, the document is used as a basis for the certification to support the decisions made throughout the work. In this way, Table 2.1 presents the group of requirements found to be applicable to the installation of the multi-sensor turret on the aircraft. It is important to refer that in this study the focus is not on assuring the compliance of these requirements but only to deliver an idea of the concerns of this modification. This should reduce the time and effort on producing the required documents to prove compliance to the requirements.

Table 2.1 – List of recommended requirements from CS-25 to consider for the installation **[6]**.

Subpart	Requirement	Description
B	25.103(d)	Stall speed
	25.251	Vibration and buffeting
C	25.335	Design airspeeds
	25.341 (a) and (b)	Gust and turbulence loads
	25.415	Ground gust conditions
F	25.1301	Function and installation
	25.1302	Installed systems and equipment for use by the flight crew
	25.1309	Equipment, systems and installations
	25.1321	Arrangement and visibility
	25.1322	Flight crew alerting
	25.1431	Electronic equipment
G	25.1503	Airspeed limitations: general
	25.1505	Maximum operating limit speed

3 Multi-sensors overview

3.1 Introduction

Electro Optical and Infrared sensors (EO/IR) cover a wide range of distinct technologies based on the targets and missions to be accomplished being these in aerial, ground or maritime environments. The particular sensors subject to this study are airborne observation systems. Depending on the application, several devices can be integrated in a turret that is installed on the aircraft. The EO/IR sensors are usually the most valuable to the mission. These multi-sensors are frequently referred as EO/IR sensors alone, however this is not accurate. These sensors are suitable for detecting, acquiring, auto-tracking and identifying targets at long ranges.

These systems are a major asset for the aircrew in many operations, such as:

- Search and rescue
- Intelligence, surveillance and reconnaissance
- Border and coastal patrol
- Force protection

In many scenarios, the ability to monitor the area of interest from high altitudes is an indispensable factor in the security or safety equation of an operation. Multi-sensor systems are fit for observing major events and demonstrations, coastguard missions, search and rescue operations and police actions. Observers are afforded a clear overview of the site even in adverse climatic conditions; command and control staff can see details on images which in other way would be impractical. This insight enables prompt intervention providing the crew precious time when under threat **[7] [8] [9]**.

To give an idea of the image provided by these devices, Figure 3.1 is a representative infrared image available to the aircrew.

Figure 3.1 – Example of IR image provided by this type of sensor **[10]**.

3.2 Most relevant characteristics of the devices

Since the sensors are not standard, their manufacturers are free to create products tailored to their clients' needs. A brief market research is undertaken allowing one to understand the typical characteristics of these sensors as well as which are the major manufacturers. Regarding the present study, the sensors' characteristics considered relevant are those which influence structural and/or aerodynamic parameters – sensor's dimensions and weight, given that their geometry is similar. In Table 3.1 there is a list of manufacturers with their respective products' dimensions and weight.

In order to ease the amount of work for the DOA by adapting a real problem to this study, there is the concern to use a sensor similar to most of the used models. Hence, the selected model – highlighted on Table 3.1 – is the one which its installation seems the most frequent and also the one with the average dimensions and weight.

Table 3.1 – List of manufacturers analysed (Data obtained from turrets' datasheets).

Manufacturer	Model	Weight (Max) [kg]	Diameter [m]	Height [m]
Airbus Defense & Space	Arghos II **[11]**	43	0,450	0,500
	Goshawk II **[11]**	30	0,450	0,350
Raytheon	NA/AAS – 52 **[12]**	60	0,457	0,193
FLIR	Star Safire III **[13]**	44	0,380	0,450
General Dynamics	V – 14 **[14]**	70	0,447	0,503
Northrop Grumman	NA/AAQ-28(V) **[15]**	210	0,406	-
Lockheed Martin	INFIRNO **[16]**	59	0,401	0,541
L-3 Wescam	MX-15 **[17]**	45	0,394	0,481
	MX-20 **[18]**	90	0,533	0,667
	MX-25 **[19]**	100	0,653	0,767
RAFAEL	Toplite EOS **[20]**	65	0,594	0,662

Regardless of the variations/differences there may be between these sensors, being it due to the different applications or just different manufacturers, there are common devices in every sensor analyzed, which are:

- Thermal imager – IR sensor that delivers thermal image. These make pictures from heat, not visible light.

- Multi-spectral sensor – This sensor allows the sensor to operate in poor conditions – fog, smoke, haze, dust, rain.
- Daylight imager – Regular camera that provides visual image
- Lowlight imager – Sensor that take in small amounts of visible light, magnifies it greatly, and projects that on a display
- Laser rangefinder – Determines the distance to a target or object
- Laser pointer/tracker – Helps in locating the target on the image

Figure 3.2 illustrates Star Safire III – a multi-sensor turret from FLIR. From the image one can also perceive the variety of lenses in the turret, which suggests a variety of functionalities present on the device.

Figure 3.2 – Star Safire III – A multi-sensor turret from FLIR **[13]**.

4 Viability analysis for the turret's installation location

4.1 Introduction

There are many locations where the multi-sensor turret can be installed on the aircraft. "Where to install it?" is a question that can have several answers, there is not a right one. Checking each location for preset criteria is usually an adequate decision-making procedure. The way one looks at this decision is subjective hence there is the need to create a methodology to assure that the result has grounds to be considered a "good" or "acceptable" result. The methodology adopted to analyze the locations is as follows:

I. Listing of all the criteria that may affect the decision;
II. Sorting of the criteria based on its priority and its consequent influence on the decision;
III. Ranking, in tiers, of each criterion by priority;
IV. Checking for dependency between criteria;
V. Identification of the possible locations;
VI. Mapping of the most adequate locations to install the sensor;
VII. Selection of the location to install the turret.

4.2 Criteria that may affect the decision and their hierarchy

In this subchapter the first three phases are described. Regarding the initial phase, the listing of all the criteria is done through brainstorm trusting the engineering judgement and experience. This phase considers operational, structural and aerodynamic issues as well as costs and aircraft maintenance, yet in a generic manner.

Table 4.1 relates the most relevant criteria to the justification for its consideration as the most relevant. Based on each criterion's definition, these are sorted by influence on the decision of the location. There are eight criteria; criterion 2 is divided into five types of interference in order to have a clearer idea of what kinds of interference there are.

In phase III, the criteria are placed in different tiers. The hierarchy is defined as tier 1 being the most relevant and tier 3 being the less relevant as shown in Table 4.2.

Table 4.1 – Definition of the most relevant criteria to the turret's location.

Criterion	Comment
1. Sensor's sight range	It was determined as one of the major needs of the system. From an operational point of view, it is mandatory that the sensor has a wide range of sight.
2. Interference with other parts	This criterion includes every kind of interference there may be. It is considered to be high priority since one must analyze if there is something already in that location.
3. Possible damage to the sensor	Possible damage to the sensor implies a shortage to the device's longevity, which creates the need for regular maintenance. Makes the modification lose its purpose in a client's point of view.
4. Pressurized areas of the aircraft	Concerns the difficulties that are imposed by the structural complexity of a pressurized area. Preference is given to the non-pressurized areas of the aircraft since there is the need to create an external structure on the pressurized areas to minimize the influence of the modification on the structure.
5. Sensor's Characteristics - Aerodynamic impact	Can be responsible for certain changes in the performance parameters of the aircraft. Although it is not a mandatory factor, it can rule out some options.
6. Sensor's Characteristics - Structural impact	Can dictate the magnitude of the support system for the turret. Regards the dimensions of the turret in a way that a certain location may need a different type of structure to be able to support the turret.
7. Structure's integrity	In a first approach to the issue, one must consider the fragility of the aircraft's local structure since it gives an approximate idea of how difficult the modification is.
8. Modification's complexity	Criterion that regards the eventual cost and size of the whole process of the modification. It is a gathering of the most important issues taken in consideration for the selection of the location.

Table 4.2 – Hierarchy of turret's location criteria.

Tier	Relevance	Definition	Criterion
1	High	Criteria that preclude the location's viability	1, 2, 3
2	Medium	Criteria that restrain the location's viability	4, 5, 6
3	Low	Criteria that hamper the location's viability	7, 8

4.3 Checking for dependency between criteria

The Design Structure Matrix (DSM) serves the purpose of analyzing the independence between criteria or tasks. To guarantee that the location criteria are independent from each other or at least just have a one-way dependency (one depends on another but not the other way around), the DSM must have a triangular configuration. This tool is useful for managing complex systems since its result allows one to find where a system can be improved **[21]**. To this particular case the DSM goes as shown in the Figure 4.1, where it is clear that the criteria in tiers 1 and 2 are independent. Both criteria 7 and 8 are dependent on higher tier criteria which confirms the hierarchy defined on Table 4.2 since it is considered acceptable that a less relevant criterion depends on a higher priority one.

DSM	1	2	3	4	5	6	7	8
1								
2								x
3								x
4								x
5							x	x
6							x	x
7								x
8								

Figure 4.1 – Design Structure Matrix which relates the interdependency of the location criteria.

4.4 Identification of the possible locations

As possible locations, it is considered every part of the aircraft where a fixation of the turret may be feasible disregarding whether it seems logical or not, though keeping in consideration the issues referred in 4.1. To identify each location the aircraft is divided into several areas, from A to Q. Each area is defined as being an area which has the same characteristics in terms of location criteria analysis. In the particular location Q, it is only illustrated the fuel tanks since it is considered the most advantageous location along the wings. Figure 4.2 consists of the bottom view of a Lockheed Martin C-130 with the locations represented and also the side view of the same aircraft.

As an important portion of this phase there is the need to search for current solutions. The results achieved should be coherent with the usual applications perceived in the market. Based on a thorough search about the locations already used to install a sensor turret or similar on a Lockheed Martin C-130, there isn't a clear convergence towards a specific location;

although, there is a group of four locations that is preferred that corresponds to locations A, B, D and P. On Figure 4.3 and Figure 4.4 are represented current applications installed on this aircraft model. On the aircraft of Figure 4.3 there are turrets simultaneously on three different locations – B, D and P – whereas on the aircraft of Figure 4.4 there is a turret installed on location A.

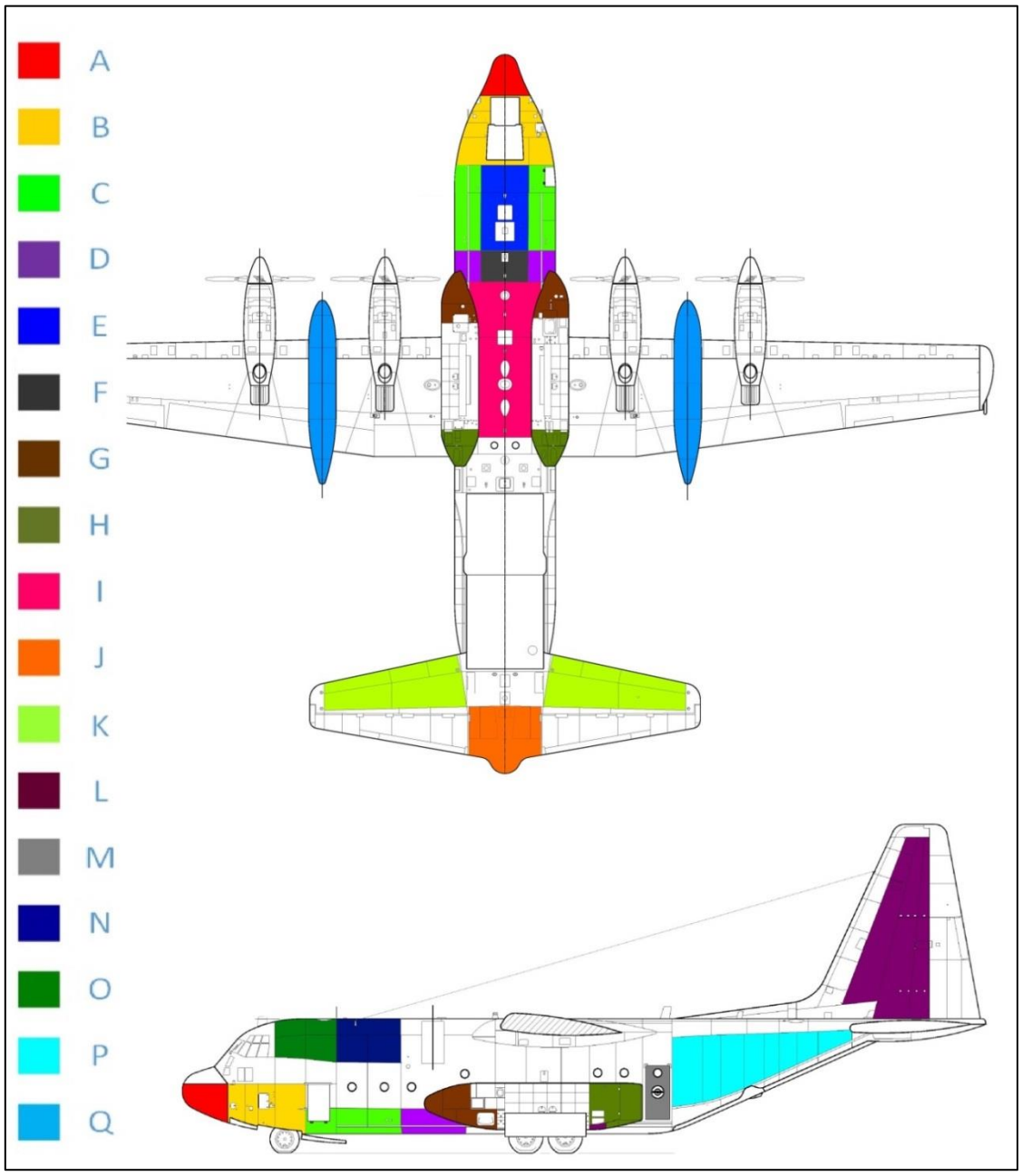

Figure 4.2 – Mapping and labeling of considered locations in the aircraft.

Figure 4.3 – Picture of the aircraft Lockheed Martin C-130 with highlighted turrets installed **[22]**.

Figure 4.4 – Picture of the aircraft Lockheed Martin C-130 with highlighted turret installed **[23]**.

4.5 Mapping of the most adequate locations to install the sensor

The assessment of each location is achieved through comparison between options; in fact the present methodology does not have the capacity of stating which of the locations are

“good” or “bad”. The comparison only allows one to decide which locations are the “better” or “most viable”. At this stage, these criteria help to narrow the possible locations for the study but it is important to state that this is a preliminary stage in which personal judgment is required. For each location, the criteria are evaluated by a three mark system, colors green, yellow and red. Green: the location meets the criteria. Yellow: the location is adaptable to the criteria. Red: The location does not meet the criteria. In Figure 4.5 it is represented the location comparison matrix which uses the marking system to relate the criteria to each location, being the former represented in the rows and the latter represented in the columns.

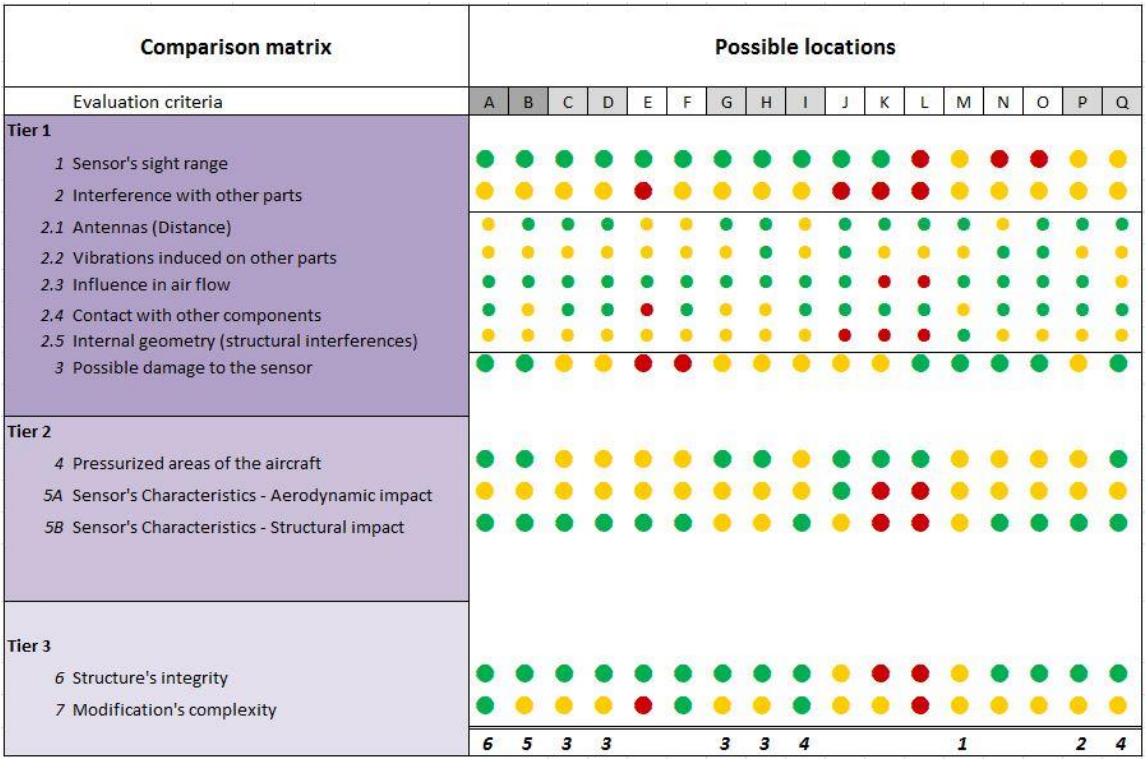

Figure 4.5 – Location comparison matrix.

As mentioned in 4.2, the criterion 2 is hereby separated into 5 narrower criteria. Since the purpose of the board is to compare each location and each mark is given on a relatively subjective basis, a list of comments on each mark is produced to help one understand the procedure that leads to the final conclusion. The list can be consulted in Annex A. Some of the marks are given based on common sense; however, there is the need to consult technical documentation of the aircraft to ground the evaluation. It is assumed that a location is ruled out as a viable option once it gets at least one red mark. The priority of the criteria defines the way each location is ranked as “better” or “worse”.

One may notice at the location comparison matrix that there are some locations highlighted in dark grey, others in light grey and others not highlighted. In addition to the last row’s information, this is a means of clearly identifying which are the locations preferred from

the evaluation. On the last row it is possible to see the result of each location's evaluation being the quantity that there appears the amount of green marks the location has obtained.

4.6 Selection of the location to install the turret

In order to define a coherent evaluating system, two assumptions are made simultaneously to the phase VII, which are: A fixed support structure to the turret is more suitable than a retractable structure due to the sturdiness of the fixed structure which allows less dependency on maintenance and which minimizes the risk of mechanism failure. The other assumption is that regardless of redundancy (which might be a plausible criterion for the client and in which case changes the priorities), needing to install only one sensor is preferred to needing to install more than one due to economical reasons. These assumptions serve the purpose of enabling one to create the comparison matrix in an unambiguous manner by defining both the preconditions and the priorities of all the criteria for the installation of the turret.

Considering the possibility of dealing with an aircraft that has been subject to previous modifications, there is the concern to suggest an assortment of viable locations and Table 4.3 lists the most viable ones according to the present methodology. As seen on current applications, there can be several locations on the same aircraft so Table 4.3 describes the concerns to bear in mind when considering the different viable locations. Regardless of the subjectivity inherent to the information present in the table, Table 4.3 is produced as a preliminary overview to the eventual difficulties regarding each location.

Table 4.3 – Summary of the viable locations.

<table>
<tr><th></th><th></th><th>Comments</th></tr>
<tr><td rowspan="2">Recommended Locations</td><td>A</td><td>• Interference with Glideslope sensor [24];
• Severe impact on the aerodynamics of the turret and aircraft;</td></tr>
<tr><td>B</td><td>• Need for an external horizontal surface to fix the turret due to the asymmetry of the location;
• Not viable from a certain turret dimension;</td></tr>
<tr><td rowspan="6">Possible Locations</td><td>C</td><td>• Need for a lens/turret protection against projectile from the wheels of the landing gear;
• Pressurized area – external fixation structure required;</td></tr>
<tr><td>D</td><td rowspan="2">• Pressurized area – external structure required between D and G;
• Possible interference with APU or AC systems [24];</td></tr>
<tr><td>G</td></tr>
<tr><td>I</td><td>• Distance to the ground may be critical;
• Distance between antennas may be critical;</td></tr>
<tr><td rowspan="2">P</td><td>• Needs a sizable structure that might influence the elevators, aerodynamically;</td></tr>
<tr><td rowspan="2">Q</td><td rowspan="2">• If in need for redundancy, these are better options;</td></tr>
<tr><td>• Complex fixation of the turret to the fuel tank;
• Need for analysis of the aircraft balance.</td></tr>
</table>

5 A framework for a design methodology

5.1 Introduction

In order to perform the modification efficiently, there is the need to follow a well-defined methodology. Stages need to be set as guidance to perform a modification as well as milestones to guarantee compliance with the preset targets along the process. An analogy is done between the domains of the Axiomatic Design (AD) and the domains considered to better describe the design methodology.

Axiomatic Design theory is used as a basis for the design of the modification. Figure 5.1 represents the domains considered by the AD methodology, where one may see the sequence of the design tasks from the beginning of the project to the end:

- The first concern is related to the customer; defining his needs– Customer Domain
- The second concern is about turning what the customer requests into functional requirements applicable to the project – Functional Domain
- Then, the functional requirements need to be satisfied by physical solutions based on design parameters; different feasible alternatives that comply with every requirement must be created in order to assess the best solution – Physical Domain
- The last domain involves the embodiment of the chosen solution and the process of performing the modification – Process Domain

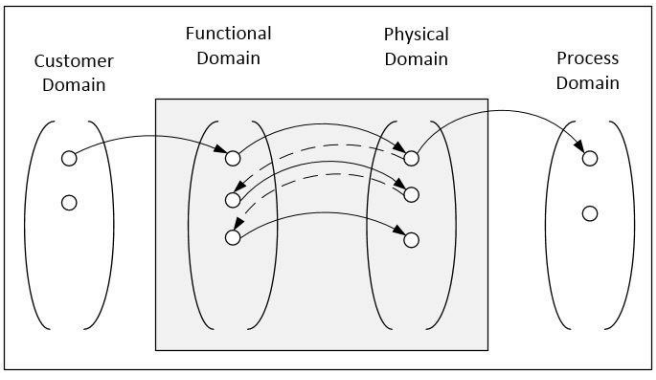

Figure 5.1 – Axiomatic Design – Sequence of design and domain interdependence **[25]**.

In Figure 5.1 one can also see the interdependence between Physical (PhyD) and Functional domains (FD). This fact means that there are decisions to be made in the PhyD that require a basis from the FD, one may need to go back to a functional analysis before being able to generate physical solutions. It is important to state that the Figure 5.1 is already adapted to

the design of the modification in study. The difference between the generic axiomatic theory and the adapted one is that in the latter, it lacks the retroactive arrows between FD and Customer Domain (CD) as well as between Process Domain (ProD) and PhyD. This is due to the fact that in the FD the customer needs are categorically defined and won't change because of the functional analysis. Similarly to the ProD, it is only reached once the PhyD is also definitively characterized. Considering the ProD, there may be the need to repeat the entire process due to unexpected limitations, being these related to economical, labor or objective purposes; although it is different from interaction between domains.

5.2 Modification design outline

Figure 5.2 demonstrates the outline of the whole project. This modification design overview has the purpose of giving one the comprehension of the whole process and also the purpose of mapping each phase in the AD domains. In Figure 5.2 there is one domain – Certification and Qualification Domain (CQD) – that is not included in the AD methodology. This is on account of certification and qualification not being design needs; these are regulatory needs that do not fit in any of the design domains. It is considered that these needs may affect the process but not in a way to be classified as a functional or physical characteristic. The independence between this external domain and the PhyD is substantiated by the simultaneous actions of the certification and qualification procedures as well as the preliminary design.

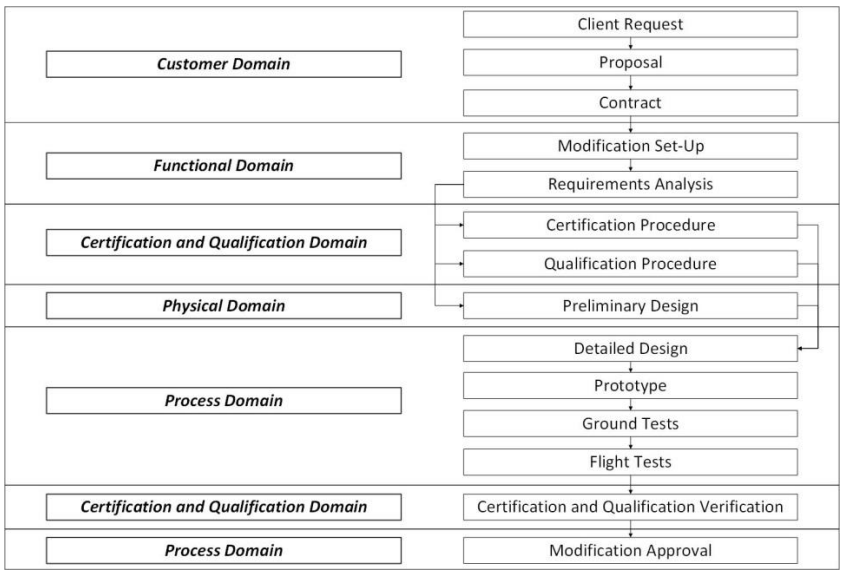

Figure 5.2 – Modification design outline.

In Table 5.1 it is visible each phase's brief description. It also relates the mapping of each phase on each domain. Since the association of a phase to a domain may be considered a subjective decision, the intent of presenting Table 5.1 is also of demonstrating the reason for each decision.

Table 5.1 – Description of the modification design outline.

Domain	Phase	Description
Customer Domain	Client Request	Initial meetings: Exposing client's needs; Defining fundamental objectives; Scheduling dates for negotiation.
	Proposal	Giving the client: Outline of the project; General steps; Budget; Schedule (setting maximums and minimums for the project); Raw order price.
	Contract	Officializing the project: Predicting results and setting the scope of work.
Functional Domain	Modification Set-Up	Initiating the modification process: Assigning a team; Checking for previous modifications to the system (aircraft or particular component); Marking the dates and references; Stating the description of the change, origin and reason for the change.
	Requirements Analysis	Laying out the needed requirements: Analyzing contractual, regulatory, functional, operational and performance requirements which the modifications interfere with; Defining decisive criteria to stand for the stages of the preliminary design
Certification and Qualification Domain	Certification Procedure	Preparation of the change certification: Establishment of the activities required to demonstrate compliance with Certification Specification; Identifying of the appropriate means of compliance for each requirement.
	Qualification Procedure	If applicable, definition of the plan to demonstrate compliance with client's requirements
Physical Domain	Preliminary Design	Development of the modification: Generation of different solutions; Choosing the most viable system; Analyzing if the system is actually viable.
Process Domain	Detailed Design	Creating the documentation necessary to perform the change: Models and installation drawings; Material, product and process specifications; Procedures; Reports
	Prototype	Materializing the solution: Performing the procedure to be subject to further tests
	Ground Tests	Performing the required ground tests (if applicable)
	Flight Tests	Performing the required flight tests (if applicable)
Certification and Qualification Domain	Certification and Qualification Verification	Assurance of the certification: Confirming that the certification status still complies with the regulations
Process Domain	Modification Approval	Finishing the modification: Getting the approval of the client and delivering the operational, maintenance and regulation documentation to all entities

Since the main focus of the present work is on the viability study of the modification, one must specify the stages which belong to FD and PhyD. These are the domains in which the design solutions are created and the most important decisions are made. Table 5.2 describes the detailing of the mentioned stages. It is also useful to understand the CQD due to its influence on the Preliminary Design (as well as due to the need for the DOA to have more information about these procedures) so it is also considered for more detailing. Figure 5.3 is the result of zooming in on the outline of the project on the referred domains and it has the purpose of showing the depth of analysis on each part of the design.

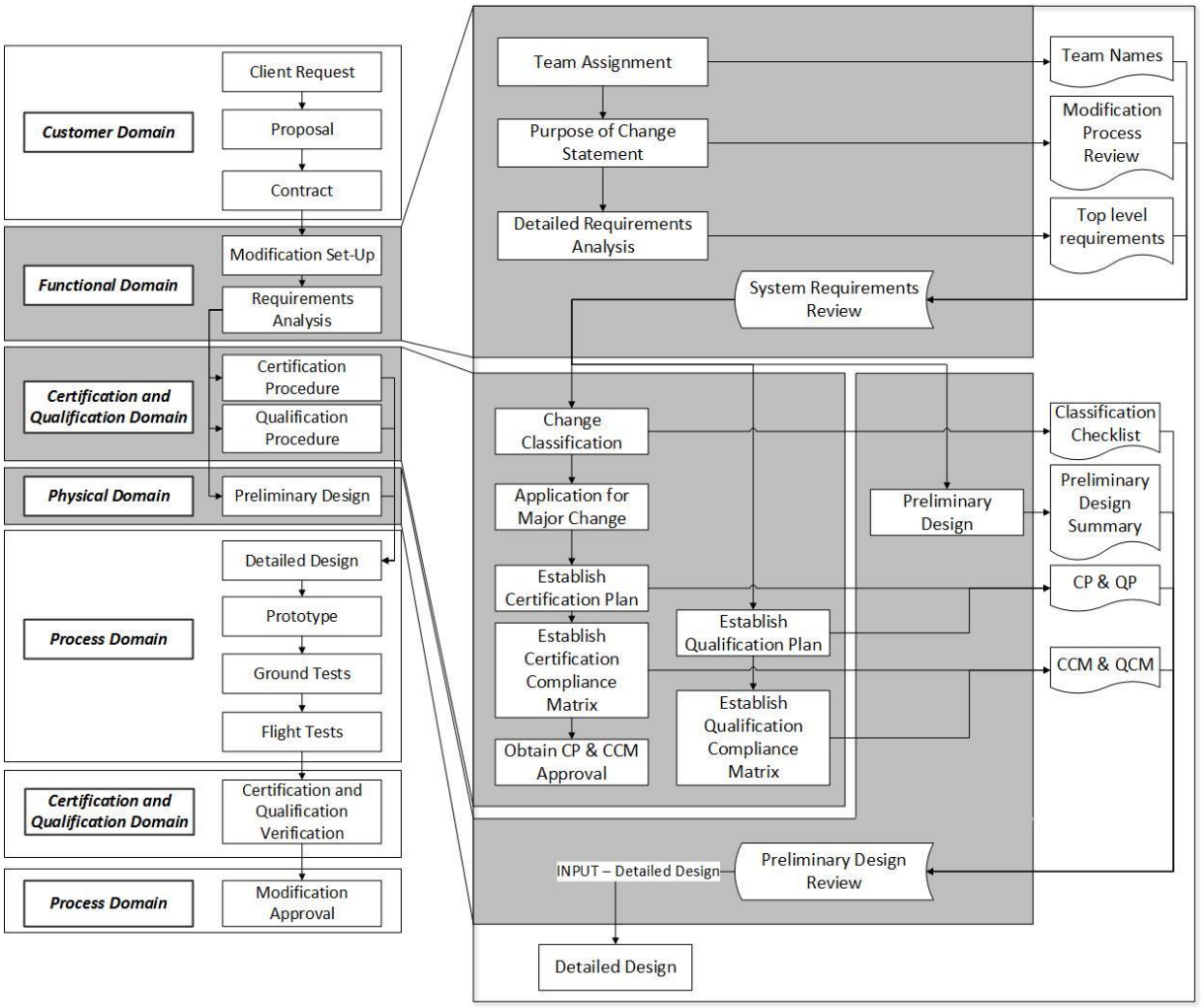

Figure 5.3 – Detailing of the relevant domains and sequence of stages for those domains.

Regarding each stage of the sequence in Figure 5.3, it is evident that some tasks are more relevant than others or even redundant, depending on the specific characteristics of the modification. It gives the freedom for the design team to adapt the methodology and the applicability of each stage to the specific modification in hands.

Table 5.2 – Description of FD, PhyD and CQD stages.

Stage	Description	Output
Team Assignment	Designating the people in charge of the design based on experience and qualification.	Team Names
Purpose of Change Statement	Stating the description and origin of change as well as the purpose for change.	Modification Process Review
Detailed Requirements Analysis	Defining general requirements from client, equipment and aircraft.	Top Level Requirements
Milestone – System Requirements Review	Assuring that the definition of the modification is complete. Relying on experience is essential for this task.	
Change Classification	Classifying as Major or Minor change.	Classification Checklist
Application For Major Change	Submitting the application for Major change to EASA.	
Establish Certification Plan	Identifying the documents and regulation necessary to perform the certification.	Certification Plan
Establish Certification Compliance Matrix	Identifying the specific requirements and the respective means of compliance to assure the certification.	Certification Compliance Matrix
Obtain CP & CCM Approval	Submitting CP and CCM to EASA and receive acceptance.	
Establish Qualification Plan	Identifying the documents and client's data necessary to perform the qualification.	Qualification Plan
Establish Qualification Compliance Matrix	Based on the client's needs, determining the means of complying with those needs	Qualification Compliance Matrix
Preliminary Design	Analyzing the sensor's possible locations, characteristics, structural link to the aircraft. Simulating the structural and aerodynamic impacts on the aircraft and sensor.	Preliminary Design Summary
Milestone – Preliminary Design Review	The client decides whether the Preliminary Design is acceptable or not. Checking for compliance with all previous requirements.	Necessary Requirements to start the Detail Design

The reviews – System Requirements and Preliminary Design – need the outputs of every stage as these are the summaries of each domain where the Design Team assesses whether the target for each stage is achieved or not.

As mentioned in Table 5.2, the Preliminary Design Review is necessary for the beginning of the Detailed Design Phase. The outcome of this last milestone may ease the workload of the entire project since it is a turning point that defines the selected system. Whether there is the

need to go back to the Physical Domain or not depends on the manufacturing viability of the system and that is the reason why one must always account for the experience of the Design Team on the Preliminary Design.

5.3 Preliminary design tasks for the methodology

In order to create a more in-depth methodology regarding the Preliminary Design with the purpose of expediting this procedure and preventing the appearance of flaws in the process, there is the need to define, for this particular modification, a set of tasks to perform. There is also the concern of creating an adjustable system, a modular group of tasks that a team may start regardless of the stage of the design process. This concern accounts for clients' requirements since on one case the client may need the designer to analyze and make every decision thus being the methodology necessary in its entire extent; on the other case the client may already know the model of the sensor, or the specific location to install the equipment, hence the designer only needs to perform a part of the methodology.

Table 5.3 describes the methodology created to aid the team in performing the preliminary design.

Table 5.3 – Preliminary design tasks.

Task	Output
1. Listing of possible sensor locations subject to further analysis	Aircraft location map
2. Location analysis and mapping of the viability of each one	Recommend locations
3. Aircraft modification for the chosen location – generating drafts of different solutions	Group of possible structural solutions
4. Selection of the most technically viable solution	Final solution proposal
5. Definition of development steps and physical requirements	Preliminary solution baseline
6. Preliminary solution development	Preliminary drawings and models
7. Analytic and numerical simulations	Preliminary analysis report
8. Development specification	Summary of the Preliminary design

As shown in Figure 5.1 there is interdependence between the Functional and the Physical domains. Regarding the tasks of Table 5.3 from the PhyD these must be performed considering functional foundations such as decision making criteria and priorities between

different criteria. These functional criteria serve as guidance to define the tasks of the Preliminary Design.

Whenever there is the need to make a decision in the Preliminary Design, that decision is based on functional criteria. Table 5.4 lists the link between a few functional requirements and the respective physical domain tasks.

Table 5.4 – Connection between Functional Domain and Physical Domain.

Functional Requirements	**Preliminary design Tasks**
• Sensor's Location: Definition of criteria to compare location	• Location analysis and mapping of the viability of each one
• Support Structure: Definition of criteria to analyze support solutions	• Selection of the most technically viable solution
• Structural needs: Parameters of material properties and geometry definition • Aerodynamic needs: Parameters of aerodynamic properties and geometry definition	• Definition of development steps and physical requirements • Analytic calculations and numerical simulations

6 Numerical modelling considerations

6.1 Experimental and computational approaches in the aircraft design industry

6.1.1 Available aerodynamic analysis methods

The aerodynamic influence on the turret's supporting structure is determined considering the airflow over the device with the goal of obtaining the pressure distribution over the turret and consequently, obtaining the aerodynamic force on the device. In order to predict the aerodynamic loads on the structure and eventual aeroelastic phenomena, the currently available tools for aerodynamic analysis are mainly grouped in two branches: Experimental testing which uses wind tunnel to simulate the real fluid flow over a scale model of the (airborne) part; and computational analysis, specifically known as Computational Fluid Dynamics (CFD), in which numerical methods and models are used to numerically solve the governing equations of fluid mechanics. Both methods are also able to consider turbulence, thermal and electric interactions and it now has the capacity of achieving high levels of accuracy.

Experimental methods

In order to predict the fluid flow behavior over a certain obstacle, mathematical equations were developed which represent an oversimplified (inviscid and non-turbulent) flow **[26]**. The need for a more reliable way of simulating fluid flow was clear. The test in wind tunnel which replicates the actual flow was thoroughly developed and it has been the most relevant tool for aerodynamics analysis. Frequently one relies on empirical results available in the literature to estimate the approximate values for some stages of the design.

Wind tunnel is a reliable means of simulating fluid flow in terms of fidelity of results, since it uses actual physical flow. It consists of a tunnel in which the object of analysis is placed, usually a scale model of a real sizable structure. An air flow is induced through the tunnel and therefore over the model and the aerodynamic parameters are then measured. Nevertheless, the wind tunnel testing has its drawbacks as well, which are the cost of the procedure, the long set-up time and the difficulty of assuring the similarity of all criteria simultaneously. Creating geometrically complex models of a product that may cause the experiment set-up to become unfeasible is a problem that also appears in wind tunnel testing. Likewise, the capacity of varying the configurations in the conceptual or preliminary design is limited **[27]**.

Computational methods

Computational methods started to prove useful for aerodynamics analysis since around 1960. Solving linear flow models for complex geometry became possible using panel methods (see more on panel methods in **[28]**; these were the first which were suitable for both subsonic and supersonic flows delivering acceptably accurate results. The development of the first methods for approaching the nonlinear equations of transonic flow took place in the early stages as well. The potential of computational methods was clear and sustained their improvement over time. The efforts during the following decades resulted in the capacity of accurately resolving shock waves and contact discontinuities in compressible flows as well as treating viscous flows and vorticity effects using computational methods. The simultaneous evolution of both numerical algorithms and computational capacity has allowed CFD tools to become faster, economical and more accurate, thus enabling CFD methods to be an essential tool for current aircraft design and aerodynamics analysis **[28]**.

Regarding complex geometries, the major concern is still the mesh generation. Techniques have been achieved based on mathematical transformations. In addition, in the last two decades, unstructured meshes have started to gain wide acceptance. Regardless of the fact that only since nearly 2000 unstructured meshes have started to be used in the industry, Euler and Navier-Stokes methods on this type of mesh have already been thoroughly developed since 1980 **[28]**.

6.1.2 Applicability of aerodynamic analysis methods in the aircraft design industry

During the distinct phases of design of an aircraft, there are tools which are better suited to each phase than the others. As for the preliminary design, the need is to have an approximate result for flight parameters to narrow down possibilities of configurations and more specifically, to create a prototype of the product; this first approach needs to be fast and economical. Regarding the detailed design, more accurate tools must be used to design components and specific characteristics of the production phase, which in turn compromise the duration and cost of the calculations. Nowadays, the cost of computational analysis is not as determining as it used to be since the once doubted enhanced computational capacity is a reality, the higher order computational schemes are not as avoided as they were, yet it is still a factor to decide whether to apply a lower order scheme on an initial phase or not **[27] [28]**.

Although still time consuming, CFD usage is now important for the aircraft industry and the main requirements for its application are: assured accuracy, acceptable computational costs and fast turn-around. Computational costs still hamper the effectiveness of modeling viscous flows with high Reynolds numbers even though there are some solutions with the purpose of reducing computational costs, such as reducing mesh requirements by using higher order

schemes, improving convergence to a steady state by using sophisticated acceleration methods, using parallel computing, among others. Another issue around the effectiveness of the use of CFD on industrial environment is the lack of proper interfaces between the CAD models and the CFD simulations. The geometry's smoothness and continuity requirements needed for flow simulation are occasionally not met **[27]**.

The computational capacity available nowadays is not unlimited. Despite the extreme breakthroughs known in this field in such short period of time, there remain many improvements to be achieved. Simulation of fluid flow requires simplification in order to make the simulation feasible. Real flow phenomena are complex due to nonlinearity or disparities of scales or many other reasons, which increases the amount of computational resources required for the simulation. Consequently, the decision depends on the amount of simplification to apply to which phenomenon or condition and one must ensure that the process remains viable and cost-effective. On a different note than the design phase – which implies a decision on the adequate method to the amount of detail needed for that phase – the decision referred above is on the relation between the resources available and the precise quality of the solution obtained. Figure 6.1 indicates the hierarchy of the models by level of simplification and contextualizes each model by its development decade. It represents the tradeoff between complexity and accuracy of flow simulation and computational resources (time and cost). Reynolds Averaged Navier-Stokes (RANS) models are the latest models represented on Figure 6.1, however, there are also recent methods available like Large Eddy Simulation (LES) and Direct Numerical Simulation (DNS); the former represents a more accurate way of treating flow separation than RANS whereas the latter is a RANS solver for turbulent flows in which velocity and pressure are known as a function of space and time (see more on **[29]**). LES is computationally highly demanding and thus there are not many studies applied to tridimensional geometries **[30]**.

One must mind that the complexity of the model does not necessarily mean better or worse results; as an example, inviscid models may provide accurate predictions of lift and drag for attached flow, yet when separation occurs (typically for high angles of attack or flow around bluff bodies) the model becomes ineffective. Hence, for a preliminary design where one just needs an approximate result for drag or lift of geometries with no separation, the inviscid model is the appropriate tool to use. This is one example in which the aerodynamicist must decide whether to use a simpler model or a more complex one **[28]**.

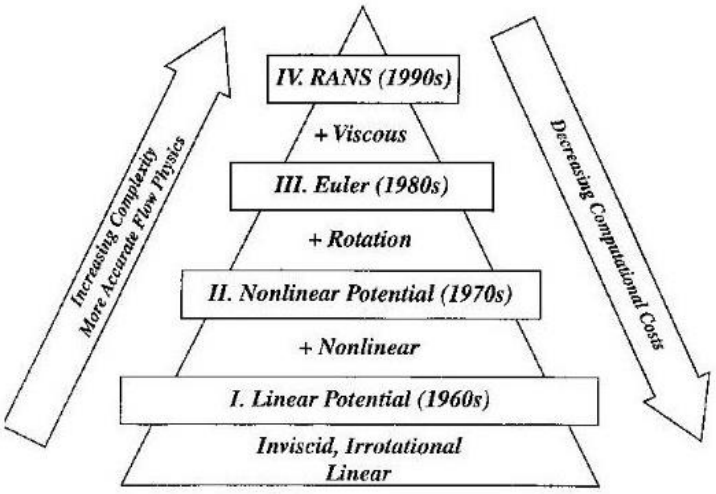

Figure 6.1 – Hierarchy of aerodynamic computational tools according to time of development **[28].**

Table 6.1 lists the major characteristics, advantages and disadvantages, of both tools for analysis: Experimental flow – Wind tunnel testing; Computational flow – CFD. Its content helps to understand the reason for the complementary usage of both tools and why wind tunnel testing is still key in the design process.

Table 6.1 – Comparison of each tool's characteristics **[27]**.

Experimental flow	Computational flow
Advantages • Known accuracy of measuring technique; • More quality of results due to real flow. Disadvantages • Scaled geometry; • Limited model flexibility; • Not always well-defined; • Low Reynolds number; • Time consuming set-up; • Increasing cost over time; • Questionable due to individual skill of aerodynamicist; • Blurry results sometimes;	Advantages • Real size geometry; • Unlimited parameter variations; • Known boundary conditions; • Real Reynolds number; • May have shorter response; • Decreasing cost over time; Disadvantages • Unknown errors; • Systematical errors due to equation usage; • Good reproducibility/objectivity; • Flow representation by model approximation; • Limited by computer capacity.

In this work the aerodynamic analysis of a flow over the turret is performed using CFD since it focuses on the preliminary stage of design; A comparison between meshes, solvers and other parameters is performed is order to optimize the CFD analysis. The decision is based on the tools' comparison showed above.

It is crucial to state that experimental analysis is not replaced by CFD; however this method becomes less used in the initial stages of design. The main purpose of wind tunnel testing is the validation of the computational algorithms and results. The complementary relation between CFD and wind tunnel allows the designer to get an optimum configuration faster and less costly maintaining the reliability of the results.

6.2 Discretization of the fluid flow governing equations

CFD is based on the governing equations of fluid dynamics – continuity, energy and momentum equations – which respectively state that the mass, energy and momentum are conserved. There are two ways of representing these equations: the integral form and the differential form. While in terms of fluid dynamics theory there is not much difference between the two, in terms of CFD algorithms the solutions are distinct **[31]**.

In order for the computers to be able to solve the equations, these must be discretized, which means transforming the problem's continuous domain into a discrete domain. Each

derivative or integral is approximated by differences, resulting in finite differences for the former and finite volumes for the latter **[31]**.

A method normally used to convert a scalar transport equation to an algebraic equation that can be solved numerically consists of integrating the transport equation about each control volume, yielding a discrete equation that expresses the conservation law on a control-volume basis **[32]**.

Several schemes of differencing the continuous governing equations into discrete domains have been developed. The following schemes are the ones which have revealed to be the most relevant for practical use through many years of CFD development. Table 6.2 lists five available differencing schemes and describes the theoretical basis of each one.

Intuitively, each scheme may be more suitable for a particular case than others; there is a reason for the development of each scheme. So there emerges the need to assess which is the most appropriate scheme to use in a particular study; the assessment is based on the trade-off between each scheme's properties and each scheme's computational demand.

The differencing schemes are assessed on the following criteria considering their ability to perform **[33]**:

- Conservativeness – The values for the transport variables must be conserved on the entire domain, hence the flux of a certain flow variable that leaves a control volume or cell must be equal to the flux that enters the adjacent cell.
- Boundedness – A general transport equation for the conservation of a flow variable has a source term which affects the property of boundedness of a scheme. Previous results from Scarborough (1958) have shown that a sufficient condition for a convergent iterative method may be represented according to the coefficients of the discretized equations.

  Boundedness is achieved by diagonal dominance **[33]**. Another requirement is that all coefficients of the discretized equations should have the same sign. If the scheme does not comply with the boundedness requirements, the solution may not converge at all or at least it may not be trustworthy.
- Transportiveness – Relation between the flow direction and the relative weight of convection and diffusion terms.
- Accuracy – The scheme must provide a stable solution; the amount of truncation error given by Taylor series which determines the level of approximation given by the scheme is also important. Whether the scheme is first order or second order (on the basis of the Taylor series truncation error) determines the level of approximation is better or worse.

Table 6.2 – Differencing schemes **[33]**.

Differencing Scheme	Description
Central	Considers the central node of the interval to be discretized. Hence it is unable to determine the direction of the flow.
Upwind	Takes into account the direction of the flow since it uses information from the anterior nodes. The solution at a given node is obtained considering the values of the upwind nodes.
Hybrid	For regimes with predominant diffusion, it applies the central scheme for resolving both diffusion and convection terms. For regimes with higher convection, it disregards the diffusion terms and uses upwind. Thus the hybrid scheme is only necessary for situations in which the nature of the flow – being it mostly diffusion in some regions and only convection in others – justifies the partial use of both central and upwind schemes.
Power-law	Fair alternative to hybrid scheme; applies polynomial expressions to evaluate the flow and it has demonstrated to be an accurate approximation to the real values of the transported variables.
QUICK	The Quadratic upstream interpolation for convective kinetics (QUICK) scheme applies a quadratic interpolation for cell face values using three-points upstream-weighted. The value for the transport variable is calculated with a quadratic function with two nodes – one on each side of the cell – and a node upstream the cell. The QUICK scheme is a second order accuracy scheme that provides more accurate results than central and hybrid schemes. It has the advantage of maintaining the upwind-weighted terms.

6.3 Turbulence modeling

Regarding viscosity and flow inertia there are two types of flow – laminar and turbulent; the first is characterized by a smooth motion of the fluid elements' and consequently, undisturbed path lines. Turbulent flow is defined by unpredictable and irregular motion of the elements. Figure 6.2 illustrates the difference between laminar and turbulent flows' path lines. The drag induced on a body is highly dependable on the type of flow since these contribute differently to the skin-friction drag and pressure drag components as well as to the separation point **[31]**.

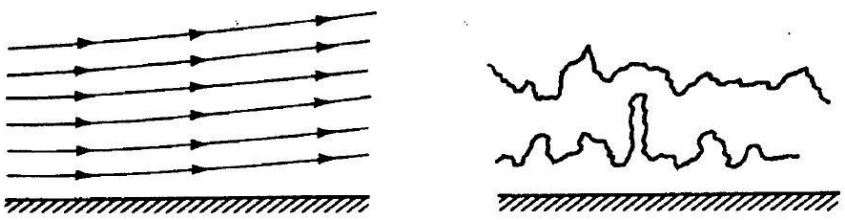

Figure 6.2 – Illustration of laminar flow regime path lines (left) and turbulent path lines (right) **[31]**.

Figure 6.3 illustrates the velocity profiles of two boundary layer flows developing over a flat plate; one being laminar and the other turbulent. The average flow velocity near the wall is larger than for the laminar flow. The skin-friction drag is directly related to the shear stress close to the wall, which in turn is directly proportional (for Newtonian fluids) to the velocity gradient at the wall; thus being evident that turbulent flows induce larger skin-friction drag than laminar flows **[31]**.

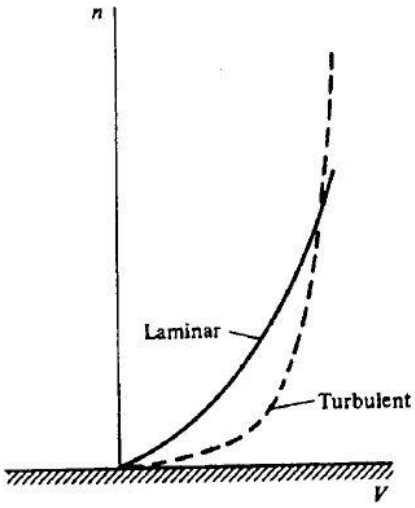

Figure 6.3 – Velocity profiles of laminar flow and turbulent flow near the wall **[31]**.

Regarding pressure drag, turbulent flows are more capable of resisting the effects of adverse pressure gradients due to their higher kinetic energy near the wall and then flow separation occurs more easily in the laminar regime than in turbulent flows. The resulting wake in turbulent flow separation is smaller than in laminar flows and the pressure drag is therefore, lower **[31]**.

Turbulence flows are characterized by fluctuating velocity fields. These variations also cause the momentum and energy values to vary. In order to make a numerical simulation feasible these small scale fluctuations are modelled by manipulating the Navier-Stokes equations (N-S equations). Averaging the instantaneous governing equations provides a computationally viable group of equations. Nevertheless, there is the need to resolve the additional unknown variables that are originated in the averaging process; these terms are solved using the turbulence models **[32]**. Figure 6.4 depicts the comparison between the real velocity contours of a flow and the RANS computational velocity contours of the same flow.

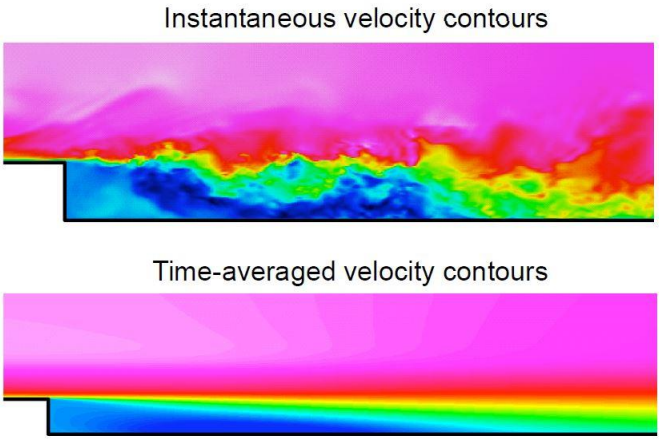

Figure 6.4 – Comparison between instantaneous and time-averaged velocity contours of a flow **[29]**.

In CFD, the preference for the usage of a certain turbulence model depends on several factors such as: the amount of accuracy needed, the available resources (time, manpower or funds) and others. It still does not exist an injective relation between the type of flow to be simulated and the turbulence model to be applied.

Since in this work the focus is on the preliminary design stage of the modification and time dependency is not considered, the approach only regards the RANS equations, despite RANS equations being also appropriate for transient state simulations. The LES approach or an eventual hybrid between the two is considered to be more suitable for the detailed design stage which involves more complex transient simulations; it introduces less error on the computation by resolving large eddies using the filtered N-S equations in an unsteady simulation. Instead of modeling time-averaged turbulence accounting for the small scales as RANS implements, LES models the eddies smaller than the filter on the N-S equations and computes the remaining large eddies. Despite having clear improvements in the accuracy of the results, LES needs to resolve turbulent eddies in both space and time domains which in turn also requires more demanding spatial and temporal discretizations; these factors cause the LES method to be avoided for a preliminary stage of design **[32]**.

There are already many studies using RANS turbulence models for both research and industrial purposes. The RANS equations model the full range of scales of turbulence and govern the transport of the averaged flow quantities. Table 6.3 lists the most used turbulence models to be used in RANS and ranks them by computational resources demand according to the “Ansys FLUENT” database. These models are two transport equation models except for Spalart-Allmaras that only has one transport equation which reduces its applicability to 3D flows or fine meshes. Its purpose is to have a low cost approximation for specific conditions of simulation.

Table 6.3 – RANS based turbulence models **[29]**.

Turbulence Model	Description
Spalart-Allmaras	• Main purpose: aerodynamic and turbomachinery applications with mild separation such as flows over airfoils or boundary-layer flows. Suitable for resolving adverse pressure gradients; • Regards a class of one-equation models where it is not necessary to calculate a length scale related to the local shear layer thickness; • Limitations: weak applicability to other types of complex engineering flows; not reliable to predict the decay of homogeneous, isotropic turbulence.
Standard k-ε	• Main purpose: it is robust and delivers reasonable accurate solutions for a wide range of applications; may be related to sub-models for resolving compressibility, natural convection, combustion and others; • Turbulence energy, k, has its own transport equation, which requires a dissipation rate, ε; dimensionally, the dissipation rate is related to the turbulence energy and a turbulence length scale; • Limitations: performs poorly for flows with larger pressure gradient, strong separation, high swirling component and large streamline curvature; for regions with large strain rate such as the one including a stagnation point, the production of k can become unphysical, resulting in inaccurate model predictions.
RNG k-ε	• The constants in the k-ε equations are derived analytically using renormalization group theory, contrarily to k-ε Standard which requires the model parameters to be calibrated by using data from benchmark experiments; • Performs better than k-ε Standard for more complex shear flows and flows with high strain rates, swirl and separation.
Realizable k-ε	• Dissipation rate equation is derived from the mean-square vorticity fluctuation, which is fundamentally different from the k-ε Standard; • Compared with the k-ε Standard, it is likely to provide superior performance for flows involving rotation, boundary layers under strong adverse pressure gradients, separation and recirculation.
Standard k-ω	• Similarly to k-ε Standard, k-ω Standard model is more versatile; there are also options for resolving specific phenomena such as compressibility effects, transitional flows and shear-flow corrections; • Better than k-ε Standard when boundary layer development is an important aspect of the flow under study. • Robust low-Reynold-number formulation down to the viscous sublayer;
SST k-ω	• The SST k-ω model uses a blending function to gradually transition from the k-ω standard model near the wall to a high-Reynolds-number version of the k-ε model in the outer portion of the boundary layer; • Contains a modified turbulent viscosity formulation to account for the transport effects of the principal turbulent shear stress; • SST turbulence model generally gives an accurate prediction of the onset and the size of separation under adverse pressure gradient.
Reynolds Stress	• Transport equations for the six distinct Reynolds stress components are derived by averaging the products of velocity fluctuations and Navier-Stokes equations. • Performs well for highly anisotropic, contrarily to the eddy viscosity models (all the above) which can only assume isotropic turbulence;

Another crucial aspect of modelling turbulence is the wall-fluid interface. Flows are affected by the presence of walls (or body surfaces); at the wall the condition of no-slip must be satisfied. Near the wall, the tangential and normal velocity fluctuations are reduced by viscous damping and kinematic blocking respectively whereas toward the outer part of the region, the turbulence intensifies by cause of the large gradients in mean velocity.

Since walls are one of the main causes for the occurrence of vorticity and turbulence, the inner region of the boundary layer must be carefully modelled in order to accurately compute the transport variables' values. Hence proper modelling of the near-wall region determines accurate computation of wall-bounded turbulent flows. Whereas k-ε, the RSM and the LES models are adequate for free stream flows, Spalart-Allmaras and k-w models consider the boundary layer effects more accurately. For the turbulence models which are not suitable for considering the viscous effects of the wall-flow interface one must include the boundary layer consideration through a near-wall treatment.

Typically, there are two ways of treating the near-wall region: wall functions and near-wall modelling. The first consists of disregarding (meshing-wise) the inner layer where the viscous effects are more noticeable and using a semi-empirical method of attaching the wall to the fully-turbulent region. The near-wall modelling resides on modelling the entire viscous region between the wall and the turbulent layer. Figure 6.5 represents both approaches to wall treatment.

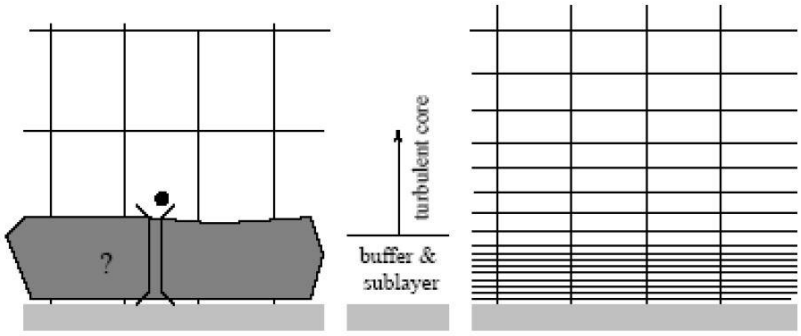

Figure 6.5 – Near-Wall treatments; Wall Function approach (left) and Near-Wall Model Approach (right) **[32]**.

The wall function approach is better suited for high Reynolds numbers flows in which the viscous effects are less relevant. This method tends to be economical, robust, fairly accurate and a valuable option for industrial usage. Although, one must mind that in this approach one does not resolve the viscous layer but assumes its effects are negligible or unvarying; this is not true for lower Reynolds numbers. These situations are better solved through near-wall modelling considering that the turbulence models are valid throughout the near-wall region **[32]**.

6.4 Meshing

In order to solve fluid dynamics equations computationally there is the need to discretize the domain in which these are applied. The numerical solvers can only calculate at discrete points and the results which are presented are from each of these discrete points. These discrete points are called nodes and these constitute the mesh. Hence the aerodynamicist faces a critical decision – where to compute the variables' values which means where to place the nodes. This decision has a crucial influence on the feasibility of the simulation since the quality of the mesh – being it coarse or too refined – may determine whether the computation is successful or not; the concern is not only around the amount of nodes on the mesh but also on its distribution along the places where it is predicted to occur complex phenomena **[28, 31]**.

Naturally, finer meshes provide more realistic results however one must compromise between mesh refinement and computational capacity; the aerodynamicist usually relies on experience in order to minimize the error in the results and consequent delays caused by poor meshing.

In order to maintain the problem tractable there must be a trade-off between mesh density, solution accuracy and simulation efficiency. Typically, regions of high parameter gradients (such as near shock waves, in boundary layer separation regions or near stagnation points) need mesh refinement so the numerical solver is able to successfully compute these gradients. Differently, regions with predictably invariable flow parameters are defined by coarser meshes to reduce unnecessary calculations **[28, 31]**.

6.4.1 Structured and unstructured meshes

There are mainly two types of meshes – structured and unstructured – which may have numerous configurations suitable for different purposes. Hybrid configurations using both types of mesh have also been developed with the objective of getting the benefits of each type of mesh.

Structured meshes consist of subdividing the domain into quadrilateral shapes in which a given node only connects four cells and never more than four. While this solution is simpler, economical and faster to use than others, it is also more suitable to straightforward cases in which there are not complex geometries involved. Using structured or block structured (separate structured meshes grouped in blocks in order to have more or less detail in certain regions) may induce issues such as decreased mesh quality, oversimplification of the geometry and deficient cell distribution in boundary areas; this last problem is, in many cases, the most significant one regarding cell count in a mesh **[34]**.

Within the group of structured meshes the principal alternatives are Cartesian meshes and Body-fitted meshes. Cartesian meshes are the first to be developed for CFD usage and are

still used for situations with simpler geometries; these meshes are only composed of non-deformed quadrilaterals which allow the use of high order discretization procedures, at the expense of a significant loss of accuracy in the treatment of boundary conditions at curved walls. Currently, with more capable processing tools, body-fitted meshes are used for almost every level of accuracy in results; these meshes allow the use of deformed quadrilaterals to fit curved surfaces in order to smooth the transition between the surface and the rest of the domain. Typical surface fitted meshes such as O-type and C-type are depicted in Figure 6.6.

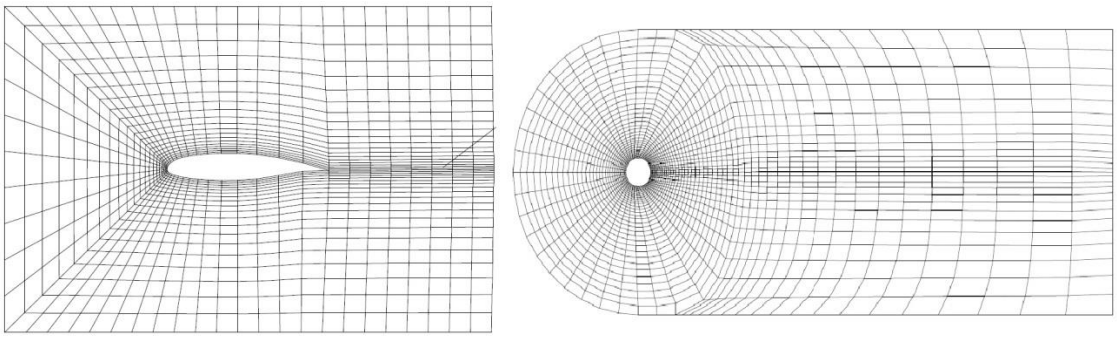

Figure 6.6 – Typical body-fitted quadrilateral meshes. (Left) C-type mesh; (Right) O-type mesh **[34]**.

Multiblock structured quadrilateral meshes, as seen on Figure 6.7, are used for cases in which there is only needed the adaptable nature of curved cells in certain near wall regions and in the rest of the domain, the cells can be non-deformed quadrilaterals.

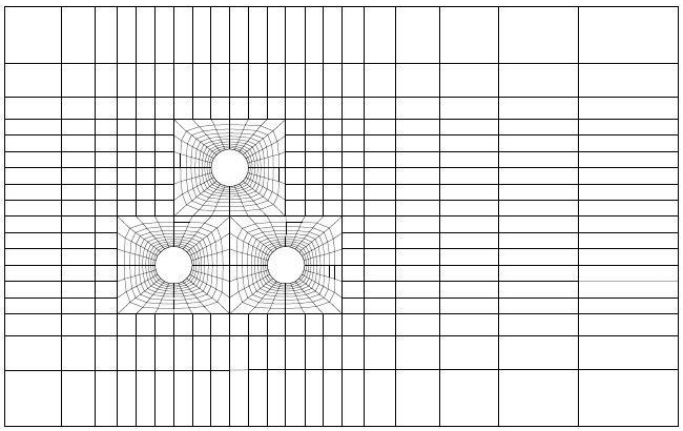

Figure 6.7 – Example of a multiblock mesh **[34]**.

The application of unstructured meshes is a more versatile method since it has the capacity to adapt to nearly every type of geometry. Its use speeds up the process of meshing, however, the algorithms must be capable of yielding the required accuracy on unstructured meshes. In addition, for the same problem and level of refinement, the amount of nodes required for unstructured meshes is far superior than for structured ones.

Figure 6.8 shows an example of a 3D unstructured mesh using tetrahedra (for the simpler case of 2D flow the mesh is typically composed of triangular shapes).

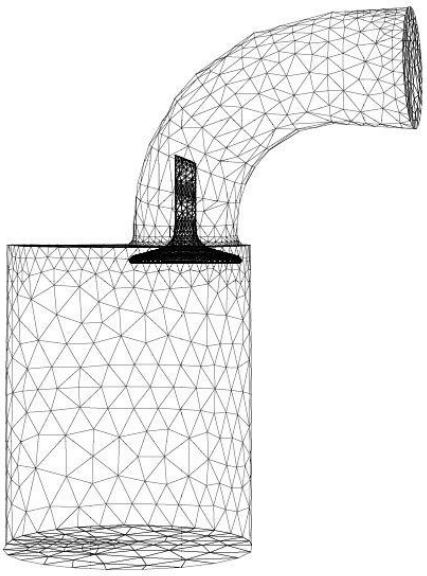

Figure 6.8 – Example of an unstructured tetrahedral mesh **[34]**.

6.4.2 Mesh quality

There are also some aspects to consider in order to obtain a suitable mesh, such as **[34]**:

- Density and distribution of the nodes on the mesh – higher node density and distribution contributes to better resolving of the critical features of the flow (separated regions, shear layers, boundary layers, shock waves and high turbulence regions for example)
- Mesh smoothness – regarding the discretization process, there appears an inevitable difference between the partial derivatives in the governing equations and their discrete approximations; that difference is the truncation error, which has to be minimized. Smooth transitions in cell volume from one cell to its adjacent results in lower truncation error.

Other issues that may reduce the accuracy of the numerical solution are related to cell shape **[34]**:

- Skewness – it is the difference between the shape of a cell and the shape of its equilateral equivalent in volume. Deformed cells provide less accuracy and may hamper the convergence to a solution. Acceptable values for skewness factor are a maximum below 0,95 and an average below 0,30.

- Aspect ratio – it measures the stretching of a cell. Usual values for the aspect ratio are below 5:1 for bulk flow and 10:1 for near-wall flow.

6.5 Solver

A fluid flow may be solved on a pressure-based or density-based algorithm. These methods were initially suited to treat specific flows; however reformulations on these methods have been carried out. This means an increase on each method's applicability to several cases.

From incompressible to mildly compressible flows, pressure-based solvers are preferred. On the other hand density-based solvers are more capable of resolving shock waves and highly compressible phenomena; hence these solvers are more suitable for high speed flows **[32]**.

Pressure-based algorithm

On this approach, the pressure field is obtained by solving a pressure equation which is achieved by manipulating the momentum and continuity equations. The velocity field's information is given by the momentum equations. To achieve solution convergence one must resort to an iterative process due to the nonlinearity nature of the governing equations and their interdependency; the solution is run through various iterations since the equations are coupled and cannot be computed in a straightforward manner.

There are two types of pressure-based algorithms – segregated and coupled – in which the equations are solved sequentially for the former and simultaneously for the latter. Figure 6.9 represents each algorithm's sequence in order to highlight the main difference in each method. In the segregated algorithm, the momentum equation is solved prior to the continuity equation whereas in the coupled algorithm both equations are solved simultaneously. Comparing both methods, the segregated one is less efficient in terms of iterations (more iterations are needed) however, it needs around half of the computer memory required by the coupled algorithm. Likewise many aspects related to computational practice aforementioned in this work, there must always be a decision which weighs the accuracy and efficiency of results and the computational efforts needed to achieve those results **[32]**.

Density-based algorithm

Similarly to the pressure-based approach, the density-based algorithm also relies on the momentum equations to resolve the velocity field. On the other hand, and contrarily to the other approach, the pressure field is obtained from the equation of state and the density field is only given by the continuity equation.

The density-based algorithm is a coupled method regarding the computation of the momentum, continuity and energy equations; other scalars that may be relevant for the solution

such as turbulence or radiation are solved segregated from the coupled set of equations. The way of solving the coupled set of equations may be either by coupled-explicit formulation or coupled-implicit formulation **[32]**.

This variation on the coupled formulation is related to linearization of the governing equations of the fluid flow. The density-based algorithm has the need to linearize the non-linear equations in order to obtain a system of equations for the dependent variables in each computational cell; an updated flow-field is then yield by the resultant linear system.

The explicit form is more desirable since it only bases the computation of an unknown variable value on existing values from other cells; it simplifies the computation by solving for all variables each cell independently. The implicit approach takes both known and unknown values from neighboring cells and computes the variables for all cells simultaneously; this increase in complexity affects the computational demand.

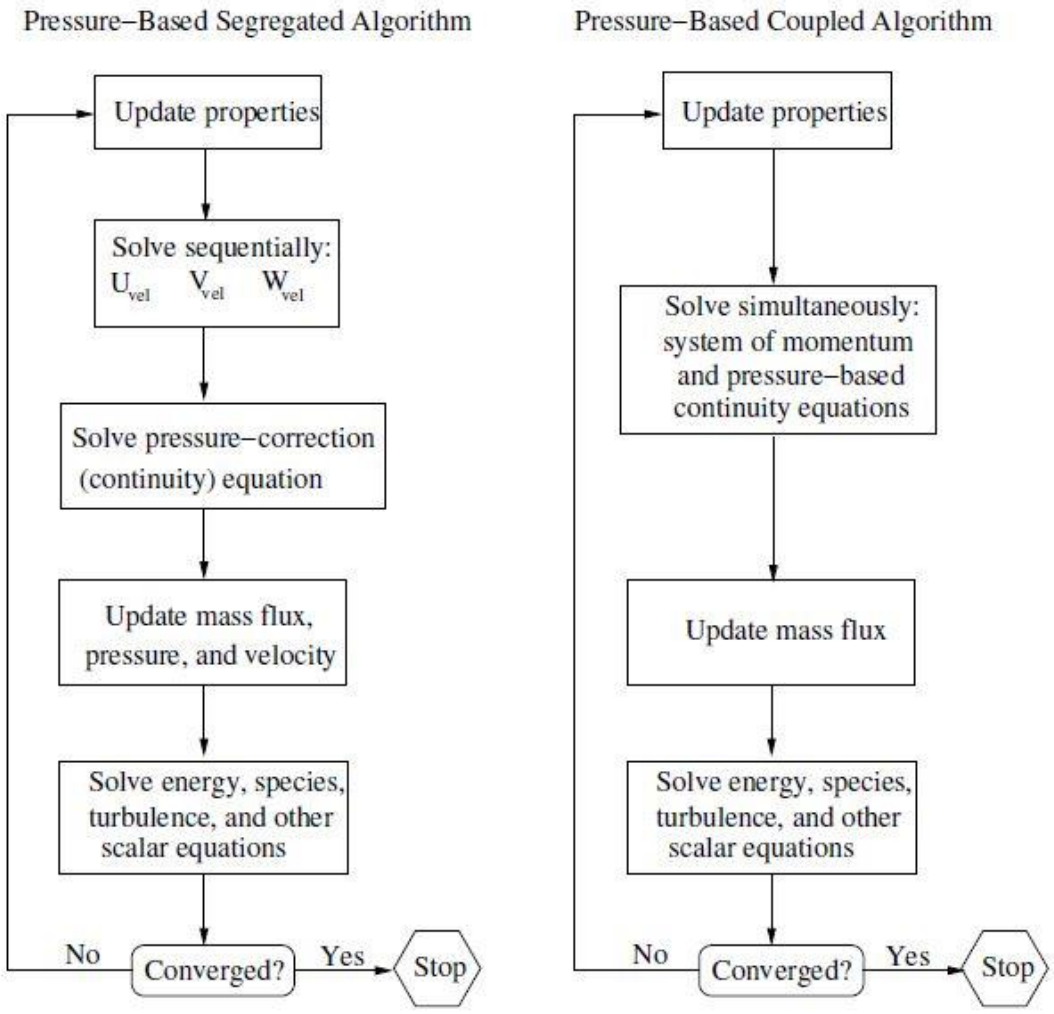

Figure 6.9 – Overview of the segregated pressure-based algorithm (left) and the coupled pressure-based algorithm (right) **[32]**.

6.6 Aerodynamic analysis methodology

6.6.1 Aerodynamic analysis methods for each design phase

Bearing in mind the required tradeoff between computational cost and accuracy of the solutions, Table 6.4 recommends the attribution of different methods – more or less complex methods – to each design phase.

Table 6.4 – Attribution of different aerodynamic analysis methods to each design phase.

Design phase	Aerodynamic analysis method	Main characteristics
Conceptual	Empiric	Estimation of the required parameters based on published data; the information obtained is limited to the conditions assumed on the others' experimental procedures.
Preliminary – static	CFD	Steady-state, 2D and 3D RANS simulations for simpler turbulence models and solver algorithms.
Preliminary – dynamic	CFD	Transient, 3D RANS simulations with vorticity and vibrations analysis for more robust turbulence models.
Detailed	CFD/Experimental	Combination of CFD simulations for LES or DNS with experimental results in wind tunnel tests and flight tests.

6.6.2 Guidelines for the aerodynamic analysis

In this chapter it is also defined the approach on the preliminary analysis report from Table 5.3. This methodology has the purpose of specifying a set of tasks for the CFD analysis by addressing the most relevant issues to consider for the installation of a multi-sensor turret on a Lockheed Martin C-130. The left column of Table 6.5 regards a general structure of a CFD analysis whereas the right column relates the specifics for the intended modification. The information present on the following table is a group of recommendations based on chapters 5 and 6, as well as on engineering judgement.

Table 6.5 – Specific recommendations on the CFD analysis for the preliminary design phase.

CFD analysis stage	Specification
Research of previous work	It is crucial to know the amount of development that has been done on the subject. This sets the ground for the analysis and the quality of the information available determines the extent of work which is feasible by computational analysis. Experimental results for velocity conditions of Mach higher than 0,4 Ma were not found. The results found only give aerodynamic information regarding drag coefficients, pressure fields around the turret, separation points and the type of vortices that appear; information regarding transient flow related to frequencies would be very useful. Although it is out of the scope of this work, there are found several documents that report the influence of the airflow on the optical performance of the sensors.
Modelling considerations	At this stage it must be defined the amount of simplification that is applied on the analysis; since the case is a relatively simple external flow, there are a few considerations to be made that do not affect the final solution. For the case of the Lockheed Martin C-130 flight conditions there is compressible flow, however, this aircraft does not reach any transonic regime. This study does not need to account for heat transfers or gravity. Geometrically, there is not an undoubtful way of knowing how much detail is enough, yet more detail typically deliver more real solutions.
Meshing	It is recommended to create a few configurationally different meshes to assess its quality. Still, an acceptable type of mesh is presented in this study. As any external flow on a plate, there is the concern of accounting for a refined boundary layer. An unstructured mesh may be a viable option for this flow since the spherical surface of the turret must adapt to the outer domain boundaries which are rectangular; the unstructured mesh may ease the geometrical adaptation, yet it may hamper the convergence and it augments the computational effort.
Defining evaluation information	Considering a steady-state simulation, the relevant information is based on the drag and pressure coefficients. The parametric study for different velocities implies a relation to velocity such as Mach number or Reynolds number. The Strouhal number is important for transient flow in order to assess the vorticity frequency.
Performing the simulations	Since the simulations are an iterative process, one starts from simpler methods and goes gradually for more complex algorithms. The chapter of the case study describes the recommended methods to perform the simulations on Table 7.8.
Method validation	At this stage, from the comparison between the experimental results and the obtained results one may identify the relation between the simulations and the reality. It is also important to assure that the behavior of the results obtained and not only the final values are congruent with the trends of the experimental plots.
Evaluation of the influence of the results	This stage has not any specific characteristic apart from the transport of these results to the structural analysis. It is crucial to be aware of how the aerodynamic analysis, and its success, influences the following phases of the design of the modification.
Assessment of compliance	There is the need to check if the results and methods applied comply with the regulations, being these external (safety agencies or clients' requirements) or internal (DOA's imposed procedures).

7 Case study

7.1 Overview of the aerodynamic analysis

In this chapter the aerodynamic impact is evaluated for the chosen characteristics such as the airplane model, the turret model and the location in which it is to be installed. The amount of impact is represented by the drag force on the turret due to the flow.

First, a series of validation simulations is required in order to validate the computational algorithm. As found in the literature, the majority of the experimental analyses are run for $Re = 3 \times 10^5$ and $Re = 3 \times 10^6$, so a series of simulations are performed for this range of Re numbers by varying the velocity of the flow.

Once validated, the intent is to do a general parametric study for a range of Re numbers that can be extrapolated to other airplanes, locations or even turret models. In this way the present work suits not only this particular case but many other possible scenarios.

There is also the need to provide information on which are the most suited parameters to set up the simulations. Comparisons between parameters are made constantly bearing in mind the tradeoff between the amount of effort and the precision and quality of the results.

7.2 Previous work on aerodynamics of turrets

To expedite the validation process, there is the need to find experimental results that can be applied to the present problem. This is important so there is no need to run a validation simulation for a simpler geometry or characteristics that represent a case that varies significantly from the one in analysis. A usual path to take for the case of a turret is to validate the algorithm with a simulation of the flow around a sphere.

For this case there are experimental results **[35, 36]** for the flow around a turret, even though the geometry might not be exactly the same for **[35]** as the one in study, it is similar and represents a fair approach considering the amount of possible error involved.

Wind tunnel testing results from **[35]** are visible in Figure 7.1 which is the plot of drag coefficient relative to a range of Re numbers from $Re = 3 \times 10^5$ and $Re = 9 \times 10^5$. The turret has a 0,23 m diameter sphere blended to a 0,20 m diameter cylindrical base.

Experimental results from **[36]** are presented on a plot of pressure coefficient along the centerline of the turret on the direction of the flow. Figure 7.2 represents the pressure distribution on the turret for a range of Ma values from Ma=0,3 to Ma=0,45. In this study, the analysis of the drag effects on the structure of the turret is done with the aid of these two types

of plots, a drag coefficient vs Re number plot and a pressure coefficient vs the degree coordinate along the centerline of the turret.

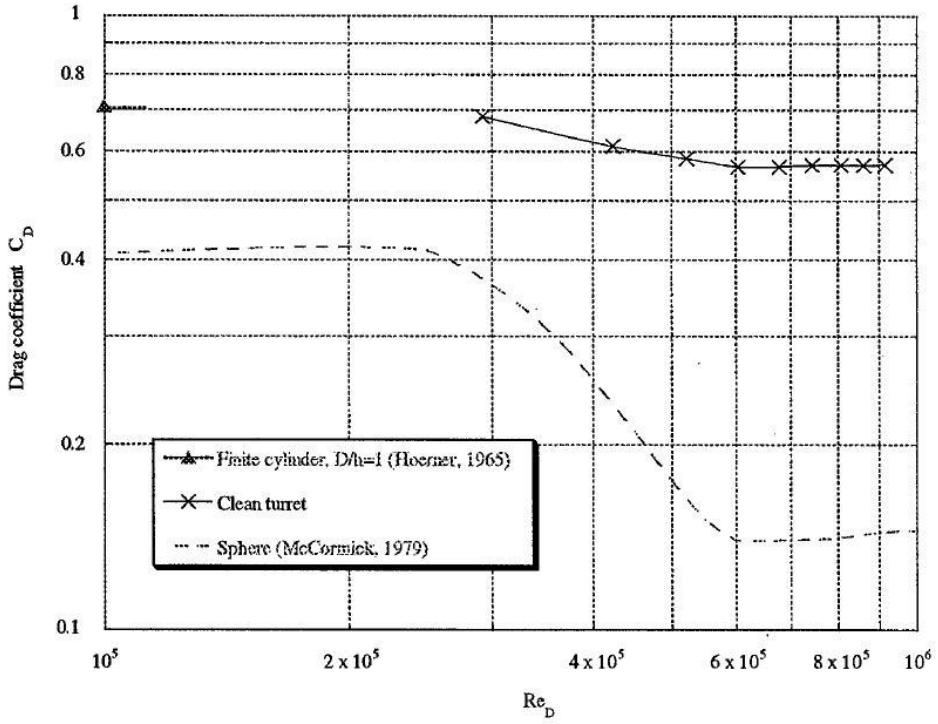

Figure 7.1 – Drag coefficient comparison **[35]**.

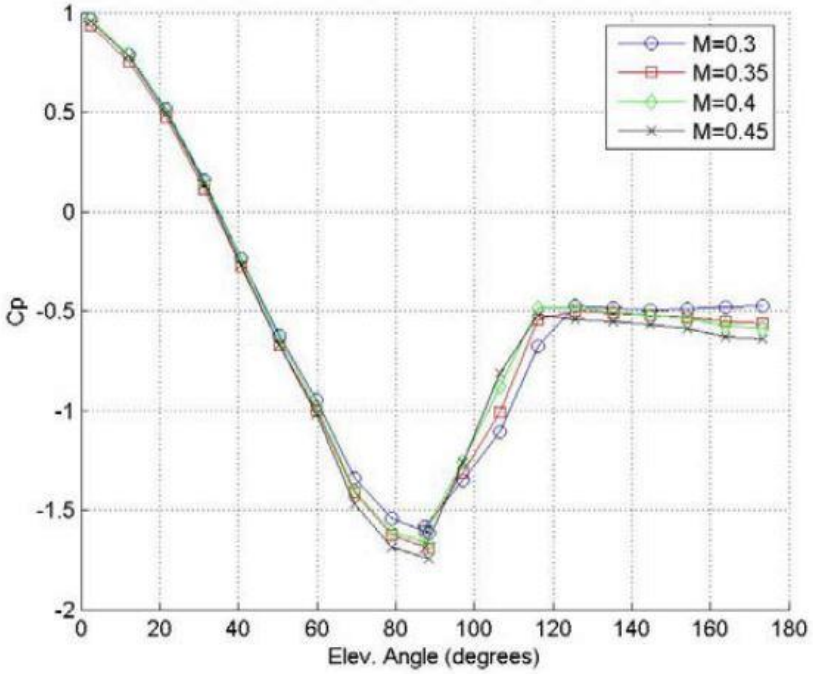

Figure 7.2 – Static pressures along the centerline of the turret. **[36]**.

The primary amount of recent work on this subject is based on computational fluid dynamics, due to the high capacity of current computers. From **[31, 37-39]** one may notice various differences regarding the exact values of drag and pressure coefficients, however, the trend of the coefficients' variation stays the same and accordingly to the experimental results. A valid drag coefficient may be overestimated by choosing to consider the highest value calculated. The divergence between the results is absorbed by the safety factor when considering the structural influence of the airflow over the turret.

7.3 Theory of the case study

Since the objective of the present stage of the study is to analyze the aerodynamic impact on the turret's structure as well as on the airframe, there is the need to understand the underlying principles of drag. Drag is defined as the component of the aerodynamic force acting on a body which direction is parallel to the freestream velocity. It is mainly composed of two components: pressure drag and skin friction drag.

Pressure drag results from forces acting normal to the surface of the body whereas skin friction drag is due to the shear stresses acting tangentially to the surface of the body. Typically, skin friction or viscous drag dominated flows are associated to streamlined shaped bodies whereas bluff bodies are related to pressure drag dominance in a flow.

The present study regards a bluff body in which pressure drag represents around 99% of the total drag. The main cause of pressure drag is the boundary layer separation and the resulting wake aft of the body – Figure 7.3. Separation results from an adverse pressure gradient which generates a turbulent wake. The flow detaches from the body whenever the pressure gradient is severe enough. Drag force is produced by the pressure differential between upstream of the turret and downstream of the turret. Since drag is mainly caused by the turbulent wake, there is a direct proportionality between the size of the wake and the amount of drag force applied to the turret. Contrarily to laminar wakes, turbulent wakes tend to appear further downstream due to the higher kinetic energy it has, which forces the separation from the boundary layer to occur later **[31]**.

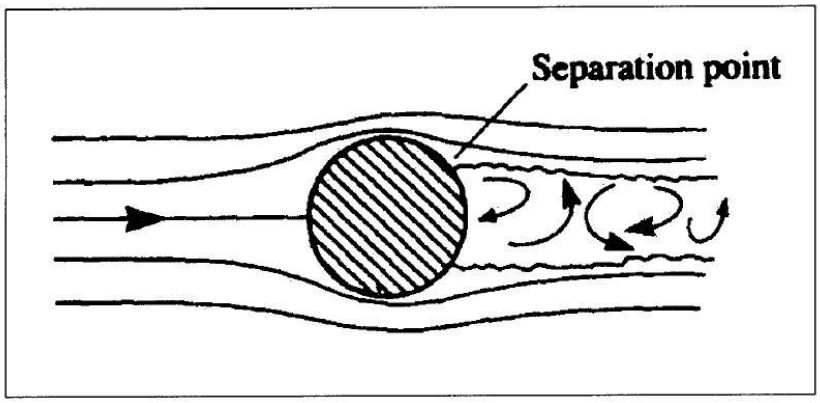

Figure 7.3 – Low pressure wake behind cylinder due to boundary layer detachment **[31]**.

Another relevant phenomenon that generates drag force is vortex shedding; vortices appear in a more visible way on flows over bluff bodies. For tridimensional flows, vortices can be formed over multiple axis of rotation which significantly increases the flow complexity; Figure 7.4 depicts the predictable vortex occurrence on a flow around a turret. For higher Re numbers, the vortex starts to give place to an irregular and intractable turbulent wake. This interaction between the turbulent wake and the vorticity contribute to an even lower pressure zone aft of the body, generating in turn, more drag. Due to computational limitations and the need to simulate transient flows, the vorticity is not considered in the present study; the focus is on the primary cause of drag forces which is pressure drag.

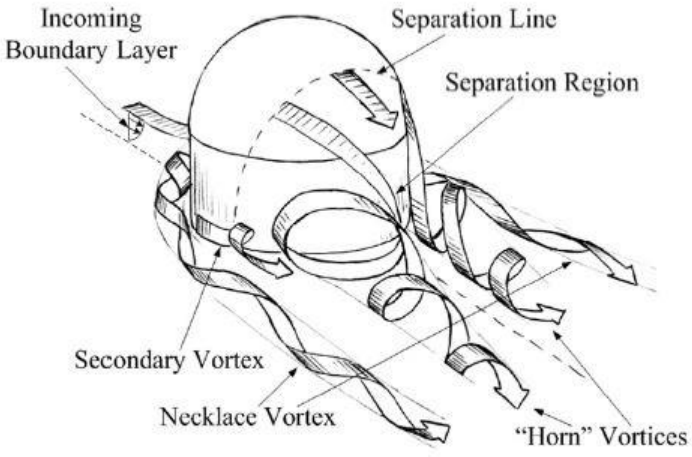

Figure 7.4 – Schematic of the vortices on a flow around a turret **[37]**.

7.4 Modeling considerations and geometries

The geometry and the setup of the study are based on several considerations, such as:

- The turret and its surroundings are symmetric about xOy plane (Figure 7.5);

- The turret's window is conformal to the hemisphere, which implies that there are not any vertices or edges on the surface of the turret;
- The surface is smooth with no roughness;
- The surroundings of the turret do not have any obstacles that may influence the aerodynamics of the turret;
- The location is as selected, at the nose of the aircraft;
- The flight conditions are assumed to not allow the accumulation of enough snow or dust that may change the aerodynamics of the turret;
- Density and temperature values are based on the altitude of the international standard atmosphere;
- Since air has negligible weight, the effect of gravity is neglected;
- Heat transfers are not considered in the present study.

As represented on Figure 7.5, the configuration of the simulation is a turret with a diameter D, on a flat surface, similarly to other studies on the subject, such as [31, 35]. The geometry of the study is thereby simplified regarding the actual geometry of the airplane and the turret's location on the airplane. In addition, the configuration analyzed is the base of the turret being coplanar to the flat surface. This is due to the consideration that the flat surface configuration is the most adverse case in terms of drag (the case in which the airflow has the direction x of figure Figure 7.5) since an inclination angle between the base of the turret and the surface softens the behavior of the streamlines (exemplified on Figure 7.6); the streamlines get less deflected in a case where the direction of the flow is not normal to the turret (different direction than x). In theory, if the flow is less obstructed there is a lower variation of pressure, which induces less drag.

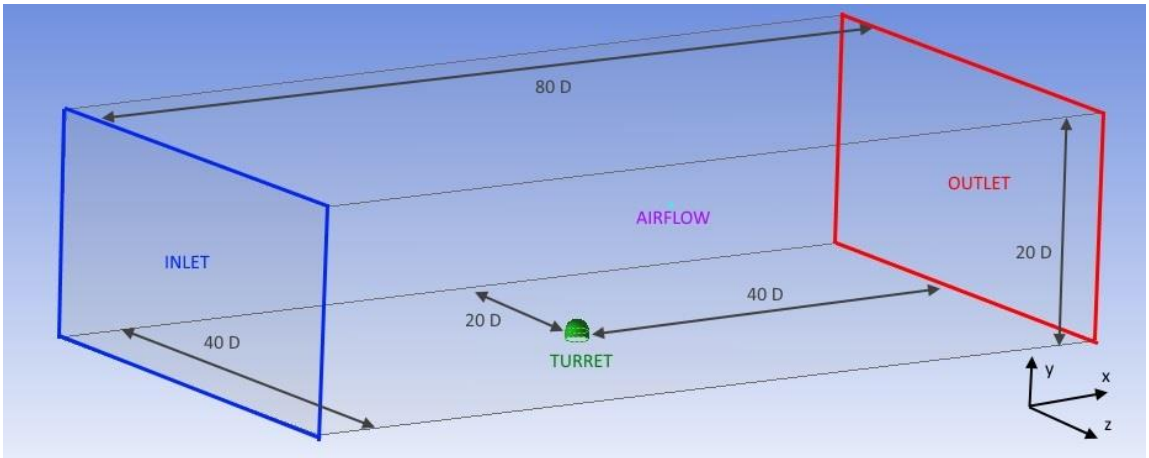

Figure 7.5 – Simulation's geometry configuration.

On Figure 7.5 it is represented the whole domain of the simulation, however only the refined mesh (discussed later) has these dimensions. The dimensions of the 2D mesh and the simpler 3D mesh are represented in their scaled images.

Figure 7.6 represents the comparison between the behavior of a streamline for the simplified configuration used in the simulations, a) – and the real configuration, b). Regarding configuration b) one may notice that since there is no boundary under the flow that could impose an acceleration of the air, the airflow only has a different direction, not a different velocity. This change in the direction of the airflow creates a smaller projected area of the turret which represents a reduction of the drag force. As Figure 7.6 shows, the deflection of the streamlines is smoother for the real configuration. In this way the study is being conservative on simplifying from configuration b) to a).

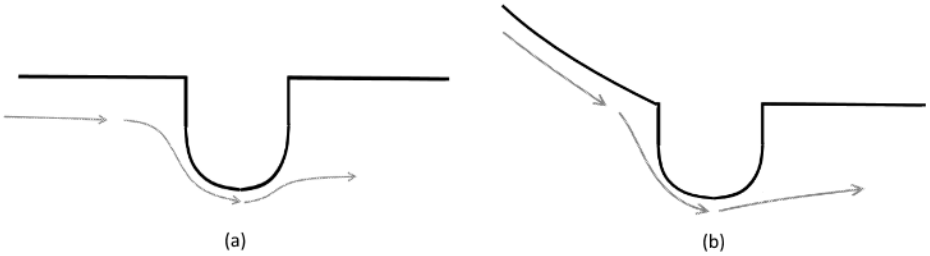

Figure 7.6 – Comparison between the flow over two configurations of turret. (a) simplified configuration; (b) real configuration.

Experimental tests for this type of study are carried out in wind tunnels. As referred in Chapter 6, CFD analysis allows one to simulate a non-obstructed airflow. The walls of a wind tunnel influence the airflow resulting in loss of accuracy in results. The geometry created in the present study is a virtual wind tunnel but with enough distance between boundaries to cancel the influence of these boundaries on the flow.

7.5 Mesh generation

In regard to mesh generation, there is the need to follow a gradual path through the relation precision vs time consumption, hence the obtained results are always useful to the analysis. Three meshes are created, one 2D and two 3D configurations. This allows one to compare the 2D and 3D simulation results and justify the need for the tridimensional analysis. In order to optimize time and enable more extensiveness of the 3D study, there are created two meshes: A simpler one with fewer elements to allow a first expedite approach to the simulation; a final and more refined mesh to assure higher results' precision, even though one might need a more refined mesh in order to identify the separation point (flows over spherical or similar shapes require a much more refined mesh since the separation point is much harder to

identify). Therefore, the mesh generation process may be divided into the mentioned three stages, the two-dimensional mesh and the tridimensional simpler first approach and final precision approach.

With the goal of simplifying the mesh and guaranteeing the best element quality, the meshes created are all structured with mapping method, which is only possible due to the basic geometries adopted. The Map type of mesh imposes that a single node can only separate 4 cells in the 2D case (see more on the mapping method in **[40]**). Regardless, for the present geometry there is a concern which is the interface between the rectangular domain required to enable mapped meshing and the circular surface of the turret. There must be assured a smooth transition between the geometries of each cell in order to prevent divergence and to improve precision in the results. Other methods such as Pave type of mesh are usually applied in complex geometries that create an irregular domain to be discretized by rectangles.

Regarding the 2D mesh, the amount of simplification is such that the geometry being studied is actually a cylinder since the projection of a sphere in a plane is a circle and creating the infinite length normal to the plane generates a cylinder. Figure 7.7**,** Figure 7.8 and Figure 7.9 represent the 2D mesh used for the simulation.

One can see in Figure 7.7 the full extent of the mesh, allowing enough distance between the inlet and outlet surfaces to the turret; this prevents the appearance of inaccuracies since there is enough space for the flow to normalize until it reaches the outlet boundary.

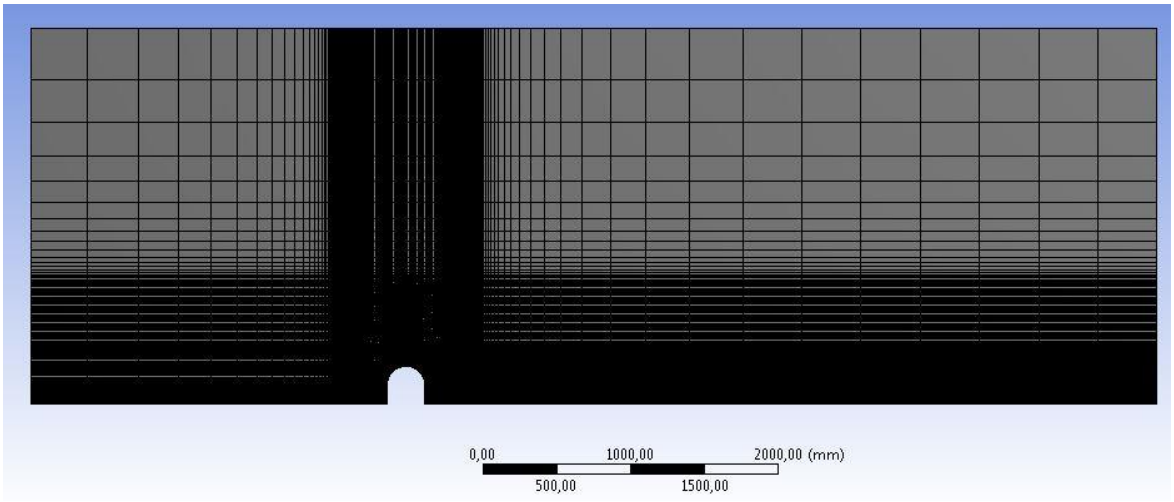

Figure 7.7 – View of the full domain of the 2D Mesh.

Figure 7.8 depicts a closer look on the surroundings of the turret surface; it also shows in green how paving method is carefully imposed in the geometry so that the size transition between cells stays as smooth as possible. One may notice the paving method on the green region since there is one node in which 5 elements meet (see more one paving method in **[41]**).

Regarding the quality of the mesh, one needs to mind that the CFD analysis is not the only concern of the study so the time spent in each stage of the process is shorter than in a fully extensive CFD study. Thus both 2D and 3D meshes are considered of an acceptable quality.

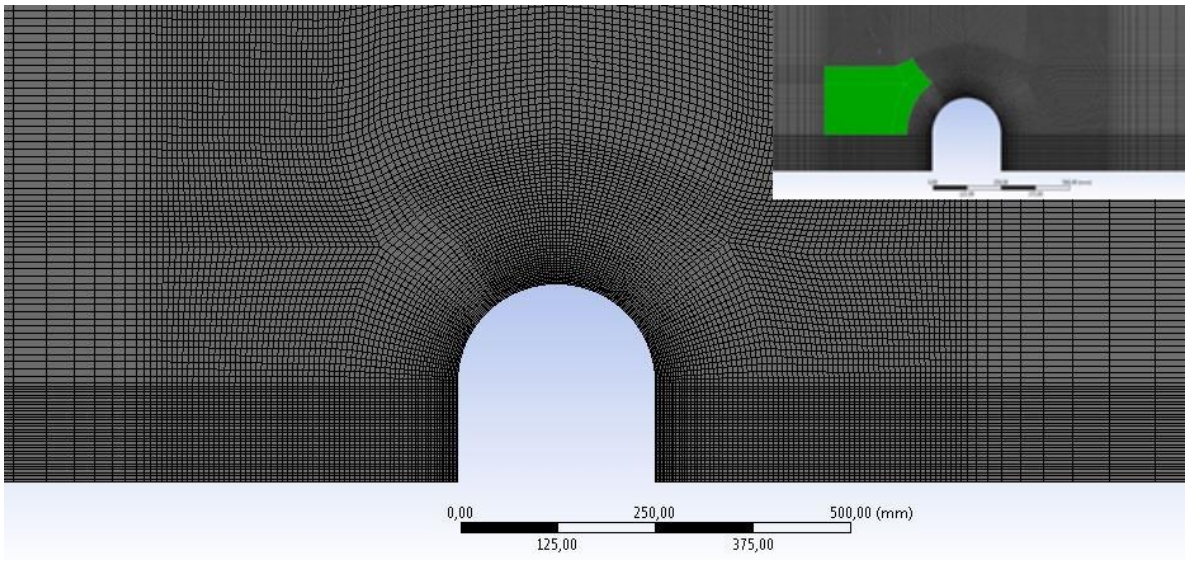

Figure 7.8 – View of the region of interest of the 2D Mesh.

In Figure 7.9 it is possible to see the boundary layer defined by smaller elements closer to the surfaces which get gradually larger as these are further away from the walls. The reason to detail the boundary layer is the presence of gradients; the parameters' variations on the boundary layer are much swifter than the variations in the freestream zone.

From Figure 7.11 to Figure 7.13 it is possible to see the first simpler 3D mesh and from Figure 7.15 to Figure 7.21 the refined final 3D mesh. In order to allow a proper comparison, Table 7.1 indicates the properties of cells on each of the meshes.

It is important to state that comparing the properties of each mesh, it is clear that the 2D mesh has higher quality due to the minimum orthogonal quality being considerably higher than the ones of the 3D meshes. It is easier to obtain less orthogonal disparities between cells in 2D than in 3D meshes. Other crucial factor that hampers the quality of these particular 3D meshes is the interface between the curvilinear surface of the turret and the planes that define the boundaries of the domain; there is always the need to distort the elements in order to maintain the mapping method throughout the whole domain. In spite of this low minimum orthogonal quality, Figure 7.9 demonstrates that for the regions that contribute for the drag coefficient the most, the orthogonal quality is reasonably acceptable. Regarding the aspect ratio, a refined mesh should have lower aspect ratio than a simpler one. The short time available leads to a disregard for the element growth in some regions of the domain. Again, like the orthogonal quality, for the regions of most interest it is guaranteed a fairly good quality of mesh. Concerning

the number of elements, as good practice there should be at least an intermediate mesh between the 35,000 one and the 130,000 one.

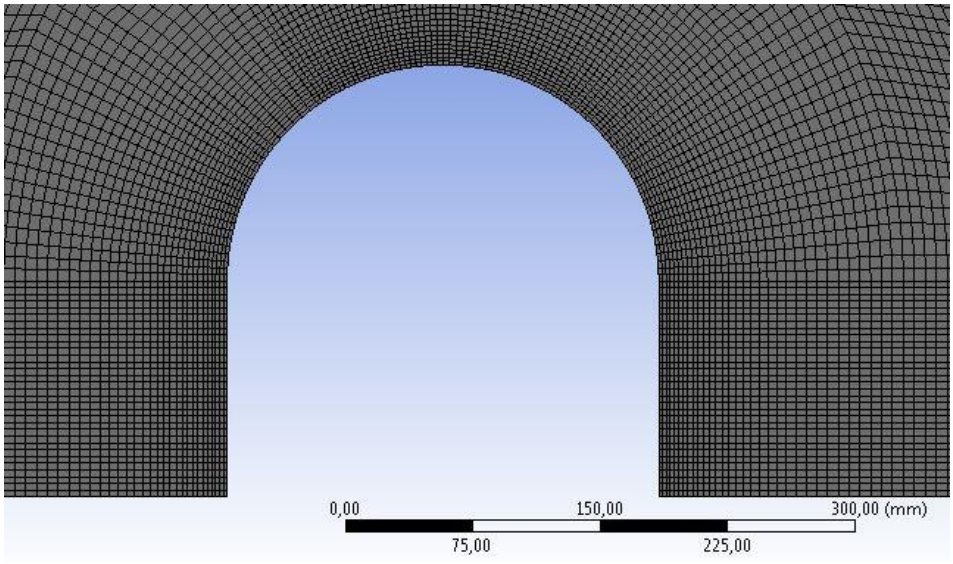

Figure 7.9 – View of the turret's boundary layer of the 2D Mesh.

Table 7.1 – Number of elements of each mesh

Mesh Designation	Number of elements	Max. Aspect Ratio	Min. Orthogonal quality
2D Mesh	24,805	10,08	0,809
3D Simpler Mesh	35,420	4,63	0,336
3D Refined Mesh	130,000	9,46	0,345

In order to apply mapping method to the entire domain, the elements on a certain surface must meet the same amount of elements on the opposite surface. As mentioned before, the curvilinear surface of the turret set a problem in the creation of the mesh. Since there is the need for more detail closer to the turret, the concentration of elements must be higher on that region. This distorts the elements as it is visible on Figure 7.10 and Figure 7.11.

In Figure 7.11 it is also possible to see how the mesh is structured. The mesh is composed of various blocks. These blocks have the purpose of giving different properties in different regions of the domain; one may see the difference in the amount of elements between the orange and blue blocks and the ones below these. Even though these blocks allow a specific characteristic – being it the growth factor of element size along a surface or even the amount of elements – on a region of the domain, it is clear by looking at the interfaces between the orange-top green and blue-top green blocks that there is a high aspect ratio that is not successfully avoided.

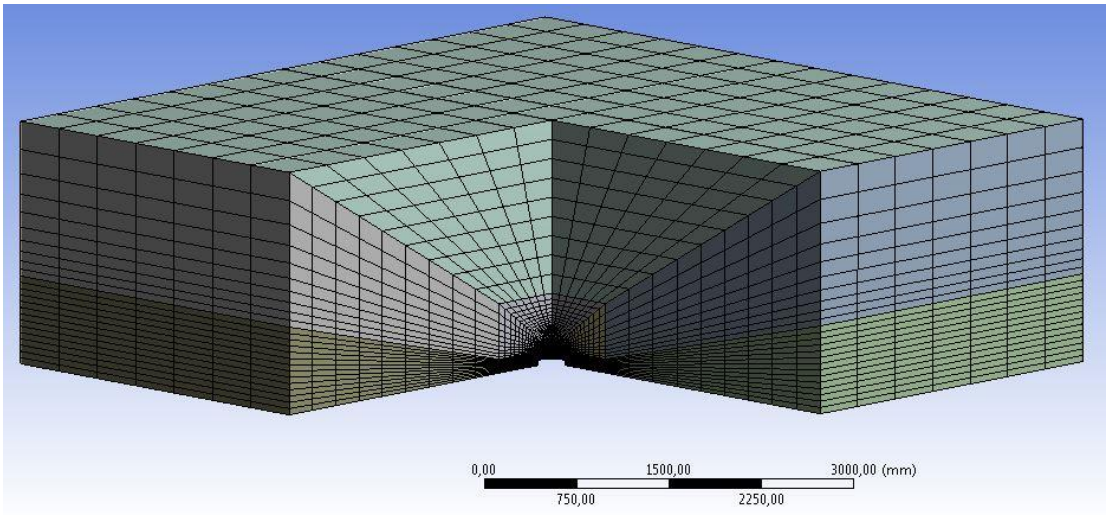

Figure 7.10 – View of the full domain of the 3D Simpler Mesh with a cutout to the center of the turret.

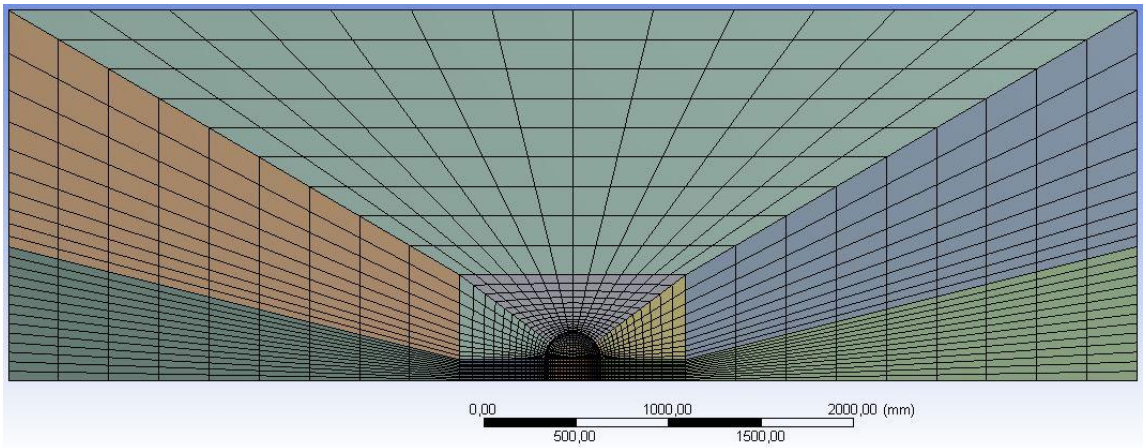

Figure 7.11 – View of the xOy plane of the 3D Simpler Mesh.

In Figure 7.12 one may see a close up to the region of the turret; it is noticeable the boundary layer on the turret. As mentioned for Figure 7.11 one can also see the distortion of the elements due to the geometric divergence from the turret's surface to the outer surfaces of the blocks.

There is the concern to maintain the region near the wall and the turret (blue and dark green blocks on Figure 7.12) well defined so there is no divergence on those elements. This is only until a certain distance from the turret. From that certain distance, new blocks – visible above on Figure 7.11 – allow a transition for a diverging trend of elements that until that point are straight (blue and dark green blocks on Figure 7.12).

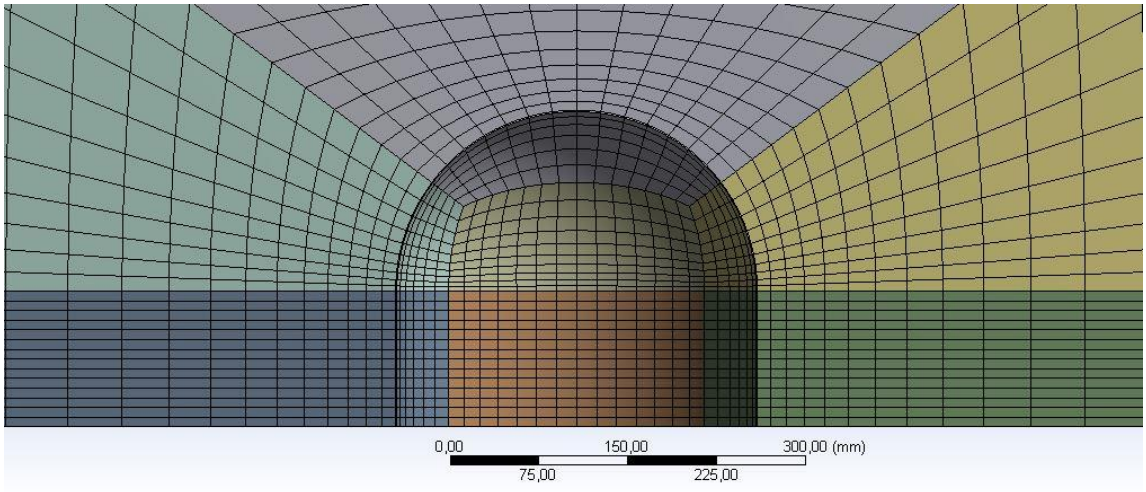

Figure 7.12 – View of the turret on the xOy plane of the 3D Simpler Mesh.

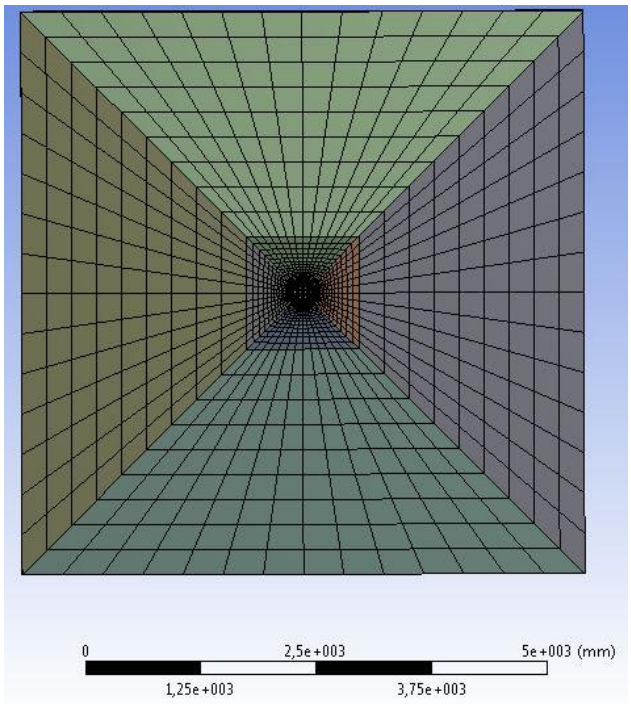

Figure 7.13 – Bottom view of the domain on the base plane of the 3D Simpler Mesh.

Regarding Figure 7.13 and Figure 7.14 it is clear the adaptation between the circular perimeter of the turret and the four sides of the rectangle; the elements are distorted similarly to what is mentioned above. These figures show the bottom view of the domain where it is also noticeable the high aspect ratio in the diagonal interfaces between the blocks. The number of divisions should be increased to obtain more cube shaped elements which would soften the transition between elements from different blocks.

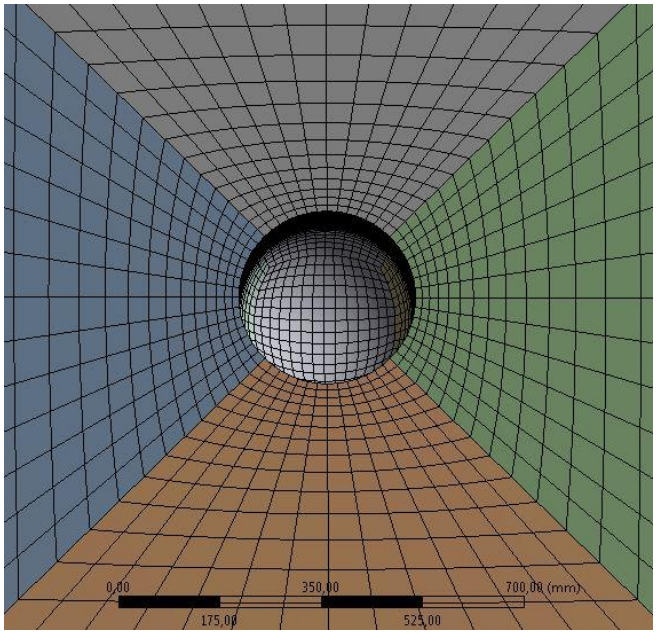

Figure 7.14 – Bottom view of the turret on the base plane of the 3D Simpler Mesh.

The main objective of refining a certain mesh is to improve its quality and subsequent accuracy of the results. This forces an increase in computational complexity so it is always necessary to optimize the process of meshing. The 3D Refined Mesh is only created in half using the full domain's symmetry to heavily reduce the number of elements in the mesh. This allows one to obtain a mesh with higher concentration of smaller elements while still creating a computationally light mesh. Symmetry should be used in the 3D Simpler Mesh however it is not necessary considering the number of elements on the mesh and the computational capacity of modern computers. One must keep in mind that the main purpose of the first tridimensional mesh is to give a first approach to the problem and to give an idea on what is more important for the particular case when working on the refined mesh.

Since the refinement is not only a matter of number of elements, there is also the concern of increasing the length and the width of the domain to assure a freestream zone around the turret. Based on notable studies in the field of external flows, distances over 10 diameters from the area of interest and the walls, inlets or outlets, usually represent a low influence of the boundaries on the region around the body of study. In the 3D Refined Mesh it is chosen distances of 40 diameters from the inlet and the turret and from the outlet and the turret, as well as 20 diameters from the turret to the top wall and the side wall.

Figure 7.15 represents the entire 3D Refined Mesh, where one can see the various different blocks by color. It is visible that this mesh is significantly more complex than the simpler one. One may separate the mesh into two regions, the one closer to the turret which has the distorted elements adapting to the curvilinear surface and the other region which has

blocks with the straight elements. These cubic and parallelepiped elements have the purpose of augmenting the size of the mesh, a necessity mentioned earlier.

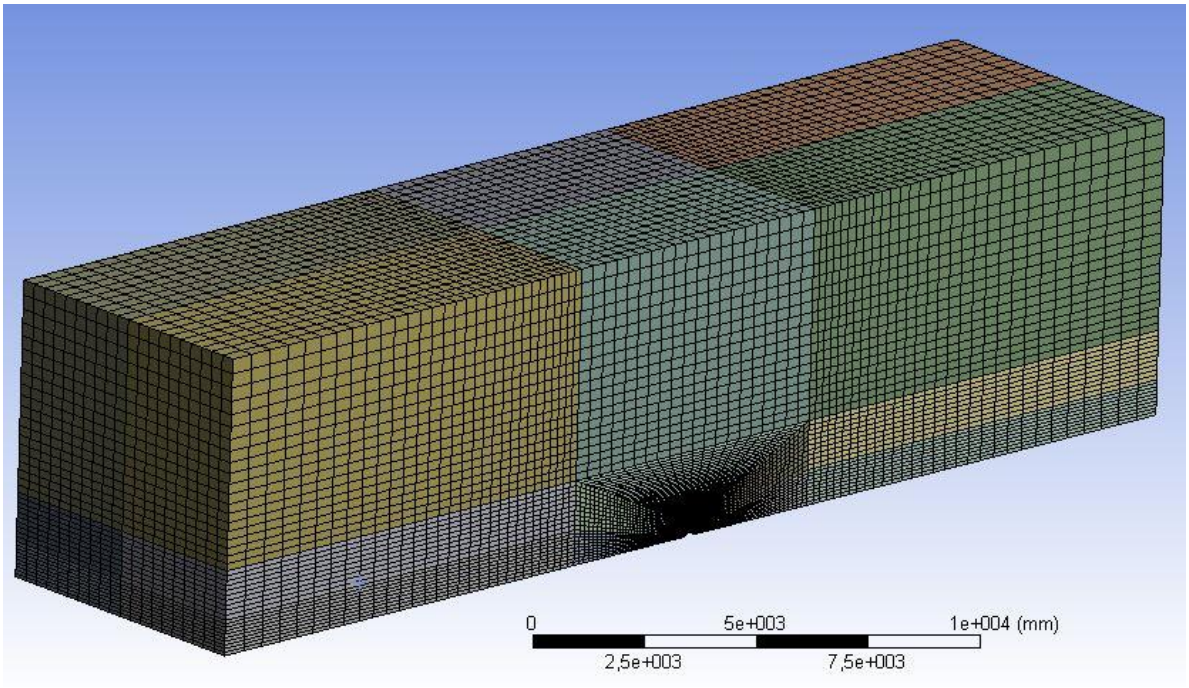

Figure 7.15 – View of the full domain of the 3D Refined Mesh.

Figure 7.16 shows the symmetry plane cutting through the centerline of the turret. In this figure one may notice the extremely different density of elements between the region around the turret and the region of non-distorted elements.

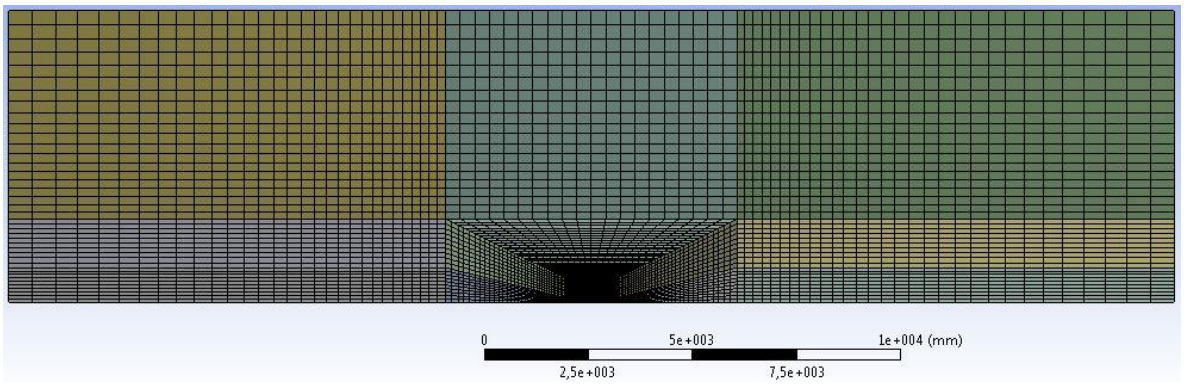

Figure 7.16 – View of the xOy plane of the 3D Refined Mesh.

Figure 7.17 depicts only the region around the turret in which it is evident the distortion of the elements in order to create a finer field of computational analysis. Similarly to the simpler mesh, there are straight lined blocks that contain the boundary layer closer to the wall and the turret and also similarly to the simpler mesh, from a certain point, two new blocks create diverging elements to the outer regions.

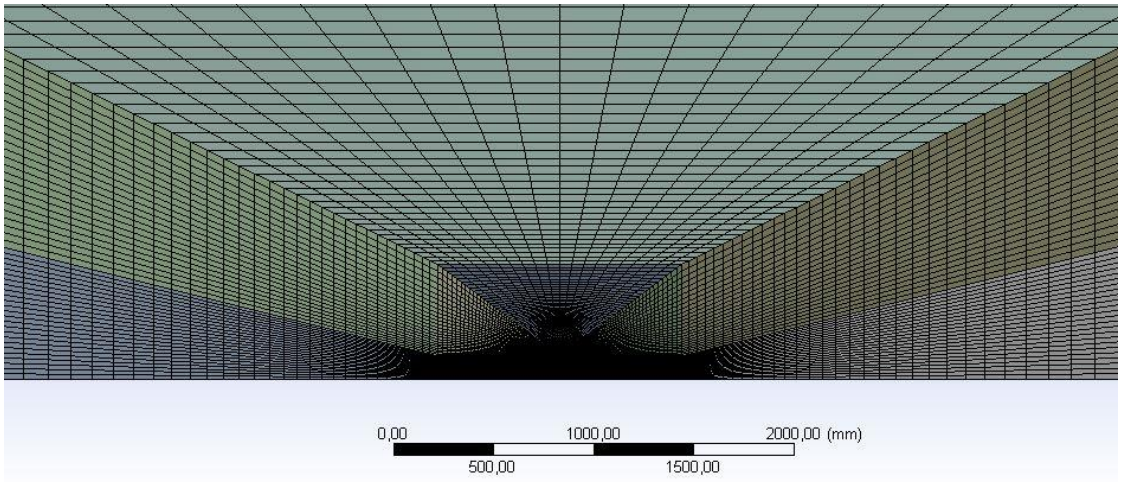

Figure 7.17 – View of a close approach on the turret on the xOy plane of the 3D Refined Mesh.

Comparing the region around the turret of both Figure 7.12 and Figure 7.18 one can see the increase of element concentration from the former to the latter. The boundary wall is better defined and high gradients of flow properties get better resolved. It is also visible that the distortion of the elements near the turret is minimized which increases the orthogonal quality in the region.

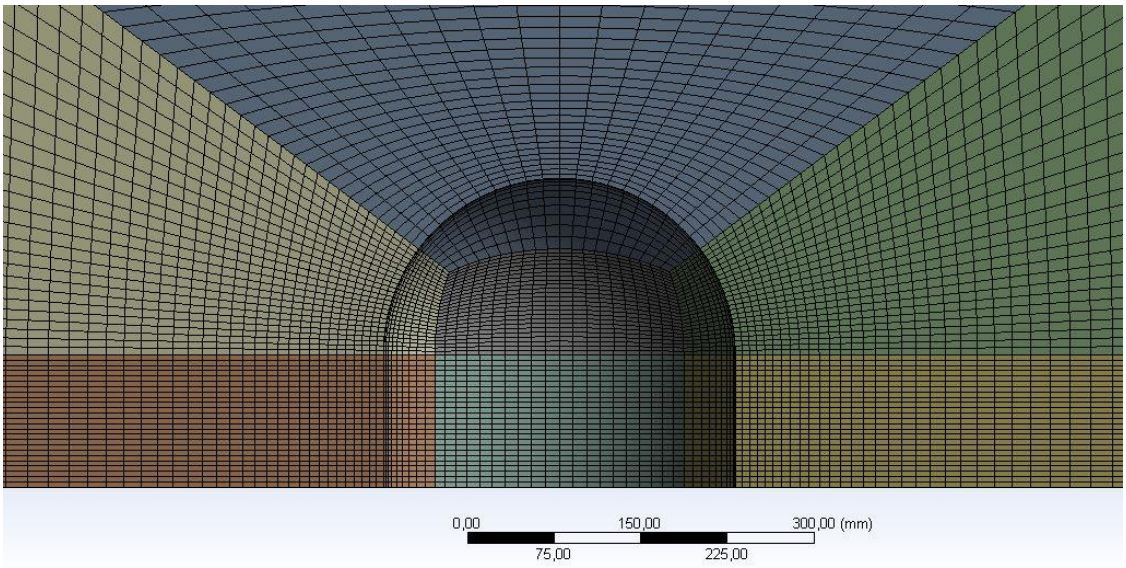

Figure 7.18 – View of the turret on the xOy plane of the 3D Refined Mesh.

The bottom view of the 3D Refined Mesh is represented in Figure 7.19, Figure 7.20 and Figure 7.21. Comparing both 3D meshes and specifically considering Figure 7.19, the blocks earlier referred as the region with straight elements do not exist in the simpler mesh.; these elements are created to enlarge the mesh. Regarding Figure 7.20 and Figure 7.21 the adaptation of the curvilinear surface of the turret to the outer blocks' rectangular shapes is better achieved in the 3D Refined Mesh.

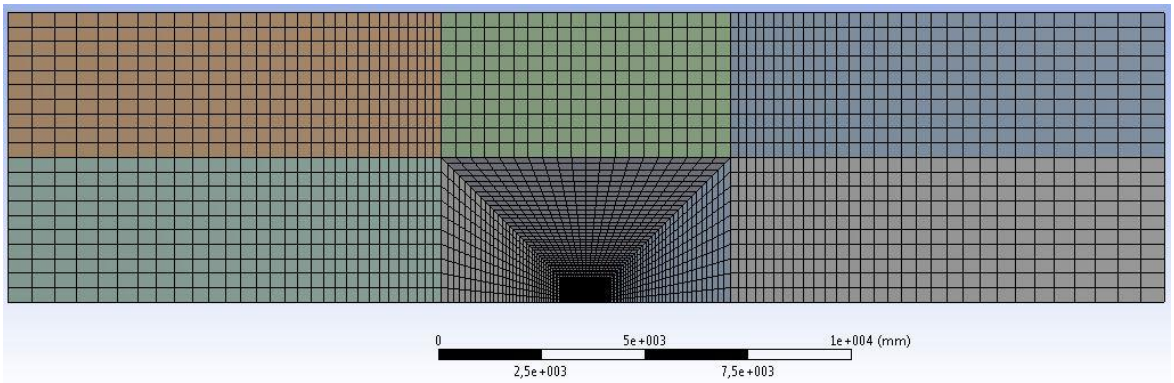

Figure 7.19 – Bottom view of the domain on the base plane of the 3D Refined Mesh.

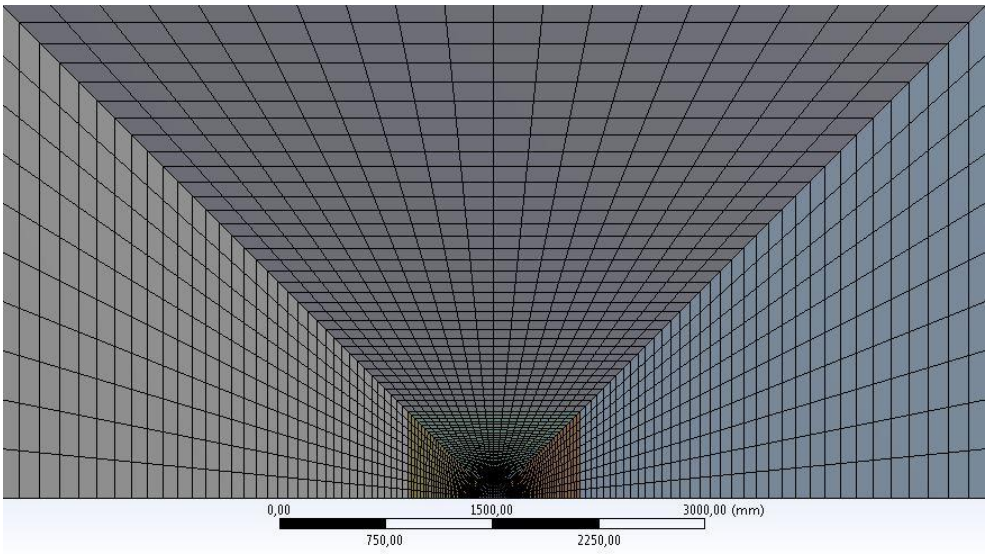

Figure 7.20 – Close approach on the bottom view of on the base plane the 3D Refined Mesh.

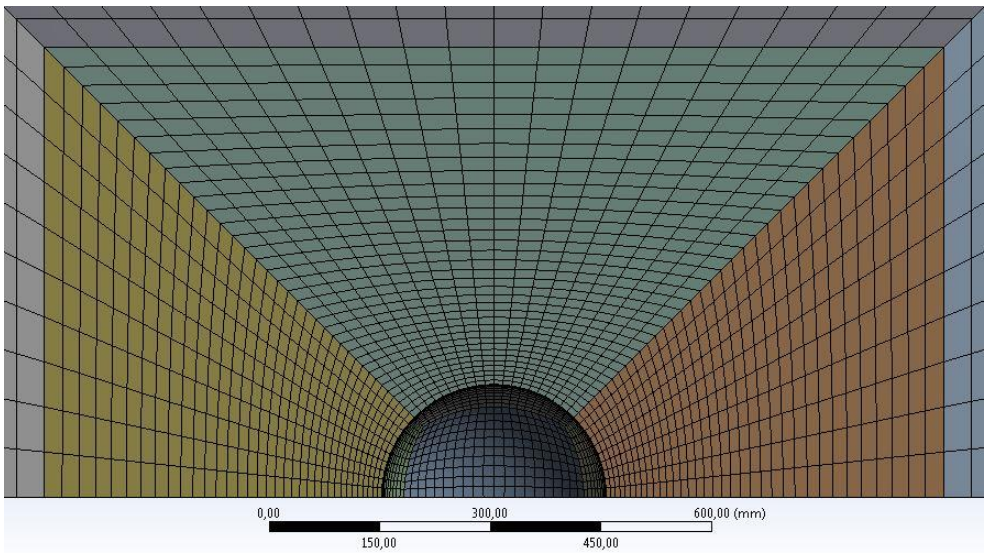

Figure 7.21 – Bottom view of the turret on the base plane of the 3D Refined Mesh.

7.6 Parameters definitions

7.6.1 Pressure coefficient

Pressure coefficient is used to express the dimensionless pressure at any point in the flow field. It is a ratio between the differential of static pressure (gauge pressure = static pressure at the point of interest – free stream static pressure) and the dynamic pressure. Pressure coefficient is defined as:

$$C_P = \frac{P - P_{ref}}{\frac{1}{2}\rho_{ref} V_{ref}^2} = \frac{P_{gauge}}{\frac{1}{2}\rho_{ref} V_{ref}^2} \quad (7.1)$$

Where

$$P_{gauge} = P - P_{ref}$$

$$P_{ref} = Reference\ Pressure$$

$$V_{ref} = Reference\ Velocity$$

$$\rho_{ref} = Reference\ Density$$

7.6.2 Drag coefficient

Drag coefficient is used to quantify the resistance of a determined object in a fluid, considering all the complex dependencies of shape, inclination and flow conditions on drag.. The non-dimensional drag coefficient is defined as de ratio between the drag force and the dynamic pressure times the surface area, S., on the object:

$$C_d = \frac{D}{\frac{1}{2}\rho_{ref} V_{ref}^2 S} \quad (7.2)$$

Where

$$D = Drag\ force$$

$$S = Object's\ projected\ area\ normal\ to\ the\ direction\ of\ the\ flow$$

Later, in subchapter 7.8, it is presented the relative difference between Cd values from several simulations. The relative difference is defined as follows:

$$|\Delta C_d|(\%) = \frac{|C_{d_1} - C_{d_2}|}{C_{d_1}} \times 100 \quad (7.3)$$

Where

$C_{d_1} = First\ drag\ coefficient\ presented$

$C_{d_2} = Second\ drag\ coefficient\ presented$

7.6.3 Reynolds number

The Reynolds number of the flow around a turret is defined as:

$$Re_D = \frac{\rho_{ref} V_{ref} D_{turret}}{\mu_{ref}} \tag{7.4}$$

Where

$\mu_{ref} = Reference\ dynamic\ viscosity\ of\ the\ air$

$D_{turret} = Diameter\ of\ the\ turret$

7.6.4 Mach number

Mach number is a non-dimensional velocity. It is useful for compressible flows in which there is a strong dependence between the speed of sound and the appearance of phenomena as shock waves. It relates the velocity of an object and the respective speed of sound on the environment in which the object is:

$$Ma = \frac{V}{a_{ref}} \tag{7.5}$$

Where

$V = Velocity\ of\ the\ object$

$a_{ref} = Reference\ speed\ of\ sound$

The speed of sound is defined as:

$$a = \sqrt{kRT} \tag{7.6}$$

Where

$k = Ratio\ of\ specific\ heats$

$R = Gas\ constant$

$T = Temperature\ of\ the\ flow$

7.6.5 Reference values

The reference values are considered to match the worst case scenario in terms of drag. As seen in Equation 9.2**,** for higher density and higher velocity, drag increases. Based on the International Standard Atmosphere (see more on ISA in **[42]**) lower altitude implies higher air density. Thus the worst case scenario is the sea level conditions.

$$P_{ref} = 1.01325 \times 10^5\ Pa$$

$$\rho_{ref} = 1.225\ kg/m^3$$

$$\mu_{ref} = 1.7894 \times 10^{-5} kg/m.s$$

$$T_{ref} = 288.15\ K$$

$$a_{ref} = 340.294\ m/s$$

Even though the airplane actually lands and takes off in sea level conditions, by this approach, one is considerably over-dimensioning the drag force since the velocities used in the simulations are applied considering maximum operating conditions and diving speed conditions. Diving speed conditions consider emergency maneuvering and ultimate load conditions on the airframe. In these conditions it is not expectable that complementary devices such as the turret in analysis maintain its operability.

Regarding velocity, there is not a single value of analysis since it is performed a parametric study varying the velocity as mentioned above. The values of the velocity parameter range from $5 \times 10^{-4}\ m/s$ to $165\ m/s$ which consists of a range of Re numbers from 10 to 3.5×10^6.

7.6.6 Projected surface area

In this study, three diameters of turret are studied. The validation simulations are done for a 2D 10 in (254 mm) turret and a 3D 12 in (305 mm) turret and the parametric study for the FLIR device is performed considering the actual diameter of the turret which is 15 in (381 mm). The projected surface area for each case is listed in Table 7.2.

Table 7.2 – Diameters and frontal surface area of the tested turrets.

	Diameter [in]	Diameter [mm]	Projected Surface Area [mm^2]
Validation 2D	10	254	57593
Validation 3D	12	305	71322
FLIR study	15	381	153770

7.7 Flow simulation setup

Since CFD simulates a fluid flow, there are several algorithms to better approximate the simulation to the actual complex phenomena. One does not know the specific phenomena present in the real flow so there has to be several different simulations in order to vary some parameters which can result in relevant discrepancies between simulations. The range of phenomena predictably present in the flow over the turret is referred above as well as the CFD's algorithms which are referred in chapter 6.

The common setup to the entire group of simulations is:

- Steady-state – Despite having the need to resort to transient analysis in order to obtain an extensive comprehension of the influence of the flow on the turret, in this study there are only simulated steady-state flows.
- Pressure-based solver – The flight conditions of the study are from incompressible flow to mildly compressible flow.

7.7.1 Boundary conditions

Table 7.3 – Different types of boundary specified for the domain.

Boundary surface	Type of boundary
Inlet	Velocity-inlet
Outlet	Pressure-Outlet
	Outflow
Midplane	Symmetry
Top, Base and Side surfaces	Wall
	Pressure far-field

Different configurations of boundary conditions are considered. Table 7.3 lists the variety of boundary types.

Velocity inlet is used for incompressible or low compressible flows. It defines the velocity field at the inlet leaving the pressure field free to adapt to the required velocity distribution.

Inlet – Since the case only considers momentum and energy equations, the inlet setup is granted by defining the velocity of the flow at the entrance of the domain (inlet) and by defining the reference temperature. The energy equation has the purpose of contemplating the ideal gas equation for the simulations in which the density of the air is considered variable.

Turbulence – The inlet setup also regards turbulence. Turbulence transported quantities may differ from type of flow. For the present case one requires both turbulent intensity and a dimensional characteristic of the mesh.

- Turbulent intensity may be defined as:

$$I = \frac{u'}{u_{avg}} \tag{7.7}$$

Where

$$u' = Root\ mean\ square\ of\ the\ velocity\ fluctuations$$

$$u_{avg} = Mean\ flow\ velocity$$

As turbulent intensity is only successfully tractable in experimental testing, varying from 10%, high turbulence, to as low as 0,05%. External flows around cars or aircrafts tend to create turbulence intensities below 1% – as a reference, for this study it is assumed 0,5% of turbulent intensity **[43]**.

- Length scale represents a dimensional characteristic of turbulence. A usual value for the turbulent length scale is around 40% of the boundary layer thickness near the bluff body (the turret). It is then assumed a value of 0,01 m of turbulent length scale **[43]**.

For the outlet, there are considered two types of boundary: Pressure-outlet and outflow. Pressure-outlet imposes that at the entire outlet surface the pressure must be the same. Outflow boundary is used when the conditions at the outlet are unknown prior to the simulation. However, this outlet boundary does not support compressibility effects. The density of the fluid must be constant in order to apply outflow boundary type.

Outlet – Gauge pressure is defined as 0 Pa since the pressure value at the outlet is free stream pressure which is the same as reference pressure. Backflow turbulence parameters are the same as the turbulence specifications at the inlet.

Using symmetry in the midplane allows one to mesh only half of the domain. All the properties of the simulated region are assumed symmetric relative to the midplane.

Regarding the other surfaces (Top, Base and Side surfaces) it is also considered two types of boundary: Wall and pressure far-field. Even though this study is an external flow, which means no physical boundaries, wall boundary is a highly viable option due to its capacity of ensuring continuity – with wall boundary the fluid does not exit or enter the domain. Pressure far-field seems the ideal boundary condition for the problem since it models a free-stream condition which is the actual case. However, it hampers the convergence of the problem since it allows the exit and entrance of air through the surface.

Wall – Since the distances between the turret and the boundaries are substantial, the blockage effect that the no-slip condition on the wall generates is minimized. The effective section area of the flow is reduced due to the region of attachment to the wall. However, this is minimized since the estimated blockage only narrows the section on around 0,08% of the nominal area. This effect has no tractable repercussion on the velocity of the flow.

7.7.2 Flight conditions

Since the purpose of the study is to assure a viable modification, one simulates the most adverse conditions to which the modification needs to comply to. In this case, the parameters that are considered variable are the velocity and the air density. These are variable since during a flight the velocity has obviously numerous values and the air density depends on the altitude. Regarding the remaining parameters that contribute for the drag (see Equation 7.2) it is noticeable that the projected surface area does not change and the drag coefficient is the subject in study. Therefore, in order to obtain the most adverse possible drag, the air density is considered the sea level reference density and the velocity is given for two cases, one considered for the maximum operating velocity and the other is for diving speed conditions in order to attend to the requirement CS 25.1503 – Airspeed limitations:general.

The most adverse flight conditions are set as follows on Table 7.4. The velocity values seen on Table 7.4 are based on specific information from the airplane. It is important to state that the Mach numbers presented are not the highest Mach that the airplane can reach. There is a simple connection between the altitude adopted to conduct the simulation and the Mach numbers presented which is: the higher the altitude, the easier it is for the airplane to reach higher Mach numbers. The rise in altitude is associated to a decrease in temperature which lowers the speed of sound. Hence, for the same velocity, the Mach number is higher at higher altitudes than at sea level conditions. As comparison, if the conditions on Table 7.4 were related to the highest Mach values that the airplane is capable of achieving, these Mach values would be as presented in Table 7.5. It is important to state that according to specific information of the airplane, these conditions assume True Airspeed (TAS) as reference for Mach calculation.

There are a few distinct definitions of airspeed, the most relevant being Indicated Airspeed (IAS) and True Airspeed (TAS). As each has its own purpose, IAS is the airspeed on

the instruments of the cockpit, it is the velocity read by the pitot tubes outside the cockpit. TAS is the speed of the airplane relatively to its surroundings. The surroundings' density plays a major role in the calculation of the Mach values since assuming a constant IAS, TAS increases for higher altitudes due to the decrease of the air's density. This increase in speed evidently causes the Mach to increase.

The Mach values in sea level conditions are the same for IAS and TAS. Otherwise, only true for altitudes higher than around 15,000 ft (for the case of the C-130H) the airplane reaches the maximum Ma number, seen on Table 7.5.

Table 7.4 – Most adverse conditions' parameters.

Conditions	Operating pressure (Pa)	Air density (kg/m^3)	Velocity ($KIAS$)	Velocity (m/s)	Mach
Maximum operating speed	1.01325×10^5	1.225	270	138,9	0,41
Diving speed	1.01325×10^5	1.225	320	164,6	0,48

As a means of assuring the most independent variation of air density near the turret, the operating pressure is defined at the farthest possible point of the domain, at the inlet.

Table 7.5 – Mach numbers associated to higher altitudes of service.

Conditions	Altitude
	Above 15,000 ft (4572 m)
Ma for maximum operating speed	0,55
Ma for diving speed	0,64

7.7.3 Solution methods

As mentioned in Chapter 6, CFD analysis is not as reliable as structural FEM analysis. Hence there needs to be given a tolerance to the results obtained through CFD methods. One way of increasing the level of confidence on the results, subsequently to the process of validation, one usually compares the solution methods used in each simulation, such as the pressure-velocity coupling and spatial discretization methods.

In a given simulation, the parameters are not necessarily the same throughout the entire set of iterations. These parameters may be altered to better suit the convergence needs. As an example, one may start a simulation by setting a laminar model for a few iterations though gradually increasing the complexity of the model during the simulation. This allows the solution to be achieved expeditiously.

During the entire process of validation as well as the parametric study there are used several configurations of simulations, combining the parameters seen on Table 7.6, Table 7.7 and Table 7.9.

Table 7.6 – Schemes of pressure-velocity coupling used in the study.

Solution Method	Scheme
Pressure-velocity coupling	SIMPLE
	SIMPLEC

SIMPLE and SIMPLEC are segregated algorithms which are similar regarding the amount of equations to be solved. These are applicable for steady state and relatively simple cases. What differs from one to another is the capacity that SIMPLEC has to apply increased under-relaxation and to use skewness correction schemes. These skewness correction schemes become very useful in cases of low quality meshes or high complexity geometries.

Table 7.7 – Turbulence models used in the study.

Solution Method	Model
Turbulence Model	Laminar
	Spalart-Allmaras
	k-ε standard
	k-ε realizable
	k-ω standard
	k-ω SST

Conducive to a more expedite convergence, several turbulence models are used in a simulation. It is a progressive process which starts with the laminar model and goes through the simpler models until it reaches the desired model in analysis. The typical relation iterations - turbulence model adopted in the study is as seen on Table 7.8. For the cases in which the final turbulence model is the laminar or the Spalart-Allmaras the process is just shortened in terms of amount of stages. Each stage involves a stop in the computation. The entire configuration of the simulation may be changed for each stage; in this study, each stage only varies in solution methods such as pressure-velocity coupling schemes, turbulence models and spatial discretization parameters.

The amount of iterations for each stage and for each turbulence model presented in Table 7.8 is based on prior experiment and convergence testing. The arrangement seen on the mentioned table is found to be the approach that results in easier convergence. From this point,

when a turbulence model is referred in a certain simulation, the process is accordingly to Table 7.8.

Table 7.8 – Setting of iterations for each stage of the simulation.

Stage	Turbulence Model			
	Laminar	Spalart-Allmaras	k-ε or k-ω STD	k-ε RZB or k-ω SST
1	All iterations			
2	30	Remaining iterations		
3	30	50	Remaining iterations	
4	30	30	50	Remaining iterations

Regarding Table 7.9 it is shown the different parameters that configure the spatial discretization used in the study.

With no significant relevance, the gradient is set as the default parameter Least Squares Cell Based due to its simplicity and low computational effort.

Since the case is steady-state, with only momentum equations in which the continuity is the most important condition to be satisfied, the pressure, density and momentum spatial discretization only regards the degree of approximation – there are no specific requirements in terms of precision such as in time dependence or higher compressibility effects. Based on initial simulations, a second order precision on the mentioned parameters delivers more consistent and stable results.

Regarding the turbulent kinetic energy and turbulent dissipation rate equations, there are not any significant changes in regard to convergence or results' precision.

The energy equation is only applicable when air is assumed as an ideal gas. Hence the computation of this equation is relatively simple and resorts to low computational effort. This allows one to select a second order precision.

Table 7.9 – Parameters of spatial discretization used in the study.

Solution Method	Parameter	
Spatial Discretization	Gradient	Least Squares Cell Based
	Pressure	Standard
		Second Order
	Density (for air as ideal gas)	First Order Upwind
		Second Order Upwind
	Momentum	First Order Upwind
		Second Order Upwind
	Turbulent Kinetic Energy (for the laminar case, there is no turbulence)	First Order Upwind
	Turbulent Dissipation Rate (for the laminar case, there is no turbulence)	First Order Upwind
	Energy	Second Order Upwind

7.7.4 Convergence criteria

Convergence may be assessed by the amount of error accumulated in the computation. Since computational analysis works with approximated terms, there remains an error in each computation. The trend of these errors or residuals must be of a decrease throughout the iterations. If the value of the residuals decreases, it means that the solution has a better approximation to the analytic result. It is assumed that the solution has converged once the residuals reach a certain level of precision. An acceptable level of precision is achieved once the residuals decrease to 10^{-5}. This convergence criterion is applied to all the equations being computed: Momentum, energy, X, Y and Z velocity components and the specific terms of each turbulence model.

Occasionally there is a concern on determining convergence as described above. This is due to a series of possibilities of results' trends. It is possible that a certain equation may adopt a periodic variation while the residuals continue to decrease. This issue is solved by verifying that equations' residuals demonstrate a stable decrease.

7.8 Aerodynamic analysis results

As mentioned, the aerodynamic study in the present work only involves static analysis. The impact assessed only regards the aerodynamic force on the turret caused by the flow. This allows the simulations to be steady-state. The primary concern is to transport the force generated on the turret to the structural study **[1]** in order to design the structure which connects the turret to the airplane. In order to obtain the force there is the need to obtain the one unknown variable on Equation 7.2 which is the drag coefficient.

7.8.1 Validation

As mentioned, the first step of the CFD process is validating the method of analysis. This is achieved by comparing experimental results to the results obtained by CFD simulation. As a means of establishing a well-defined process of validation and comparison of results, one starts by the simpler options and advances to the more complex and theoretically better suited methods. This sets ground for the initial simulations that are performed on a 2D domain.

The validation is performed for two different flow velocities in which the first corresponds to $Re = 8{,}66 \times 10^5$ and the second to Mach between Ma=0,3 and Ma=0,4. These conditions are chosen so the results may be comparable to published experimental data. The experimental data available imposes these conditions on the process of validation.

The parameters used to represent the results are the pressure distribution around the centerline of the turret and the overall drag coefficient that the flow causes to the turret. Figure 7.22 is related to the first case of validation and Figure 7.24 represents the pressure distribution on the centerline of the turret for Mach between Ma=0,3 and Ma=0,4. Figure 7.26 is the plot of drag coefficient containing published experimental results from Snyder (1998) and computational results from the present study which partially represent the results from the parametric study which is discussed later.

For conclusion purposes, which include the validation process and the comparisons between computational values, the results presented are achieved for the most refined mesh; Figure 7.27 represents the comparison between results from the simpler mesh and the refined mesh. This comparison is useful to understand the influence of the mesh quality on the results.

The published results presented in this document are obtained by reading the plots presented in the documents. This introduces an error to the comparison of the results which would be avoided if the plots were presented exactly as these appear in the publications. However, in order to optimize the results section the method is chosen as stated. In addition, the amount of error introduced to the results is believed to have no significant impact on the analysis and subsequent conclusions.

On Table 7.10 it is possible to see the similar Cd results for 2D simulations from this study and from Schwabacher (2000) in which the reference values used are accordingly to the ones used in the present work. This may ground the method used for the study to perform the 2D simulations, however these are not experimental results.

Table 7.10 – Drag coefficient results for 2D computational studies.

Case of analysis	Computed drag coefficient
2D result from Schwabacher (2000)	0,16
2D result from present study	0,18

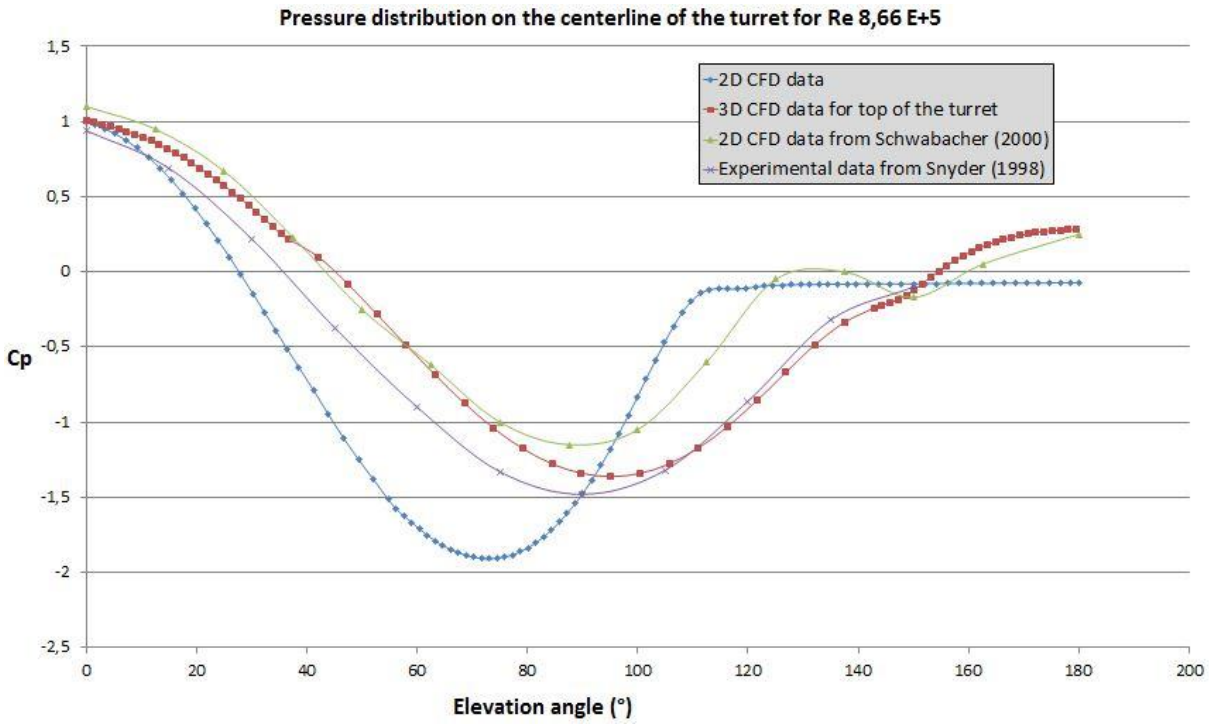

Figure 7.22 – Pressure distribution plot on the centerline of the turret for $Re = 8{,}66 \times 10^5$. Blue – 2D computational results obtained in this study. Red – 3D computational results obtained in this study. Green – 2D computational results from Schwabacher (2000). Purple – Experimental results from Snyder (1998).

On Figure 7.22 it is presented the published 2D results from Schwabacher (2000) and the experimental results from Snyder (1998) as well as the 2D and 3D computational results obtained in the present study. These published results have conditions similar to the present study so the comparison is possible. On this plot the pressure coefficient values are related to the region of the domain in which they are measured or computed; in this case the region is the centerline of the turret on the same direction of the flow. The fact that the four results start at pressure coefficient 1 for 0 degrees means that it is a stagnation point of the flow. A stagnation

point occurs when the velocity field at that point is zero, meaning that the dynamic pressure is 0 at that point. From the definition of the pressure coefficient one may notice that it consists of a ratio between the gauge pressure at the location in analysis and the dynamic pressure of the freestream uninfluenced flow. If both these quantities are equal (Cp = 1) it means that all the dynamic pressure is transformed into static pressure. Then, the stagnation point is where the static pressure is maximum. The result plots may not start exactly at 1 since turbulence or any other disturbances to the results such as computational or experimental approximations may cause the theory not to be exactly applied.

On Annex B.1 it is represented the pressure and velocity magnitude fields for the 2D validation case and on Annex B.2 it is represented the pressure field, the pressure coefficient around the turret and the velocity magnitude field for the 3D validation case.

The results are obtained considering viscid flow, which implies viscous forces. Figure 7.23 regards the potential solution for the pressure coefficient around a sphere and around a cylinder. Potential flow does not involve drag.

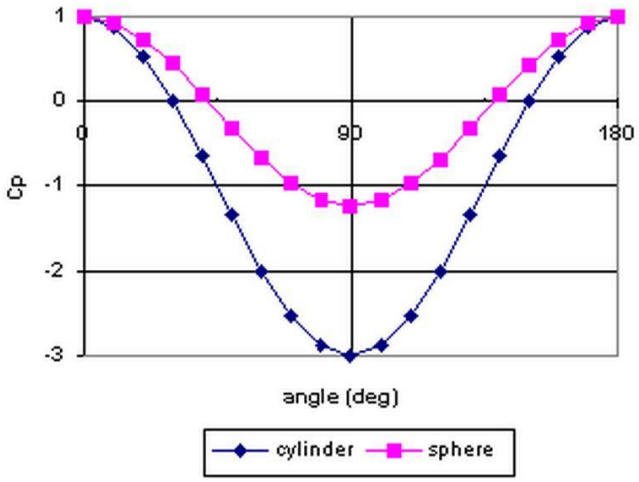

Figure 7.23 – Pressure distributions for centerline cuts through a circular cylinder and a sphere **[44]**.

Comparing the results from Figure 7.22 to the potential solutions for the sphere and the cylinder one may notice that there is a separation point on the viscid flow results that does not occur in the potential flow. This separation point is due to the adverse pressure gradients that the flow is subjected to and it does not have the capacity to stay attached to the turret. The detachment occurs at the separation point. These separation points are presented in Table 7.11. One may see that the separation in the 2D cases is visible whereas the 3D results show a slightly smoother separation; this may be explained by the geometric differences as discussed next.

By looking at the difference between the sphere and cylinder potential cases one may see that the cylinder causes the flow to diverge much heavily than the sphere since the

minimum pressure coefficient is much higher in the cylinder case. This occurs due to the geometry of the sphere and the cylinder; the 2D section of these geometric objects may be the same, however, the sphere induces less blockage effect to the flow due to the third dimension factor. Hence, the 2D meshes represent cylinders and not spheres; this is the main reason for not achieving satisfactory results with 2D analysis for this case. The separation points are accordingly to what is referred on the sphere geometry; a later separation demonstrates that the fluid has lower blockage to its movement.

Table 7.11 – Separation points for validation case of $Re = 8{,}66 \times 10^5$.

Case	Angle of separation point (°)
2D computational results	115
3D computational results	140 (approximately)
2D computational data from Schwabacher (2000)	130
Experimental data from Snyder (1998)	140 (approximately)

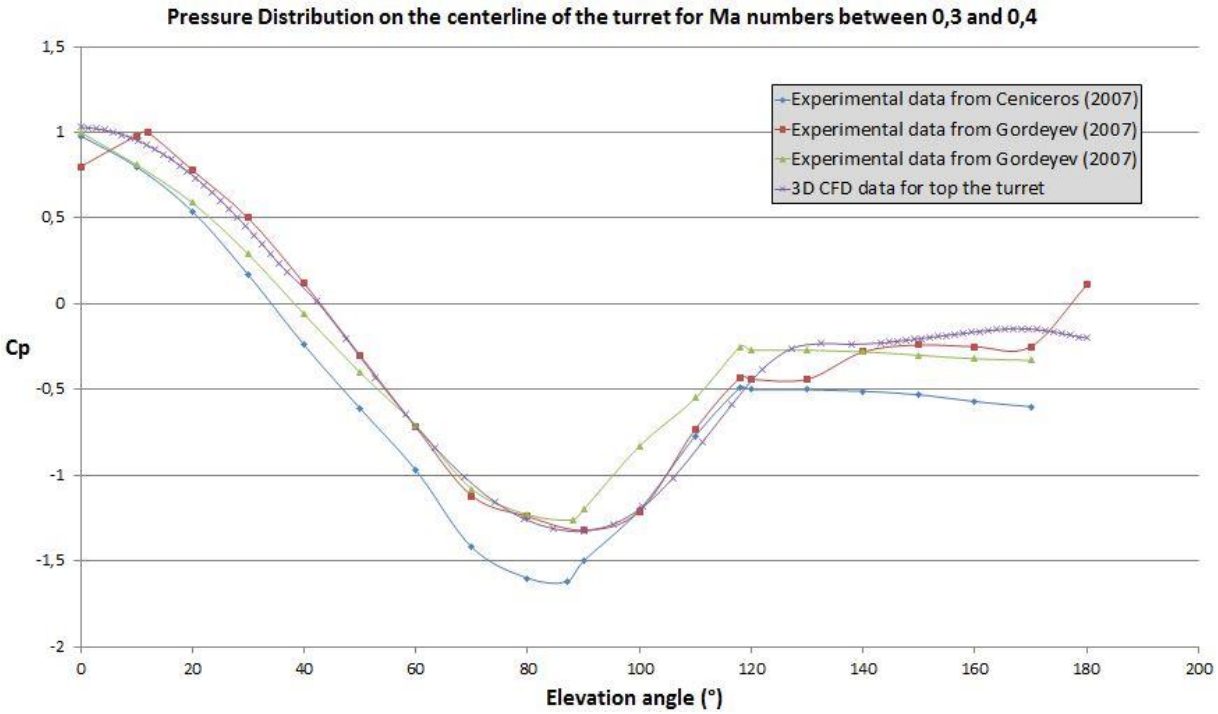

Figure 7.24 – Pressure distribution plot on the centerline of the turret for Ma between 0,3 and 0,4. Blue – experimental results from Ceniceros (2007). Red – experimental results from Gordeyev (2007). Green – experimental results from Gordeyev (2007). Purple – 3D computational results obtained in this study.

On Figure 7.24 it is presented experimental results for velocity conditions of between Ma=0,3 and Ma=0,4. This is the second stage of the validation process and for these

conditions, as well as the conditions of $Re = 8{,}66 \times 10^5$ discussed previously, the 3D computational analysis shows to be representative of the actual flow conditions. Apart from a slightly distinct separation point, the 3D computational results obtained in this study prove to be of considerable reliability.

Contrarily to what is expected, as seen on Table 7.12, the results for a higher flow velocity show the separation point occurring sooner than in the results for $Re = 8{,}66 \times 10^5$. Theoretically, the separation is easier to occur in low speed flows, which is the reason for generating higher drag.

Table 7.12 – Separation points for validation case of Ma between 0,3 and 0,4.

Case	Angle of separation point (°)
Experimental data from Caniceros (2007)	120
Experimental data from Gordeyev (2007) (Red)	120
Experimental data from Gordeyev (2007) (Green)	120
3D computational results from the present study	130

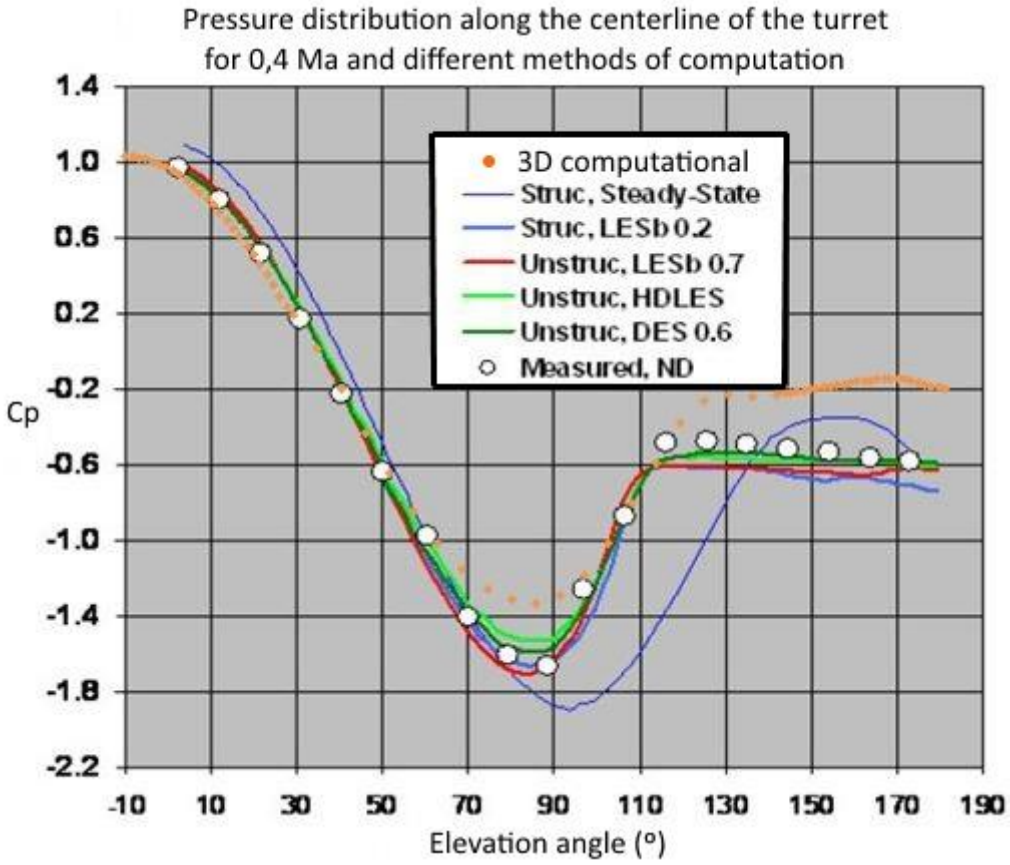

Figure 7.25 – Comparison between computational 3D results of pressure coefficient for Ma=0,4 from Ladd (2009) **[38]**.

On Figure 7.25 (Plot adapted from **[38]**) it is presented the comparison between an experimental result and computational results from Ladd (2009) and the 3D computed results from this study. One may notice two curves which are not as similar to the measured curve as the others. These two curves are from steady-state simulations which may explain the disparity from the transient ones. There are used more complex computational methods to obtain the results from **[38]**.

Similarly to Figure 7.24 the separation point of the computed curve occurs latter in the flow, which might result in lower drag. Visibly, the drag values obtained for the computed curve are lower than the drag obtained from the other simulations on Ladd (2009). This is based on the gap of 0,4 on the Cp values between the results from this study and the other results; this gap is read from the values of Cp after the separation.

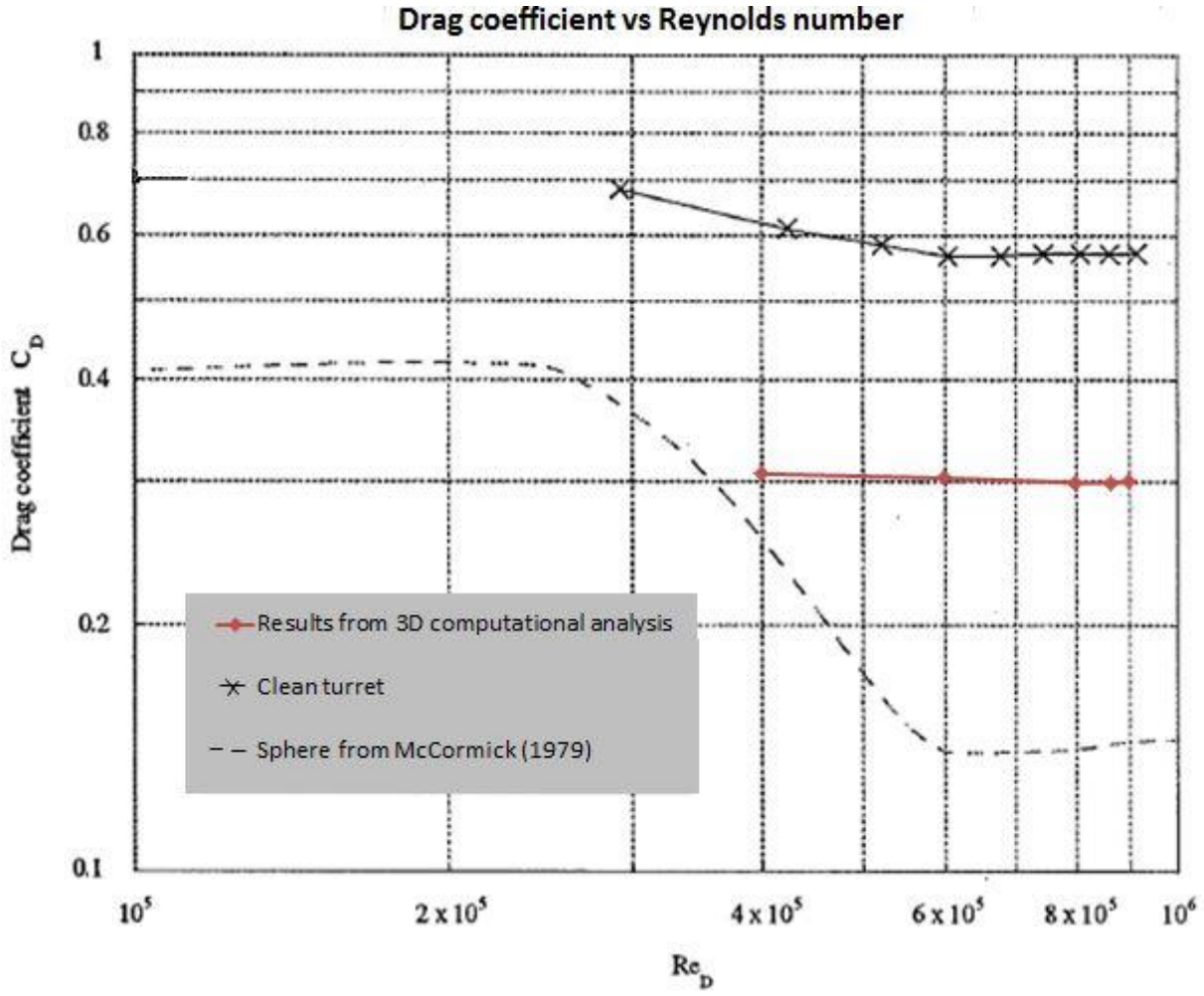

Figure 7.26 – Drag coefficient plot for the validation process.

Figure 7.26 regards the comparison between the drag coefficients for the experimental results from Snyder (1998), the computational results from the present study and the results for a sphere from McCormick (1979). One may notice a substantial discrepancy between the turret's experimental and computational results. For validation purposes it is recommended that the results obtained by the method of this study should be considered with a factor of 2 since the computational results represent around 50% of the experimental results as clearly visible on Figure 7.26.

Contrarily to other published results, Figure 7.26 presents the experimental results from Synder (1998) as these are presented.

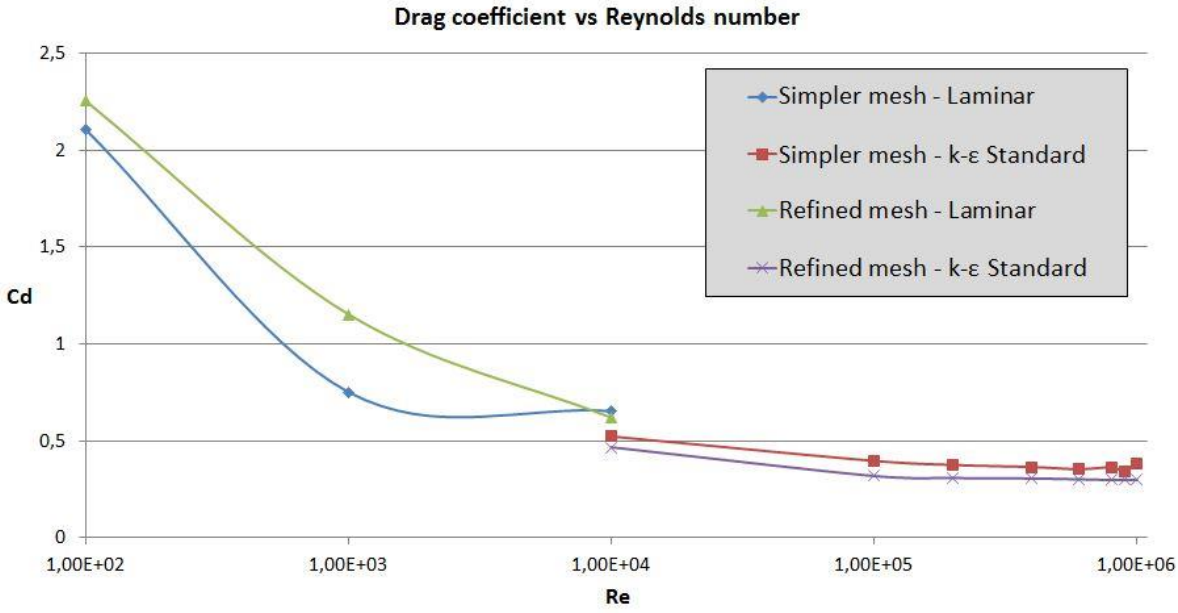

Figure 7.27 – Drag coefficient plot, comparison of simpler mesh and refined mesh.

Still related to the process of validation, there is the need to justify the use of a refined mesh over a simpler and less computationally demanding mesh. Figure 7.27 is the plot that related the drag coefficient values with the Reynolds number. It compares the simpler mesh results to the refined mesh results. Whereas between the results obtained with k-ε Standard, the trend of the results is similar it is clear that for the "Laminar" turbulence model comparison, the simpler mesh fails to assure a stable trend of the results. It is visible that for the transition from $Re = 10^2$ to $Re = 10^4$ the refined mesh results show a better-defined convergence to the lower values of drag coefficient than the simpler mesh. Particularly, the difference between the Cd values for $Re = 10^3$ demonstrates a lower accuracy from the simpler mesh.

Table 7.13 – Analysis of different outlet boundary parameters.

Outlet boundary parameter		Cd	|ΔCd| (%)	Iterations
Outflow		0,37731	-	86
Pressure outlet		0,37733	0,01	89
Remaining parameters of the simulation				
Re	2,00 E+5	Gradient	LSCB	
Ma	0,03	Density	Standard	
V (m/s)	9,58	Momentum	First order upwind	
ρ (kg/m^3)	1,225 (constant)	Pressure	First order upwind	
Turbulence Model	Laminar	Turbulent kinetic energy	-	
Solver	SIMPLE	Turbulent dissipation rate	-	
Outlet Boundary	-	Energy	-	

Table 7.13 presents the analysis of different outlet boundary parameters. It regards the two distinct configurations for the outlet boundary parameter which are “outflow” and “pressure outlet”. It also contains the remaining information for the simulation which is the same for both configurations in order to assure that the results’ variation only depends on the parameter being altered. However the independence between the remaining parameters and the variation of the results has a limitation since there may exist a higher variation for a different set of parameters such as higher velocity. To avoid this issue, it is also performed a comparison for higher velocities as seen on Table 7.16.

Regarding the result, it is clear that the outlet boundary condition has no influence on the drag coefficient value. As mentioned, this only states that for the simulation’s configuration described, there is no influence in the value of drag coefficient. It is not inferable for other set of parameters. From the amount of iterations needed for each simulation one can conclude that the amount of computational effort is around the same using one parameter or the other and it also allows one to contemplate that results for this set of parameters are simply and easily obtained.

For this analysis and also applicable for the following, the set of parameters is decided considering engineering judgement always regarding the simpler methods of computation and also the conditions that better describe the actual problem. Parameters of energy and turbulence are not applicable since the air density is constant and the turbulence model is laminar which implies no turbulence.

Table 7.14 – Analysis of different momentum discretization schemes.

Momentum discretization schemes		Cd	|ΔCd| (%)	Iterations
First order upwind		0,35086	-	207
Second order upwind		0,28337	19,24	264
Remaining parameters of the simulation				
Re	4,00 E+5	Gradient	LSCB	
Ma	0,06	Density	Standard	
V (m/s)	19,17	Momentum	-	
ρ (kg/m^3)	1,225 (constant)	Pressure	First order upwind	
Turbulence Model	k-ε standard	Turbulent kinetic energy	First order upwind	
Solver	SIMPLE	Turbulent dissipation rate	First order upwind	
Outlet Boundary	Pressure-outlet	Energy	-	

In Table 7.14 is described the analysis of different momentum discretization schemes. The comparison between “first order upwind” and “second order upwind” is subsequent of a decision regarding this parameter – which scheme to use in the simulations. The decision is made based on the complexity of the case. In this study, the momentum equations is one of the most important in computation since the problem does not involve extreme compressibility and it also does not regard heat transfer which simplifies the problem and makes the momentum equation the drive of the computation.

The difference between first order upwind and second order upwind is only based on the level of precision of each one since one is of first order precision and the other is of second order precision. The result goes accordingly to what one expects – higher precision involves more computational effort. A difference of around 20% between first order and second order precision confirms the level of influence of the momentum equation on the drag coefficient and it also demonstrates that first order precision is not acceptable on the computation of the problem.

Table 7.15 – Analysis of different air properties on low speed flow.

ρ (kg/m^3)	Cd	|ΔCd| (%)	Iterations
1,225 (constant)	0,27162	-	227
Ideal gas	0,27165	0,01	295

Remaining parameters of the simulation			
Re	2,00 E+5	Gradient	LSCB
Ma	0,03	Density	Standard
V (m/s)	9,58	Momentum	First order upwind
ρ (kg/m^3)	-	Pressure	First order upwind
Turbulence Model	k-ε standard	Turbulence kinetic energy	First order upwind
Solver	SIMPLEC	Turbulent dissipation rate	First order upwind
Outlet Boundary	Pressure outlet	Energy (for “Ideal Gas” case)	Second order upwind

Similarly to the analysis of the outlet boundary condition, Table 7.15 shows that different air properties for relatively low speed do not produce practically any difference in the drag coefficient. This is as expected since for Ma=0,03 the compressibility effect is irrelevant. The case considering a higher flow speed is assessed and the result is visible on Table 7.16.

Due to the incompressibility condition for Ma=0,03, the air density for each case is approximately the same. However, for the air as “ideal gas” case, the equation of energy is computed. This distinction could affect the final result since the approximations from discretization of the equations could introduce a reduction in precision of the computation. This unknown behavior of the computation is the main reason for using “second order upwind” on the energy equation calculation.

The increased amount of iterations from one case to another is clear and it may be justified by the energy equation that needs to be accounted for in the “ideal gas” case.

Table 7.16 – Analysis of different air properties on high speed flow.

ρ (kg/m^3)	Cd	|ΔCd| (%)	Iterations
1,225 (constant)	0,29897	-	340
Ideal gas	0,27435	8,23	323
1,225 (constant) for outlet boundary “outflow”*	0,29967	0,23	242

Remaining parameters of the simulation			
Re	2,13 E+6	Gradient	LSCB
Ma	0,3	Density	Standard
V (m/s)	102	Momentum	Second order upwind
ρ (kg/m^3)	-	Pressure	First order upwind
Turbulence Model	k-ε Standard	Turbulent kinetic energy	First order upwind
Solver	SIMPLEC	Turbulent dissipation rate	First order upwind
Outlet Boundary*	Pressure-outlet	Energy	Second order upwind

Table 7.16 shows the analysis of different air properties for relatively high speed flows. Ma=0,3 is commonly referred to as the initial stage in which the compressibility effect appears. For these conditions, the simulation is set up with the more robust parameters, such as the k-ε turbulence model, “SIMPLEC” solver and the energy equation calculation.

Since in Table 7.13 the comparison between outlet boundaries is done for a speed of Ma=0,03, in Table 7.16 there is a third simulation that allows one to compare the outlet boundaries “outflow” and “pressure-outlet” for high speed. One may see that for “outflow” outlet boundary, the computation lasted 100 iterations less than for “pressure-outlet” outlet boundary. This means that with “outflow” the computation is “lighter” than with “pressure-outlet”. Regarding the result, a 0,23% variation is negligible, yet it cannot be referred as non-existing. One cannot take a clear conclusion regarding the precision of each parameter. The decision for using “pressure-outlet” is based on the inability of considering compressibility effects on the density parameter (using “ideal gas”) with “outflow” outlet boundary.

As one may conclude that the outlet boundary condition is not as relevant in terms of influence on the drag coefficient, one may also deduce that, as expected, the compressibility of the air influences the results. Considering the air’s density as constant for conditions of Ma=0,3 or above is not acceptable as demonstrated by the 8,23% variation between both parameters.

Table 7.17 – Analysis of different solvers.

Solver		Cd	|ΔCd| (%)	Iterations
SIMPLE		0,37733	-	89
SIMPLEC		0,37605	0,34	239
Remaining parameters of the simulation				
Re	2,00 E+5	Gradient	LSCB	
Ma	0,03	Density	Standard	
V (m/s)	9,58	Momentum	First order upwind	
ρ (kg/m^3)	1,225 (constant)	Pressure	First order upwind	
Turbulence Model	Laminar	Turbulent kinetic energy	-	
Solver	-	Turbulent dissipation rate	-	
Outlet Boundary	Pressure Outlet	Energy	-	

In spite of not generating much difference between drag coefficient's values, the analysis of different solvers visible on Table 7.17 shows the increase in the amount of iterations when using the "SIMPLEC" solver. It is computationally heavier than "SIMPLE".

On the other analysis tables, one may contemplate a trend on the amount of iterations. On every simulation that uses "SIMPLE" solver, the number of iterations is usually below 100. On simulations for "SIMPLEC" solver, the number raises to over 200 iterations. One may conclude that for "SIMPLE" solver, the solution converges faster than for "SIMPLEC".

Nonetheless, based on the several simulations performed throughout the study, it is evident that "SIMPLE" solver starts to diverge for low speed flows (around Ma=0,08) so it is only applied for initial iterations. "SIMPLEC" is then a more robust solver which is applied for higher speed flows. In conclusion, the "SIMPLEC" solver needs higher amounts of iterations in order to reach a solution; however it allows one to perform more demanding simulations.

Table 7.18 – Analysis of different turbulence models on low speed flow.

Turbulence Model		Cd	|ΔCd| (%)	Iterations
Laminar		0,37733	-	89
Spalart-allmaras		0,35992	4,61	90
k-ε Standard		0,35259	6,56	91
Remaining parameters of the simulation				
Re	2,00 E+5	Gradient	LSCB	
Ma	0,03	Density	Standard	
V (m/s)	9,58	Momentum	First order upwind	
ρ (kg/m^3)	1,225 (constant)	Pressure	First order upwind	
Turbulence Model	-	Turbulent kinetic energy (except “laminar” case)	First order upwind	
Solver	SIMPLE	Turbulent dissipation rate (except “laminar” case)	First order upwind	
Outlet Boundary	Pressure-outlet	Energy	-	

Table 7.18 shows the analysis of different turbulence models on low speed flows. This parameter is one the most discussed parameters in CFD. Since the turbulence model is a mathematical approach to simulate a mainly random behavior of particles, there are better suited turbulence models to particular situations but there is still to be found a turbulence model that accurately simulates the behavior of turbulence rather than approximating it.

This analysis is performed in two stages: the low speed and the high speed flows. The velocity is directly related to turbulence and for that reason there appears the need to separate laminar flow and turbulent flow. Table 7.18 regards a configuration close to the transition phase in terms of turbulence. The models appropriated for low speed are the simpler ones since the flow is close to laminar – the laminar model may be considered suited to return an acceptable result. The “Spalart-Allmaras” and the “k-ε Standard” regard turbulence which implies that the conditions of the flow are at least on the laminar-turbulent transition.

The three models result in distinct values of drag coefficient, being that the approach with any turbulence is 4,61% and 6,56% different than the approaches that consider turbulence. These results demonstrate that turbulence implies less drag which corresponds to the main principles of drag effects. Regarding the comparison between both turbulent models, there cannot be stated a well-defined conclusion on which is the best model.

Table 7.19 – Analysis of different turbulence models on high speed flow.

Turbulence Model		Cd	|ΔCd| (%)	Iterations
k-ε Realizable		0,29385	-	335
k-ω Standard		0,28314	3,64	372
k-ω SST		0,26447	10,00	354
Remaining parameters of the simulation				
Re	2,84 E+6	Gradient	LSCB	
Ma	0,4	Density	Standard	
V (m/s)	136	Momentum	Second order upwind	
ρ (kg/m^3)	Ideal gas	Pressure	First order upwind	
Turbulence Model	-	Turbulent kinetic energy	First order upwind	
Solver	SIMPLEC	Turbulent dissipation rate	First order upwind	
Outlet Boundary	Pressure-outlet	Energy	Second order upwind	

Table 7.19 shows the second stage of the analysis of turbulence models. As mentioned earlier, the solver used for higher speed flows is “SIMPLEC” due to its capacity of converging with no manipulation of under-relaxation terms of the simulation. This justifies the amount of iterations and its difference to the results in Table 7.18.

The results of drag coefficient for the particular turbulence models are significantly distinct. CFD results are only reliable to some extent – there has to be a range of acceptable values as a result of a certain simulation. In this case one may consider a range between 0,30 and 0,26 for the drag coefficient. There is not a clear method for considering a turbulence model more appropriate than other; yet, each turbulence model is created upon certain grounds. The challenging task is to associate these grounds to the considerations of the study.

As an example and considering these results as the drag coefficients in which one is interested in, for safety reasons one is recommended to be conservative which means consider the highest value of drag coefficient obtained. Also for safety reasons one must apply a safety factor to the coefficient’s value. For this example, a valid approach is considering the value as 0,30 and applying a 1,5 safety factor which means a final value of drag coefficient of 0,45.

Table 7.20 – Analysis of different turbulence properties.

Turbulence intensity / Turbulent length scale	Cd	|ΔCd| (%)	Iterations
TI 0,5% / TLS 0,01m	0,29406	-	244
TI 1% / TLS 0,05m	0,29687	0,96	245
TI 5% / TLS 1m	0,33506	13,94	244

Remaining parameters of the simulation			
Re	8,66 E+5	Gradient	LSCB
Ma	0,12	Density	Standard
V (m/s)	41,5	Momentum	Second order upwind
ρ (kg/m^3)	1,225 (constant)	Pressure	First order upwind
Turbulence Model	k-ε Standard	Turbulent kinetic energy	First order upwind
Solver	SIMPLEC	Turbulent dissipation rate	First order upwind
Outlet Boundary	Pressure-outlet	Energy	-

Table 7.20 shows the analysis of different turbulence properties. This analysis is of most relevance for the study since usual values for these properties have wide ranges of values. This implies that a flow might have strongly distinct characteristics from the actual flow. There are a few means of characterizing the turbulence of a flow. However it usually takes two parameters, one regarding the strength or intensity of the turbulence and the other regards a dimension or a geometric factor of the flow. For an external flow it is common to consider turbulent intensity and turbulent length scale which as default is considered as TI 5% and TLS 1 m.

As default the values are not applicable to the actual flow, there are compared three different sets of turbulence properties: the default parameters, the maximum parameters considerable for this type of flow and an average reasonable set of parameters. The results demonstrate a clear divergence from de coefficient values obtained for the lower parameters to the ones obtained for the default parameters. This means that there is a notable influence of the turbulence properties in the result of drag coefficient. A variation of around 1% between the maximum acceptable values for the turbulence properties and the average values considered also means that it is a safe approximation.

For some turbulence models on higher speed flows, these parameters and its decrease also result in a relatively easier convergence. Based on the various simulations performed the momentum equation shows to be slightly sensitive to these parameters.

7.8.2 Parametric study

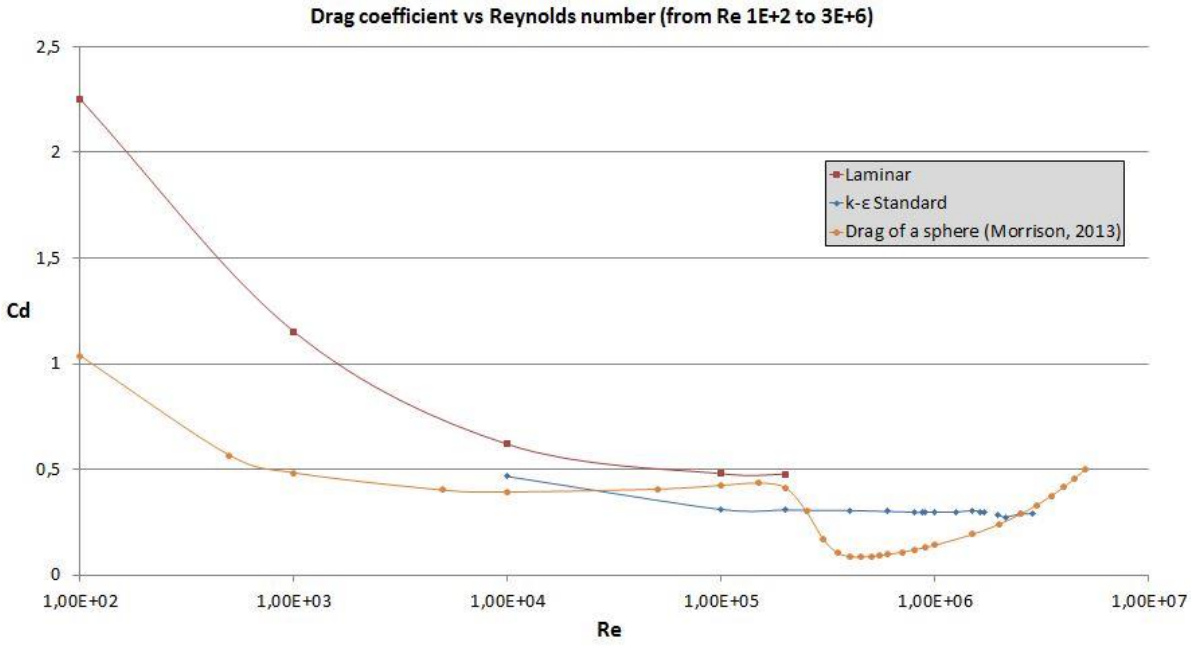

Figure 7.28 – Parametric study of drag coefficient around a turret for Reynolds varying from $Re = 10^2$ to $Re = 3 \times 10^6$. Red – results obtained considering laminar flow. Blue – results obtained considering turbulent flow. Orange – published results for drag of a sphere from Morrison (2013).

After the validation is completed, there is the need to apply the computational analysis to the region and conditions of interest. A parametric study is performed with the purpose of giving not only the information on the most adverse drag force to which the turret is to be subjected but also on the entire range of operability of the turret. This may be relevant for purposes of analyzing the behavior of the turret in terms of structural fatigue or applying this information on another installation.

As seen on Figure 7.28 the flow is considered to assume a laminar nature from low speeds until it reaches $Re = 10^4$; from this point to around $Re = 2 \times 10^5$ it is assumed a transition phase regarding turbulence so both laminar and turbulent simulations are performed. From $Re = 2 \times 10^5$ to around $Re = 3 \times 10^6$ the flow is considered fully turbulent.

Lacking experimental data to compare to within the range of Re here presented, there is presented a comparison to a known simpler case – flow around a sphere from Morrison (2013). This has the goal of finding similarities between the sphere case and the turret case in study, which is a half of a sphere coupled to a cylinder base. Although it is important to mention the major difference from both cases – the sphere case has no obstruction to the geometry whereas the turret is attached to a surface. This alters completely the behavior of the flow around the object in study.

One may notice the similar decrease in drag coefficient for the laminar region whereas on the region of around $Re = 4 \times 10^5$ the Cd of the sphere drops significantly and then, from around $Re = 7 \times 10^5$ it starts to rise. For the turret, the Cd converges to around 0,3 with no considerable variations.

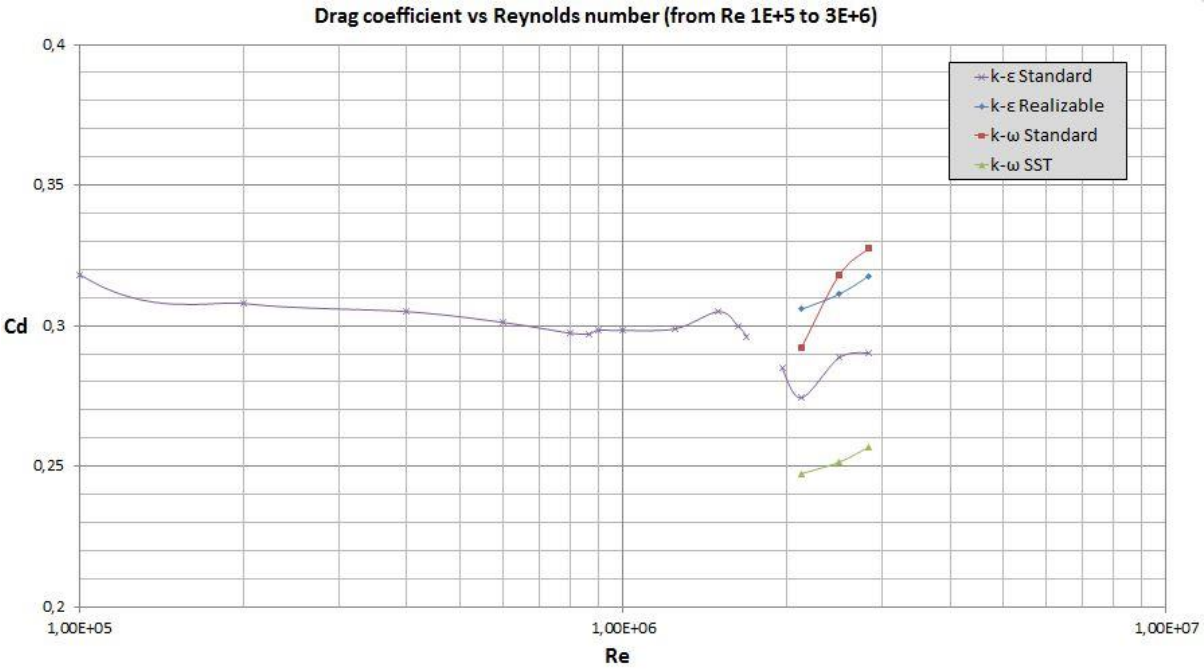

Figure 7.29 – Comparison of different turbulence models for Reynolds varying from $Re = 1 \times 10^5$ to $Re = 3 \times 10^6$.

Figure 7.29 focuses on just the turbulent phase of the turret computational results. In order to understand the influence of the turbulence model chosen, simulations for Ma=0,3, Ma=0,35 and Ma=0,4 are performed for other three turbulence models as seen on the figure. One may notice that the four turbulence setups delivered the same trend in the Cd values – increasing from Ma=0,3 and Ma=0,4 – which also goes accordingly to the sphere case discussed from Figure 7.28. The results obtained with the turbulence model "k-ε Standard" also show a slight drop for the conditions around $Re = 1{,}50 \times 10^6$ with a subsequent increase afterwards around $Re = 2{,}05 \times 10^6$. Comparing this situation with the sphere case, there might exist a relation between both curve behaviors. However, it is important to consider that the scale of the plot in Figure 7.29 is much more sensitive and in which any variation on the curve is much more easily visible. In addition, comparing the variation of Cd on the drop on the purple curve to the variation of the Cd values on the different turbulence models, it is clear that the range of variations is similar. This inhibits one to relate the drop on this curve to the drop in the sphere's curve.

The discontinuity verified in the "k-ε Standard" curve, which represents flow velocities between 82 m/s and 94 m/s, is related to the divergence of the solutions associated to these

parameters. This may ground that an unknown phenomenon for this range of Reynolds numbers may induce the drag coefficient to decrease. Consequently, it may raise the doubt whether the drop in this curve may be related to the one visible on the sphere's curve or not. Although the region of Re in which the drops occur are considerably different as well as the magnitude of the Cd values' decline, it cannot be concluded that the curve from the turret has the same trend as the curve obtained for the sphere; further study on this subject is required in order to assure a conclusion.

Table 7.21 – Drag forces for the most adverse flight conditions.

Conditions	Drag Coefficient	Validation factor	Safety factor	Drag Force (N)
Maximum operating speed	$0{,}2951 \approx 0{,}3$	2	1,0	1636
Diving speed	$0{,}3012 \approx 0{,}3$	2	1,5	2272

Drag values for the most adverse flight conditions are the main output of the CFD analysis since these are the values for which the structural design of the turret's supporting frame is conducted **[1]**. Table 7.21 shows the drag forces obtained for both flight conditions. Drag coefficient is related to the Cd value computed from the analysis. The validation factor relates the difference between the computed values and the experimental results as referred previously. A safety factor is assumed before any structural design influence in order to increase the reliability on the results; once in the structural design, there are other safety factors involved. The values of drag force are interpreted as the maximum aerodynamic static impact on the turret caused by the flow.

8 Conclusion

8.1 Concluding remarks

- A group of requirements to comply throughout the process is identified, as seen on Table 2.1; this regards the certification context in which the modification is inserted;
- A suitable location for the installation of turrets is chosen for the Lockheed Martin C-130 and also a method of analyzing locations is created applicable to other aircrafts;
- A design approach which has the purpose of reducing cost and time to the DOA's design process is successfully achieved;
- A specific methodology is created to serve as support for the design team of the DOA whom is responsible for the installation of a turret on an aircraft;
- Regarding the case study, which may have different characteristics by varying conditions such as the location of installation, the model of the sensor, or the type of aircraft, it is carried out focusing on the aerodynamic influence of the flow on the turret and consequently on the structure which is attaching the turret to the airframe. Many conclusions are made regarding the aerodynamic analysis:
    - The computational methods used demonstrate to be expedite and accurate so, for that reason, suitable to conduct the analysis.
    - A 2D simulation has geometrical limitations that hamper the reliability on the results. A 3D study proves to be essential for this flow geometry;
    - A steady-state simulation has limited applicability for the study; it only allows considering aerodynamic impact as aerodynamic static force.
    - The turbulence models tested vary from the simplest models to some of the most robust models for the RANS approach. LES and DNS simulations may be tested, however, the results should not be significantly different. These approaches are not usually suited to practical purposes since the results' variations are absorbed by the safety factors of the design process.
    - Based on the quality parameters evaluation, the meshes created are acceptable.

8.2 Future developments

- The main focus of this work, regarding the design process, lies on the preliminary design stage, so the development of detailed design procedures is naturally the following necessity;

- As additional work, it is important to validate the method of analyzing the installation locations on other aircrafts;
- Regarding the aerodynamic analysis:
    - The experimental results found are clearly distinct from the computational solutions obtained which may induce a concern subject to further validation;
    - Since steady state simulations have limitations, further transient simulations are required to treat the important issue of flow induced vibrations;
    - Due to the characteristics of the actual flow, the considerations made to simplify the analysis generally demonstrate to be solid and of low influence on the results; still, in future work, it is important to assure the independency between these simplifications and the results, for certification purposes; on the other hand, relevant geometrical considerations such as the turret having a non-conformal window may justify an in-depth study since it may alter the whole configuration of the flow.
    - A more extensive work on the architecture of the mesh is certainly going to improve the simulation. The solution values are not expected to vary greatly yet the convergence will be easier to attain. In addition, a further transient study requires both more refined and enhanced quality meshes. The reason for this necessity is the aforementioned difficulty in identifying precisely the separation point of the flow. This has been subject of innumerous studies.
- As part of a larger project, the aerodynamic influence on the turret is one of the required subjects to be studied. A structural impact is also carried out by Doloshytskyy (2015) **[1]**. Yet, it still remains to be studied the electric and electronic needs of the mentioned modification. Very useful information regarding the impact of the airflow on the optical performance of turrets is provided **[37]**.

Bibliography

[1] Doloshytskyy, Y. “Electro-optical/Infrared sensor turret integration on an aircraft – structural impact on LOCKHEED MARTIN C-130 and project design methodology”, FCT-UNL, 2015.

[2] Anderson, D. D. “Design for Manufacturability & Concurrent Engineering”, Cambria, California: CIM Press, 2004.

[3] Atkinson, R. “Project management: cost, time and quality, two best guesses and a phenomenon, its time to accept other success criteria”, International Journal of Project Management 17, 1999.

[4] ECOLE POLYTECHNIQUE FEDERALE DE LAUSANNE, Group of Thermal Turbomachinery, “Aeroelasticity in turbomachines”. [Online]. Available: http://gtt.epfl.ch/page-63561-fr.html [Accessed 2015 08 31].

[5] EASA, [Online]. Available: https://www.easa.europa.eu/the-agency. [Accessed 2015 07 20].

[6] EASA, CS-25 Amendment 17 Certification Specifications for Large Aeroplanes.

[7] FLIR, “Star SAFIRE III”, [Online] Available: http://www.flir.com/surveillance/display/?id=63504 [Accessed 2015 08 31]

[8] AIRBUS DEFENCE&AEROSPACE, “ARGOS-II HD / ARGOS-II HDT”, [Online] Available: http://www.defenceandsecurity-airbusds.com/web/guest/argos_ii_hd [Accessed 2015 08 31]

[9] LOCKHEAD MARTIN, “INFIRNO”, [Online] Available: http://www.lockheedmartin.com/us/products/infirno.html [Accessed 2015 08 31].

[10] FLIR, “FLIR Military & Defense – Maritime Patrol” [Online]. Available: http://www.flir.com/surveillance/display/?id=64967 [Accessed 2015 08 31].

[11] AIRBUS DEFENCE&AEROSPACE, “Airborne Optronics”, technical datasheet, 2014.

[12] RAYTHEON, “AN/AAS-52”, technical datasheet, 2015.

[13] FLIR, “STAR SAPHIRE III”, technical datasheet, 2011.

[14] GENERAL DYNAMICS, “V-14”, technical datasheet, 2015.

[15] NORTHTOP GUMMAN, “AN/AAQ-28(V) LITENING”, technical datasheet, 2012.

[16] LOCKHEAD MARTIN, “INFIRNO”, technical datasheet, 2010.

[17] L3-WESCAM, “MX-15”, technical datasheet, 2014.

[18] L3-WESCAM, “MX-20”, technical datasheet, 2014.

[19] L3-WESCAM, “MX-25”, technical datasheet, 2014.

[20] RAFAEL, “Toplite EOS”, technical datasheet 2015.

[21] T. U. Munchen, “DSMweb.org,” [Online]. Available: http://www.dsmweb.org/. [Accessed 16 03 2015].

[22] Planobrazil, [Online]. Available: http://www.planobrazil.com/wp-content/uploads/2013/10/AC-130U.jpg [Accessed 2015 08 31]

[23] LOCKHEED MARTIN, “Lockheed Martin Delivers Landmark 300th C-130J Super Hercules”, [Online]. Available: http://www.lockheedmartin.com/us/news/press-releases/2013/december/131218ae_lockheed-martin-delivers-300th-c-130j.html [Accessed 2015 08 31].

[24] OGMA, “Internal document”

[25] Coelho, A. M. “Fundamentals of Axiomatic Design - 1. Introduction,” DEMI-FCT/UNL, UNIDEMI.

[26] Schonberger, J. R. “Flow control about an airborne laser turret”, Monterey, California. Naval Postgraduate School, 1980.

[27] AGARD, “Special Course on Engineering Methods in Aerodynamic Analysis and Design of Aircraft”, AGARD Report 783, 1992.

[28] Jameson, A. “A perspective on computational algorithms for aerodynamic analysis and design”, Progress in Aerospace Sciences 37, 2001.

[29] ANSYS, “Introduction to ANSYS FLUENT – Turbulence Modeling” [Software Documentation] 2010.

[30] Morgan, P. E., Visbal, M. R. “Large Eddy Simulation of Flow Over a Flat-Window Cylindrical Turret with Passive Flow Control”, AIAA 2010-916

[31] Schwabacher, G. J. “Computational fluid dynamics testing for drag reduction of an aircraft laser turret”, Air Force Institute of Technology, 2000.

[32] ANSYS, “ANSYS FLUENT 12.0 Theory Guide” [Software Documentation] 2009.

[33] Conde, J. M. P. “Computational Fluid Dynamics” DEMI-FCT/UNL, UNIDEMI.

[34] ANSYS, “ANSYS FLUENT 12.0 User’s Guide” [Software Documentation] 2009.

[35] Snyder, C. H. “Wind tunnel testing for drag reduction of an aircraft laser turret”, Air Force Institute of Technology, 1998.

[36] Gordeyev, S., Post, M. L., McLaughlin, T., Ceniceros, J., Jumper, E. J. “Survey of optical environment over hemisphere-on-cylinder turret using suit of wavefront sensors”, 37th AIAA Plasma dynamics and Lasers Conference, AIAA-2006-3074.

[37] Gordeyev, S., Jumper, E. “Fluid dynamics and aero-optics of turrets” Progress in Aerospace Sciences 46, 2010.

[38] Ladd, J., Mani, M., Bower, W. “Validation of aerodynamic and optical computations for the flow about a cylindrical/hemispherical turret” 27th AIAA Applied Aerodynamics Conference, AIAA 2009-4118

[39] Mathews, E., Wang, K., Wang, M., Jumper, E. “LES analysis of hemisphere-on-cylinder turret aero-optics” University of Notre Dame, Notre Dame, IN 46556, 2014.

[40] Hannaby, S. A. “A mapping method for mesh generation” Comput. Math. Applic. 16, 1988.

[41] CUBIT, “CUBIT 13.2 – User Documentation”, [Software documentation]

[42] Cavcar, M. “The International Standard Atmosphere (ISA)”, Anadolu University, Turkey

[43] ESI-CFD, “ESI users documentation” [Online], Available: http://www.esi-cfd.com/esi-users/ [Accessed 2015 08 31].

[44] Strumolo, G. S. “Seminar on industrial problems ISDP: Inverse Shape Design Procedure” Scientific Research Laboratory Ford Motor Company, 1999.

Annex A

Criteria		Location	Decision/Justification
1		L	As it is on the side, it would need sensors in both sides and the K area is blocking the sensors' sight
		M	Not under the fuselage enough
		N, O	Being in the top of the fuselage does not allow any range of sight
		P	To have an adequate sight range it would need a sensor in both sides and it would have to be in the lowest part of the area P
		Q	The only way is to attach a supporting structure to the fuel tank with the sensor facing down
2	2.1	A	Antenna 20 must be relocated if an interference is detected
		E	The distance between the sensor to antennas 17,18 e 19 must be checked
		F	The distance between the sensor to antennas 17,5 e 6 must be checked
		N	The distance between the sensor to antenna 3 must be checked
	2.2	A, B	nose landing gear
		C,D,F,G,E, I	main landing gear
		E, I	there are some antennas in that space
		K	elevators
		L	rudder
		M	door M
		P	elevators
		Q	flaps and ailerons
	2.3	K	elevators
		L	rudder
		Q	wing and flaps
	2.4	B	interphone and liquid oxygen drain/vent - must mind these components when designing the fixation
		C,D,F	These locations meet the FAP C-130H but there are usual modifications in these locations that one might have to consider
		E	Interference with the nose landing gear sliding cover
		G,H	Possible interference with the main landing gear cover
		M	Door M
	2.5	A	PI - Landing Gear Hydraulic Pumping (**IPB - Hydraulic Systems**). Bleed Air Anti-Icing system (**IPB - Pneumatic System**). Pitot Static Systems (**IPB - Pneumatic System**)

		B	PI: external interphone (**TMC**). Booster hydraulic system ground test connection access, Liquid Oxygen Valve/Vent (**TMC**). Hydraulic Brake Piping (**IPB - Hydraulic Systems**). Metering Valve (**IPB - Hydraulic Systems**). Electrical Components (**IPB - Electrical Systems**). Battery Equipment (**IPB - Electrical Systems**)
		C	PI - fuselage drainage holes (**TMC**) Hydraulic Brake Piping (**IPB - Hydraulic Systems**). Flight Deck Air Conditioning System (**IPB - Pneumatic System**). Electrical Components (**IPB - Electrical Systems**). Battery Equipment (**IPB - Electrical Systems**). AFT Center Equipment (**IPB - Electronic System**)
		D,E,F	PI - fuselage drainage holes (**TMC**)
		G	I - Refrigeration Unit PI - Cargo compartment refrigerator access (**TMC**). Water separation drains (**TMC**). Air intake Drain (**TMC**). Hydraulic Vent (**TMC**). Landing Gear Failing Drainage Holes (**TMC**). PI - APU air intake door (**TMC**). Hydraulic Brake Piping (**IPB - Hydraulic Systems**). APU Bleed Air Supply system (**IPB - Pneumatic Systems**)
		H	PI - single point refuel drain valve/adapter drain. Fuel Pump seal drain. Hydraulic Brake Piping (**IPB - Hydraulic Systems)**
		I	PI - fuselage drainage holes
		J	I - elevator trib tab motor access, Controls inspection access, Pressure seals and structural inspection, Rudder and elevator controls and electrical access, Rudder and elevator, controls and electrical access, AFT empennage draining holes. PI - Elevator and Rudder Controls (**TMC**)
		K,L	I - anti-icing
		N,O	PI - IFF (**IPB - Electronic System**)
		P	PI - Auxiliary Hydraulic Piping (**IPB - Hydraulic Systems**). Caution with AFT Fuselage Electronic (**IPB - Electronic System**)
		Q	PI - Fuel Tank
3		C,D	Susceptible to dust and rocks from the nose landing gear
		E,F	Dangerously close and behind the nose landing gear
		G,H,I	Close to the ground
		J,K	High temperatures may affect the sensor and the exhaust gas may affect the sensor's lenses
		P	In the location that enables a full range of sight, the sensor may be too close and behind the main landing gear
4		C,D,E,F,I, M,N,O,P	Pressurized area of the aircraft
5A		A,B,C,D,E, F,G,H,I	A bigger sensor may affect the aircraft's aerodynamics. The location is in the fuselage where the air flow is well difinied
		J	May affect the Cd critically
		K,L	Bigger size is critical to the good functioning of the elevators and rudder

	M,N,O	The aerodynamics must be checked if considering a bigger sensor
	P	The only way to reduce the impact is to create an aerodynamic external structure to support the sensor
	Q	The wing balance affects the flight performance of the aircraft. Needs Sensors on both wings
5B	A	Relatively simple fixation needing only structural reinforcements
	B,C,D,N,O,P	Needs small external structures to support the sensor
	G,H	Needs bigger external structures to support the sensor
	J	Sensitive location of the airplane (Structural and Operational-wise)
	K,L	Sensitive and small areas, not viable
	M	It is an attachment to the door, it is limited
	Q	Structurally, does not affect much the wing
6	A	near the bulk head
	B,C,D,E,F,I,N,O,P,Q	Frames
	G,H	near the frames
	K,L	Sensitive location of the aircraft
	M	There is the need to guarantee the resistance of the door
	J	There are many vital components in a small space
7	A	Hole + Fixation (relatively simple)
	B,C,D	Requires an external structure
	E	Landing gear sliding door and many antennas (interference)
	F,I	Hole + Fixation (Mind the distance between antennas!)
	G,H	Involves a big external structure to support the sensor
	J	Numerous interferences (operational, structural, geometrical) that may not allow the fixation
	K,L	Sensitive areas and critical operational functions
	M	Concern about the link between the door and the sensor, as well as the type of fixation. It no longer is as a door.
	N,O	To provide a good sight range, there would be necessary a huge arm to the sensor
	P	Might need sensors on both sides or a big external structure
	Q	Difficulties in attaching the structure of the sensor to the fuel tank

Annex B.1

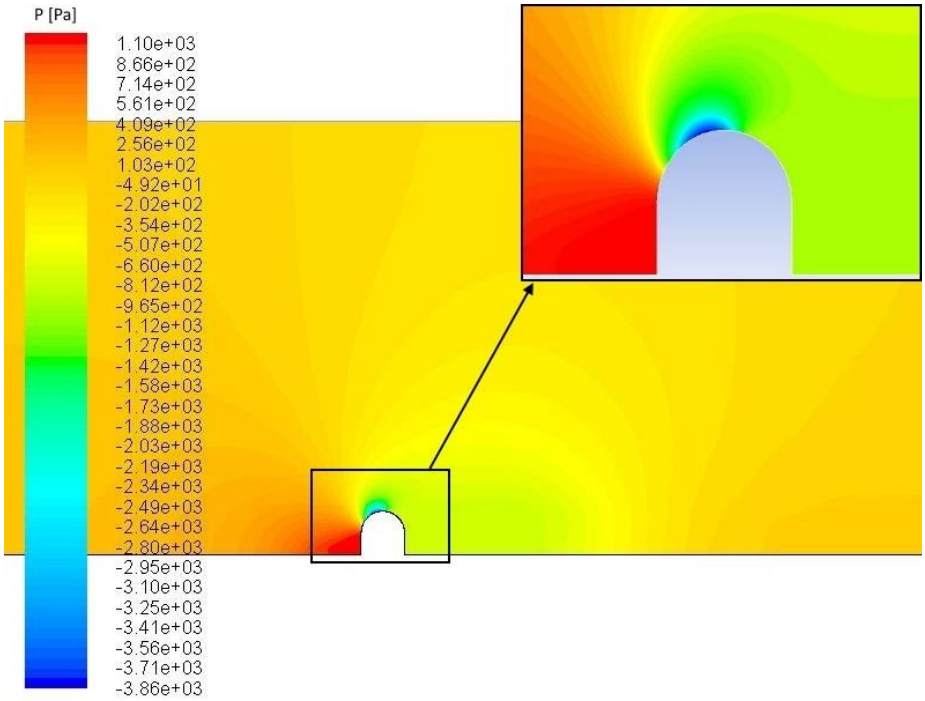

Annex – 2D pressure field for validation conditions of $Re = 8{,}66 \times 10^5$.

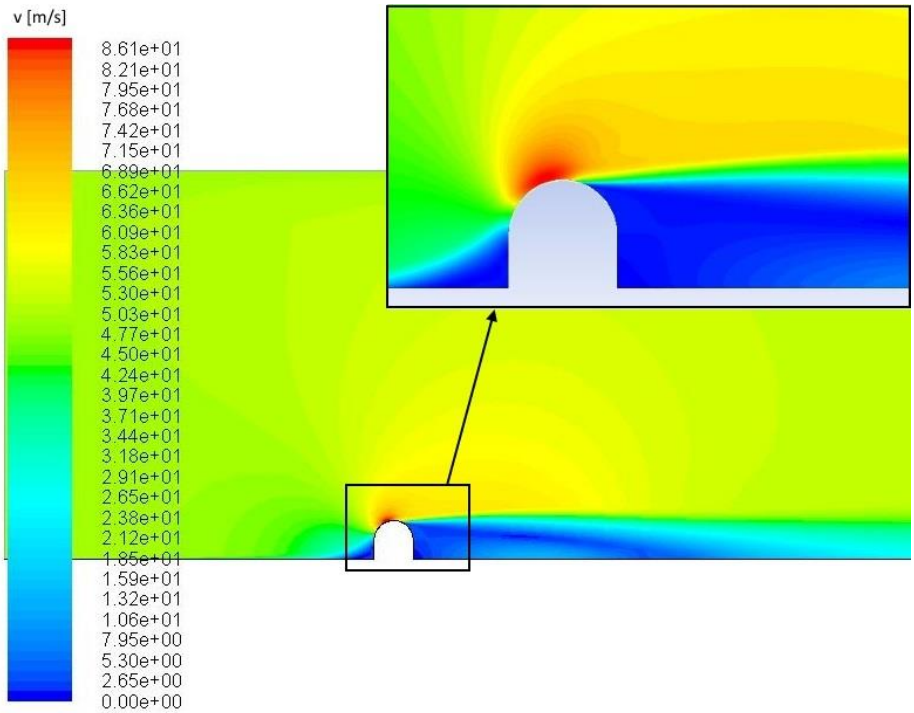

Annex – 2D velocity magnitude field for validation conditions of $Re = 8{,}66 \times 10^5$.

Annex B.2

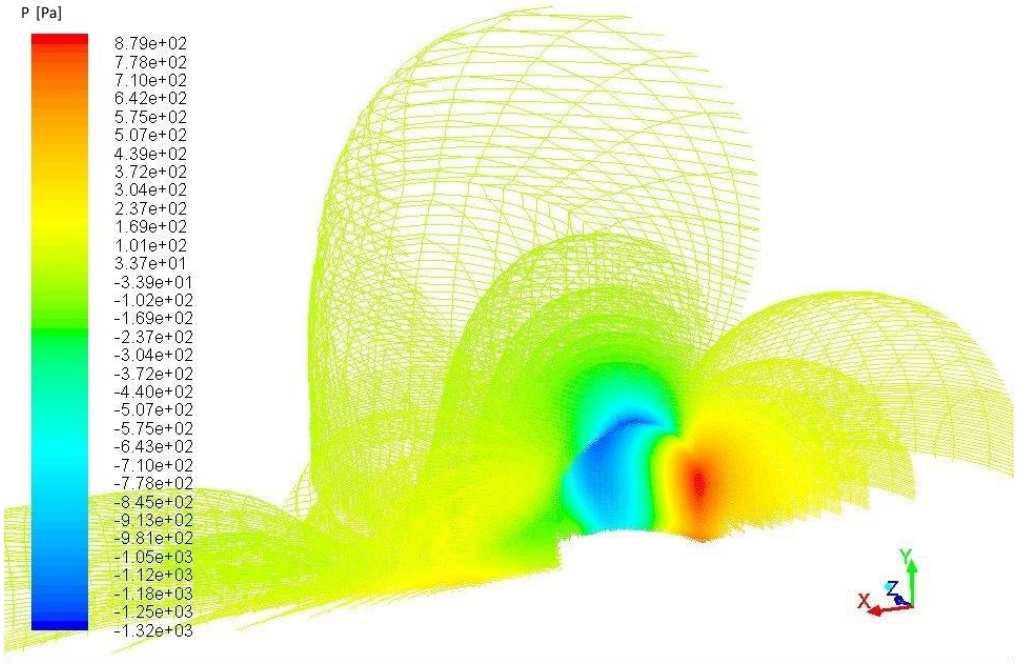

Annex – 3D pressure field for validation conditions of $Re = 8{,}66 \times 10^5$.

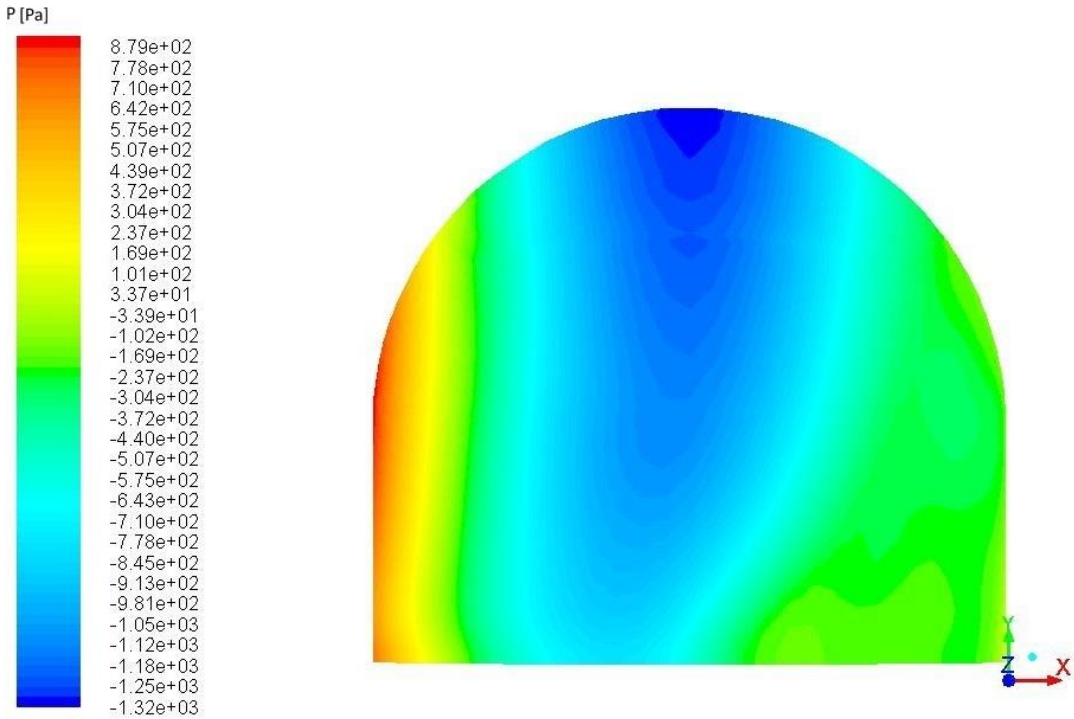

Annex – 3D pressure contours around the turret for validation conditions of $Re = 8{,}66 \times 10^5$.

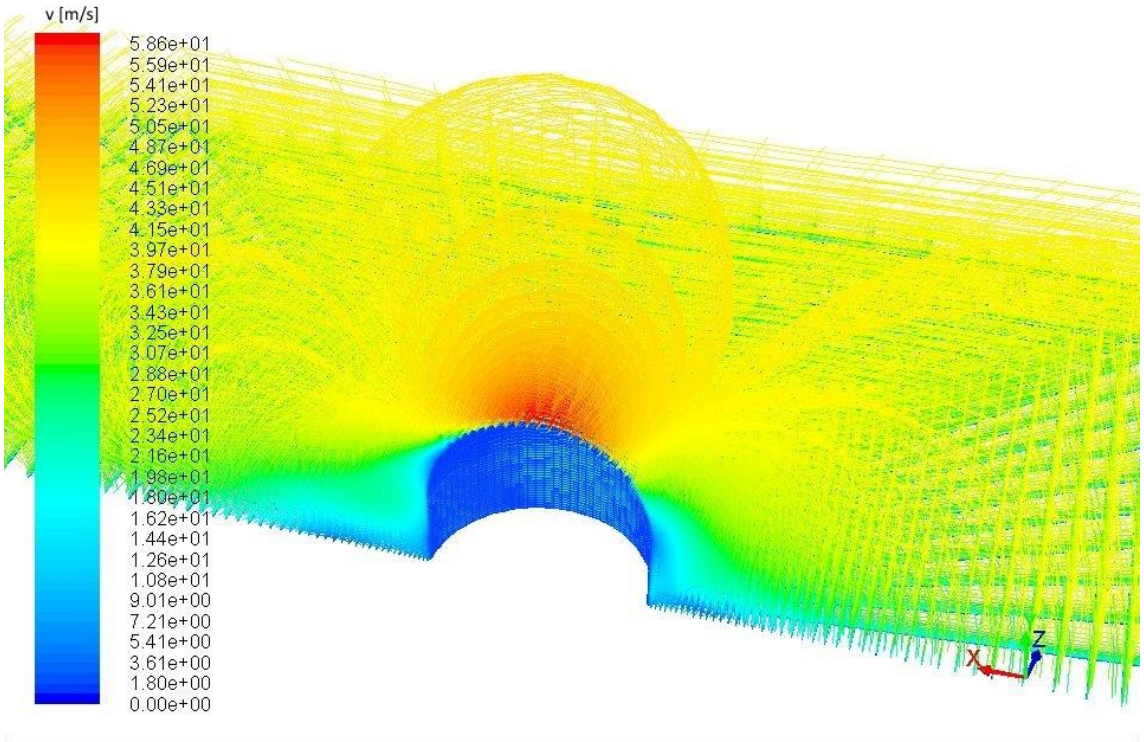

Annex – 3D velocity magnitude field for validation conditions of $Re = 8{,}66 \times 10^5$.